

1245

TRIPLET EXCITONS IN QUASI-ONE-DIMENSIONAL
MOLECULAR CRYSTALS

A low temperature spectroscopic study of
1,4-dibromonaphthalene

J. M. J. VANKAN

TRIPLET EXCITONS IN QUASI-ONE-DIMENSIONAL MOLECULAR CRYSTALS

A low temperature spectroscopic study of
1,4-dibromonaphthalene

PROMOTOR: PROF. DR. E. de BOER
CO-REFERENT: DR. IR. W. S. VEEMAN

TRIPLET EXCITONS IN QUASI-ONE-DIMENSIONAL MOLECULAR CRYSTALS

A low temperature spectroscopic study of
1,4-dibromonaphthalene

PROEFSCHRIFT

TER VERKRIJGING VAN DE GRAAD VAN DOCTOR
IN DE WISKUNDE EN NATUURWETENSCHAPPEN
AAN DE KATHOLIEKE UNIVERSITEIT TE NIJMEGEN, OP GEZAG VAN
DE RECTOR MAGNIFICUS, PROF. DR. J. H. G. I. GIESBERS,
VOLGENS BESLUIT VAN HET COLLEGE VAN DEKANEN
IN HET OPENBAAR TE VERDEDIGEN
OP VRIJDAG 15 APRIL 1983
DES NAMIDDAGS TE 2 UUR PRECIES

door

JOHANNES MARIA JOSEPH VANKAN

geboren te Heerlen



krips repro meppel

1983

Op deze pagina wil ik iedereen van harte bedanken, die op enigerlei wijze heeft bijgedragen tot de totstandkoming van dit proefschrift.

Op de eerste plaats mijn dank aan alle medewerkers van de afdeling Molecuulspectroscopie voor de jarenlange samenwerking. Met name Christ Weijtens heeft een eigen bijdrage aan dit onderzoek geleverd. De experimenten beschreven in hoofdstuk VI zijn door hem verricht.

Bijzonder grote dank gaat uit naar de technische staf van het Laboratorium voor Hoge Magneetvelden, de heren Klaas van Hulst, Henk Mulleman en Jos Rook, voor de assistentie in de vele nachtelijke uurtjes. Harold Myron dank ik voor zijn grote interesse en "stimulating discussions".

Op diverse medewerkers van andere afdelingen van onze faculteit heb ik in de afgelopen jaren een beroep mogen doen. Met name wil ik noemen de heren Jan Noordik en R. Curtis Haliwanger (Universiteit van Colorado) van de afdeling Kristallografie, waar onder meer de kristalstructuur van het 1,5-DBN werd opgelost. Abko van Zeist verrichtte op het Laboratorium voor Organische Chemie de moeilijke synthese van de verbindingen 1,5-DBN en 1,8-DBN, terwijl Louis Jetten (afdeling Vaste Stof Chemie) kristallen van 1,4-DBN uit de oplossing heeft gegroeid.

Verder heb ik assistentie gehad van vrijwel alle dienstverlenende afdelingen van de faculteit der Wiskunde en Natuurwetenschappen. In het bijzonder wil ik noemen de (Service) Instrumentmakerij (o.l.v. de heren Henk Verschoor resp. Paul Walraven). Nauwe samenwerking is er geweest met de heer Wil Corbeek, die de 4π -rotator heeft vervaardigd, een waar meesterwerk.

De uitgave van het proefschrift werd mogelijk gemaakt door de hulp van Désirée van der Wey die het manuscript typte, Ellen van Eldik die het netwerk verrichtte, John Slippens (afdeling Illustratie o.l.v. Wim Verdijk) die de tekeningen maakte en de medewerkers van de afdeling Fotografie o.l.v. Huub Spruyt, die het fotografische gedeelte voor hun rekening hebben genomen.

Tenslotte bedank ik Lies voor haar geduld en ondersteuning.

Dit onderzoek is uitgevoerd onder auspiciën van de Nederlandse Stichting voor Chemisch Onderzoek (SON) en met ondersteuning van de Nederlandse Organisatie voor Zuiver Wetenschappelijk Onderzoek (ZWO).

What is matter? - Never mind

What is mind? - It doesn't matter

*Ter nagedachtenis van mijn
schoonvader*

*Aan mijn ouders
Voor Lies*

CONTENTS

CHAPTER I

INTRODUCTION	1
I.1 Historical survey	1
I.2 Some physico-chemical background	1
I.3 Molecular triplet excitons in quasi-linear systems	3
I.4.1 Motivation	9
I.4.2 Outline of presentation	11
I.5 References	12

CHAPTER II

THEORETICAL CONSIDERATIONS	13
II.1 Introduction	13
II.2 Molecular triplet states	13
II.2.1 Zero-field splitting	13
II.2.2 Spin-orbit coupling (SOC)	16
II.2.3 The Zeeman interaction	18
II.3 Excitons in molecular crystals	20
II.4 Linear chain triplet excitons	24
II.5 Annihilation of triplet excitons	28
II.6 References	36

CHAPTER III

EXPERIMENTAL CONDITIONS	37
III.1 Sample preparation	37
III.2 Zone-refining	38
III.2.1 Zone-melting	38
III.2.2 Zone-sublimation	39
III.3 Crystal growing techniques	41
III.4 The spectrometer	42
III.4.1 Zero magnetic field	42
III.4.2 Magnetic field experiments	45

III.5	Typical experiments	50
III.5.1	Emission experiments	50
III.5.2	Time-resolved experiments	50
III.5.3	Excitation spectroscopy	51
III.6	References	52

CHAPTER IV

OPTICAL PROPERTIES OF THE LOWEST TRIPLET STATE

	OF 1,4-DIBROMONAPHTHALENE CRYSTALS	53
IV.1	Phosphorescence emission	53
IV.2	Delayed fluorescence	60
IV.2.1	General aspects	60
IV.2.2	The DBN case	62
IV.3	$S_0 \rightarrow T_1$ Absorption	64
IV.4	Concluding remarks	68
IV.5	References	69

CHAPTER V

	TIME-RESOLVED MEASUREMENTS	70
V.1	Introduction	70
V.2	A kinetic model for an exciton-trap system	70
V.3	Experimental results	76
V.3.1	Phosphorescence emission	76
V.3.2	Delayed fluorescence	80
V.4	Discussion and conclusions	83
V.5	References	85

CHAPTER VI

MAGNETIC RESONANCE ON LOCALIZED EXCITED TRIPLET

	STATES IN 1,4-DIBROMONAPHTHALENE	86
VI.1	Introduction	86
VI.2	Optically detected magnetic resonance (ODMR)	86

VI.3	Microwave induced delayed phosphorescence (MIDP)	88
VI.3.1	Determination of the absolute decay rates k_u	89
VI.3.2	Determination of the relative decay rates k_u^r	90
VI.3.3	Determination of the relative steady-state populations $N_u(0)$	91
VI.3.4	Determination of the relative populating rates $P_u(0)$	92
VI.4	The DBN case	92
VI.5	Results and discussion	93
VI.6	References	96

CHAPTER VII

MAGNETIC FIELD EFFECTS ON 1,4-DIBROMONAPHTHALENE

	PHOSPHORESCENCE EMISSION	97
VII.1	Introduction	97
VII.2	Steady-state experiments	100
VII.3	Time-resolved experiments	104
VII.4	References	108

CHAPTER VIII

	PHYSICAL AND CHEMICAL IMPURITIES IN DBN	109
VIII.1	Effects of different crystal growing techniques	109
VIII.2	The isomer 1,5-dibromonaphthalene	110
VIII.3	The isomer 1,8-dibromonaphthalene	114
VIII.4	References	116

	SUMMARY	117
--	---------	-----

	SAMENVATTING	119
--	--------------	-----

	CURRICULUM VITAE	121
--	------------------	-----

Parts of the contents of this thesis have been or will be published elsewhere:

J.M.J. Vankan, W.S. Veeman, Chem. Phys. Lett. 89, 258 (1982),

J.M.J. Vankan, W.S. Veeman, Chem. Phys. Lett. 91, 358 (1982),

J.M.J. Vankan, W.S. Veeman, Chem. Phys. Lett. 92, 519 (1982),

J.M.J. Vankan, W.S. Veeman, Chem. Phys. Lett., accepted for publication,

Ch.H.L. Weijtens, J.M.J. Vankan, W.S. Veeman, Spectr. Lett.,

accepted for publication in vol. 15/12,

J.M.J. Vankan, R.C. Haltiwanger, W.S. Veeman, to be published.

CHAPTER I

INTRODUCTION

1.1 Historical survey

There is a large class of organic compounds that exhibits a long-lived afterglow, when irradiated by ultra-violet light. Wiedemann reported observations of this kind in 1888, performing experiments on organic dyes dissolved in gelatine. Half a century later, in 1933, Jablonski [Ja33] proposed that a metastable intermediate state was responsible for this phenomenon. During the second world war it was suggested for the first time that this intermediate state was in fact an excited triplet state. Terenin [Te43] and Lewis and Kasha [Le44,Le45] attributed the afterglow to a radiative, spin-forbidden transition from the triplet state to the ground state. The term "phosphorescence" was introduced to indicate the phenomenon.

Since in a triplet state two electrons have parallel spins, it is paramagnetic. This photo-induced paramagnetism was measured by Lewis, Calvin and Kasha in 1949 [Le49] and by Evans in 1955 [Ev55]. Definite proof for the triplet nature of the metastable state was obtained in 1958 by Hutchison and Mangum [Hu58] through Electron Spin Resonance experiments on naphthalene present in a single crystal of durene. These experiments make use of the fact that a triplet state has three spin components which in a large magnetic field give rise to three Zeeman states $|m_S = +1\rangle \equiv |+1\rangle$, $|m_S = 0\rangle \equiv |0\rangle$ and $|m_S = -1\rangle \equiv |-1\rangle$.

Molecular triplet states have been the subject of numerous studies since then, especially since the discovery, that transitions between the three spin components can occur and can be detected optically even in the absence of a magnetic field [Sc68].

1.2 Some physico-chemical background

Studies of triplets are very often dealing with aromatic molecules, such as benzene, naphthalene, anthracene and their derivatives (Fig. I.1).

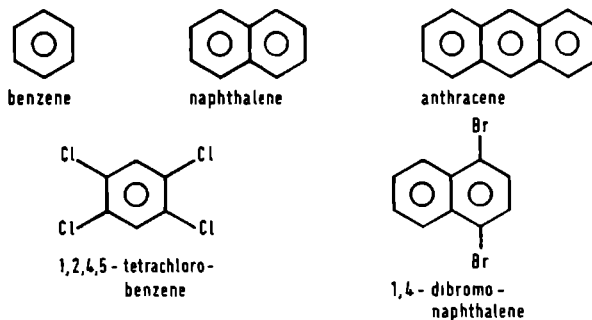


Fig. I.1 *Some aromatic systems.*

In a theoretical description of such molecules, the valence electrons of the individual atoms are considered to move in orbits, described by molecular orbitals (M.O.'s). These orbitals may have different symmetry properties and it is common practice to classify them into three types: σ , π and n-orbitals. The bonds that form the structural skeleton of the aromatic ring system are formed by the σ -orbitals and are called σ -bonds. In these σ -bonds one will always find the highest electron density in the molecular plane between the atoms. The π -orbitals, on the contrary, are delocalized over the molecule (indicated by the circles in Fig. I.1) and are represented by linear combinations of carbon $2p_z$ -orbitals. For π -orbitals the maximum electron density is found above and below the molecular plane, while the molecular plane itself is a nodal plane. Non-bonding orbitals (= n-orbitals) are found in molecules that contain hetero-atoms such as nitrogen or oxygen. Two compounds of this type, well known from phosphorescence studies are benzophenone and 1,4-diazanaphthalene (quinoxaline).

An electron present in the highest occupied molecular orbital (HOMO), n in the case of for example benzophenone, π in the case of naphthalene, can be promoted to the lowest unoccupied π^* molecular orbital (LUMO) by absorption of an UV photon. In this way an $n\pi^*$ or a $\pi\pi^*$ excited state is formed. Since during this electric dipole transition a change of spin

angular momentum is quantummechanically forbidden, the excited state has the same spin-multiplicity as the ground state. For the molecules discussed in this thesis the ground state is a singlet state and therefore, immediately after excitation, the excited state also will be a singlet state ($S = 0$). However, the electrons with antiparallel spins present in different orbitals may align their spins parallel via a non-radiative process called intersystem crossing. These parallel electron spins give rise to a triplet state ($S = 1$) with a lower energy than the corresponding singlet state (reduced interelectronic repulsion). Radiative decay from the excited state back to the ground state may occur both from the excited singlet state and from the triplet state. The first case is spin-allowed and is termed "fluorescence". The latter is spin-forbidden and termed "phosphorescence". Because of the spin-forbidden nature of the phosphorescence the triplet lifetime ($\sim 10^{-3} - 10$ s) is much longer than the excited singlet lifetime ($\sim 10^{-9} - 10^{-7}$ s). Transitions between the singlet and triplet manifold can in fact only occur because spin-orbit coupling mixes some singlet character into the triplet state. Therefore it is said that phosphorescence intensity is "stolen" from the allowed singlet-singlet transitions. When heavy substituents like bromine or iodine are present, spin-orbit coupling is relatively strong, which results in appreciable singlet-triplet mixing. This usually not only results in strong phosphorescence but also allows direct excitation from the ground state into the triplet manifold. In fact, this method of direct triplet excitation has been used for most of the experiments presented in this thesis.

1.3 Molecular triplet excitons in quasi-linear systems

In the case that no intermolecular interactions would exist in molecular crystals, an excitation would remain on the molecule that was originally excited. Such situations may be found in very dilute mixed crystals of an aromatic molecule in an inert molecular host crystal. In real neat crystals, though, intermolecular interactions are important and as a result the excitation in principle will no longer be localized on a single molecule but it can be thought to be transferred from molecule to molecule. In fact the molecules in the crystal can be considered to be

excited collectively and such a collective excitation is called an "exciton". Depending on the spin angular momentum one can distinguish between singlet and triplet excitons. Frenkel in 1931 [Fr31] was the first to describe these molecular "tight binding" excitons, called "tight binding" because the excited electron and the remaining hole travel tightly bound through the crystal.

In an ideal crystal excitons are described with band theory. In such a model the exciton has a wave-like character and is delocalized over a large number of molecules. The number of states in the band equals the number of molecules over which the excitation is delocalized. In fact, these bands arise because the intermolecular interactions lift the degeneracy of the excited states of the individual molecules. The nature of these intermolecular interactions is very different for singlet and triplet excitons. For singlet excitons the dominant interaction is the interaction between the molecular transition dipole moments. For triplet-singlet transitions the transition dipole moments are approximately zero and triplet exciton transport occurs mainly through interactions, arising from intermolecular electron exchange (see Chapter II).

Since intermolecular interactions determine the character of the exciton transport, it is obvious that the crystal structure is a very important key to understand the transfer topology. Two very well known systems that have a special crystal structure are 1,4-dibromonaphthalene (DBN) and 1,2,4,5-tetrachlorobenzene (TCB) (Fig. I.1). In these crystals the molecules are stacked in such a way that the aromatic rings are parallel to each other. Consequently, there is a large overlap between the π -orbitals and therefore a large interaction in the stack direction. The spatial distance between the different stacks is large and as a result the interactions between the stacks are extremely small. Altogether, the excitation transfer topology in these crystals is characterized as (quasi-)one-dimensional.

The lifetime of a triplet exciton is limited by several factors. First, the exciton can decay to the ground state, either via a radiative process (phosphorescence) or via a radiationless transition whereby the transition energy is converted into heat. Secondly, the exciton can get trapped at a molecule which has a lower triplet energy than the exciton energy. This is possible in a real crystal because there will always be physical

imperfections and chemical impurities. Molecules near such imperfections or impurities can be somewhat distorted and may have a lower triplet state than the exciton band (X traps). An impurity molecule itself can also act as a trap (Y trap). An exciton, when trapped, becomes a localized excitation at this trap molecule. Subsequently, this excited trap can decay to the ground state. When the trap energy is only slightly lower than that of the host, thermal "detrapping" may occur so that the energy transfer may eventually proceed further, notwithstanding the fact that the exciton path was disrupted by a trap.

Another event that shortens the lifetime of a triplet exciton, can occur when two triplet excitons meet. Annihilation of the excitons may be the result of such an encounter. This process, responsible for delayed fluorescence, will be discussed later.

Ever since the application of band theory to the description of electronic excitations in molecular crystals, it was suggested that energy transport in such systems can be described in two limits: wave-like (coherent) or diffusive (incoherent). Coherent transfer occurs in principle, when the electronic excitation remains in the same delocalized crystal eigenstate (exciton) throughout the time of observation. A coherent state is characterized by a definite wave vector, which reflects the translational symmetry of the lattice. Incoherent transfer comes about from the "scattering" of the excitation into different eigenstates at times short compared to the experimental time scale. An exciton may be "scattered" by an impurity or defect that has either a higher or lower triplet energy than the host. Also, scattering may occur from the interaction with lattice vibrations (phonons). The motion of the exciton in this incoherent limit is usually referred to as "hopping" and it is expressible through classical rate equations and diffusion equations that describe the random walk motion. In this statistical hopping model it can be shown [Mo65] that the trapping efficiency in a linear system is much less than in a higher-dimensional system. Table I.1 gives the number of visited lattice sites for N jumps of the exciton. For a one-dimensional system the trapping efficiency appears to be three orders of magnitude smaller than for a higher-dimensional system. This has been assumed to be a reason that it is relatively easy to observe exciton phosphorescence emission in linear systems.

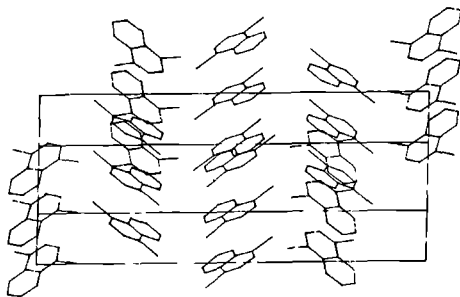


Fig. I.2.A
 The different stacks of molecules in the DBN crystal structure. Three molecules of each stack are shown.

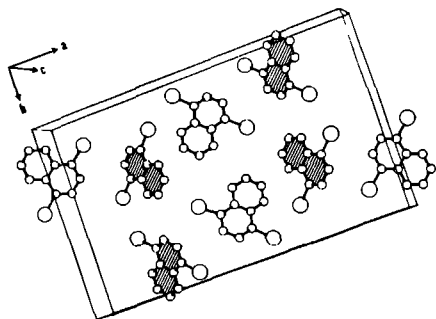


Fig. I.2.B
 The eight molecules in the DBN unit cell. The molecules of the lowest energy sublattice have been shaded.

Table I.1 *Number of visited sites for*

	N jumps	10^8 jumps
1-dim	$\frac{8}{\pi} \sqrt{N}$	$2.5 \cdot 10^4$
2-dim	$\frac{\pi N}{\log N}$	$4 \cdot 10^7$
3-dim	$0.6 N$	$6 \cdot 10^7$

The remainder of this thesis will be largely dedicated to experiments on the one-dimensional system 1,4-dibromonaphthalene (DBN). Fig. I.2A shows for DBN the different stacks, whereas fig. I.2B shows the eight molecules in the unit cell. The space group is $P_{21/a} (C_{2h}^5)$ and this implies that normally there are only four molecules in the unit cell. Consequently, the eight molecules form two independent sublattices, each of a set of four molecules. These two sublattices are not related via a symmetry operation of the space group. Table I.2 gives some crystallographic data on the DBN crystal structure [Tr61,Be78].

Table I.2 *DBN crystal structure data.*

Space group :	$P_{21/a} (C_{2h}^5)$
Z :	8
a(Å) :	27.230
b(Å) :	16.417
c(Å) :	4.048
$\beta(^{\circ}) = \angle (a,c)$:	91.95

In optical experiments the effect of the two sublattices I and II is to double all absorptions [Ca67], each sublattice appearing at its own specific absorption energy. For DBN it is known [Ca67] that the singlet exciton bands corresponding to the two sublattices differ by 85 cm^{-1} , the triplet exciton bands by 50 cm^{-1} (Fig. I.3). Confining ourselves to triplet state properties, at low temperatures only exciton emission from the lowest sublattice is observed due to the unfavourable Boltzmann-factor. At higher temperatures ($> 60 \text{ K}$ [Sc74]) also exciton emission from the second sublattice may be observed. In theory one would expect the absorption of each sublattice to be split into a "Davydov-doublet". The four molecules in each sub-set give rise to four states that can be labelled $A_g, B_g, A_u,$ and B_u according to symmetry. Since the electric dipole operator transforms as a u-irreducible representation, transitions of the type $g \leftrightarrow g$ and $u \leftrightarrow u$ are forbidden and one expects to observe the A_u and B_u state as separate absorptions. However, no splitting of this

type ("Davydov-splitting") has been observed for DBN to date and therefore it is concluded that the interchain interaction is extremely small ($< 0.05 \text{ cm}^{-1}$) in DBN. On the other hand, the intra-chain exchange interaction in DBN is relatively large ($J \approx -7.5 \text{ cm}^{-1}$) as compared to TCB ($J \approx 0.3 \text{ cm}^{-1}$). Since for a linear system this value is directly related to the triplet exciton bandwidth ($W = 4 J$, Chapter II) it follows that DBN is a case of large triplet exciton bandwidth ($\sim 30 \text{ cm}^{-1}$) in contrast to TCB ($\sim 1.2 \text{ cm}^{-1}$).

Triplet excitons, described within the band model, are characterized by a wave vector \bar{k} . Quantummechanical selection rules only permit optical accessibility of the band in the region of the $\bar{k} = 0$ state. In a linear system this $\bar{k} = 0$ state is either found at the top or at the bottom of the band, depending on the sign of the exchange interaction. This sign is negative for DBN [Ho72] and the $\bar{k} = 0$ state is at the bottom of the band. The sign is positive for TCB and consequently in that case the $\bar{k} = 0$ state is found at the top of the band.

In Fig. I.3 the important optical properties of DBN have been summarized in a Jablonski diagram.

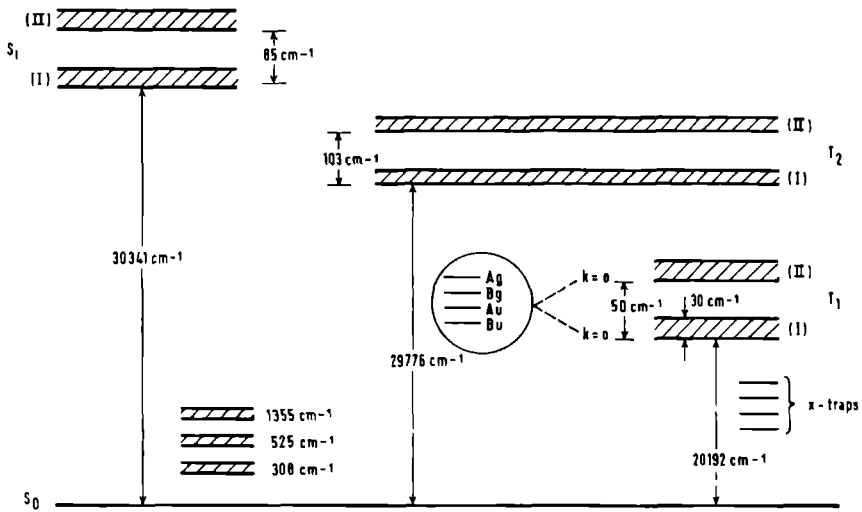


Fig. I.3 Optical properties of DBN. The data are taken from Castro and Hochstrasser [Ca67] (vacuo corrected for λ in air).

1.4.1 Motivation

Both DBN and TCB are key substances for studying the dynamical behaviour of triplet excitons in molecular crystals. A large number of papers has been published, which deal with these two compounds [Bu79]. The research on both systems has shown that for several reasons the TCB system is an easier model compound for the study of triplet excitons than DBN. First, in DBN for a so far unknown reason, no zero-field transitions between the triplet exciton sublevels can be observed in contrast to the TCB system. Such zero-field experiments make it possible to go beyond the $\bar{k} = 0$ selection rule and study the dynamical behaviour of $\bar{k} \neq 0$ excitons [St80]. Second, many different trap states can be detected in DBN single crystals in contrast to TCB, where only one trap state is observed. This fact plus the fact that in DBN we have to deal with an extra crystallographic sublattice make the trapping dynamics much more complicated for the DBN system than for TCB. Third, crystal specimens of DBN are very sensitive to the way of preparation, in contrast to TCB, as will be shown in this thesis.

Although the DBN system is very complex, there was a very clear first motivation why we chose the DBN system for our studies. As will be pointed out in Chapter VII, our first goal was to try and detect changes in trap phosphorescence emission intensity when the $|+1\rangle$ Zeeman component of a trap was made to cross the $|-1\rangle$ Zeeman component of the exciton in a large magnetic field. The DBN system was very suitable for this purpose since it exhibits exciton and trap phosphorescence emission at such an energy difference that magnetic fields of ~ 15 Tesla can bridge this difference. Furthermore, the DBN system was more suitable than the TCB system because the optical characteristics of the flexible light guide used in the magnetic field experiments, favour by far the transmission of DBN phosphorescence emission. However, these experiments (which were nevertheless also tried on TCB and benzophenone) were unsuccessful and although a magnetic field dependent increase of trap emission intensity was observed (Chapter VII), this could not be due to level anticrossing effects. The analysis of this observation led us into the complicated problem of the triplet exciton dynamics in DBN. Therefore we decided to make a close and careful examination of the lowest triplet state as

related to absorption, emission, delayed fluorescence, trapping dynamics and crystal quality. It appeared that the results of this study could not only explain the effects observed in a magnetic field but also provides a very detailed picture of triplet exciton dynamics in linear systems.

It will be shown in this thesis that for the study of triplet excitons real crystals of DBN cannot be treated as "infinitely" long linear chains. Rather, we propose that crystals of DBN should be considered as a collection of linear cages, which are confined by high energy scattering centers (Fig. I.4) [Wi78]. These cages appear to be strongly isolated from one another and therefore the excitons generated within different cages have different physical properties. When there is no trap present in or nearby a cage an exciton may be reflected several times at the cage ends before leaving the cage, either by hopping to a neighbouring stack or hopping to a neighbouring cage. In this way a *coherent* exciton with a relatively long lifetime may leave the cage via an *incoherent* hopping process. Because the cages behave as isolated units, the excitons generated in the different units can have very different lifetimes, each lifetime being determined by the specific conditions describing the particular cage. Emission from triplet excitons will only be observed when the conditions that determine the exciton lifetime, favour a long exciton lifetime. In practice this means, that a cage which encompasses such an exciton will have to be rather small in order not to contain a trap.

Also experiments will be discussed which suggest that some of these cages in DBN are formed because of a very small amount of the isomer 1,5-dibromonaphthalene. This isomer acts as a triplet barrier since it has a triplet energy 65 cm^{-1} higher than the corresponding DBN triplet state. On the other hand, this same contamination appears to be a very efficient energy leak for singlet excitons in DBN. When two triplet excitons in DBN collide, a singlet exciton can be formed which subsequently traps at 1,5-dibromonaphthalene molecules. The fluorescence emission of this contamination then can be used as the monitor for triplet-triplet annihilative processes that occur in DBN.

Further it is tried to introduce barriers by growing mixed crystals of DBN with perdeuterated DBN. The deuterated compound has a higher triplet energy than the parent molecule and therefore should function as a cage

former. Indeed a strong increase of exciton phosphorescence is observed, in these mixed crystals.

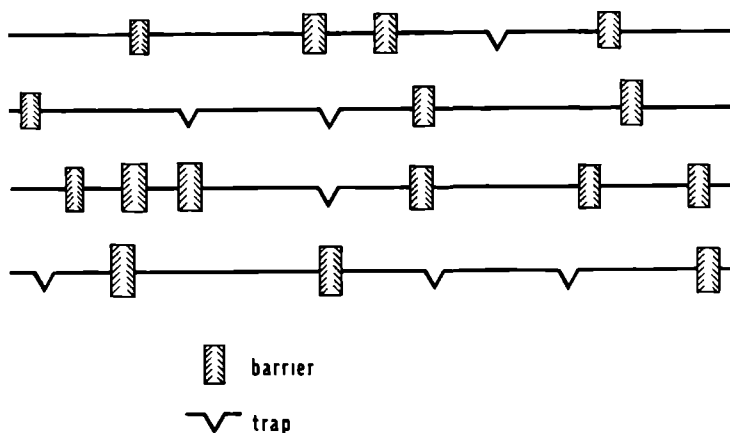


Fig. I.4 *Schematic representation of a collection of linear cages. Barriers have been indicated by a block and traps by a dip.*

1.4.2 Outline of presentation

In Chapter II some important theoretical aspects of triplet states in general and linear triplet excitons in particular will be given.

Chapter III is dedicated to experimental details and some typical experiments will be discussed.

Chapter IV describes the experiments on phosphorescence emission, delayed fluorescence and absorption.

Chapter V gives the results of time-resolved experiments using short laser pulses.

In Chapter VI we present additional proof, obtained from magnetic

resonance experiments, for the conclusions obtained in Chapters IV and V.

In Chapter VII it is described how a large magnetic field influences the dynamics of the DBN system.

In the last chapter, Chapter VIII, the effect of two compounds, 1,5-DBN and 1,8-DBN, present as a possible contamination in 1,4-DBN, and of physical imperfections will be discussed. The compound 1,8-DBN is proposed as a possible new system for studying excitons in molecular crystals.

1.5 References

- [Be78] J.C. Bellows, E.D. Stevens, P.N. Prasad, *Acta Cryst.* B34, 3256 (1978).
- [Bu79] D.M. Burland, A.H. Zewail, in *Adv. Chem. Phys.* XL, 369 (1979).
- [Ca67] G. Castro, R.M. Hochstrasser, *J. Chem. Phys.* 47, 2241 (1967).
- [Ev55] D.F. Evans, *Nature* 176, 777 (1955).
- [Fr31] J. Frenkel, *Phys. Rev.* 37, 1276 (1931).
- [Ho72] R.M. Hochstrasser, J.D. Whiteman, *J. Chem. Phys.* 56, 5945 (1972).
- [Hu58] C.A. Hutchison, B.W. Mangum, *J. Chem. Phys.* 29, 952 (1958).
- [Ja33] A. Jablonski, *Nature* 131, 839 (1933).
- [Le44] G.N. Lewis, M. Kasha, *J. Am. Chem. Soc.* 66, 2100 (1944).
- [Le45] G.N. Lewis, M. Kasha, *J. Am. Chem. Soc.* 67, 994 (1945).
- [Le49] G.N. Lewis, M. Calvin, M. Kasha, *J. Chem. Phys.* 17, 804 (1949).
- [Mo65] E.W. Montroll, *J. Math. Phys.* 6, 167 (1965).
- [Sc68] J. Schmidt, J.H. van der Waals, *Chem. Phys. Lett.* 2, 640 (1968).
- [Sc74] R. Schmidberger, H.C. Wolf, *Chem. Phys. Lett.* 25, 185 (1974).
- [St80] A.J. van Strien, J.F.C. van Kooten, J. Schmidt, *Chem. Phys. Lett.* 76, 7 (1980).
- [Te43] A.N. Terenin, *Acta Physicochim. URSS* 18, 210 (1943).
- [Tr61] J. Trotter, *Can. J. Chem.* 39, 1574 (1961).
- [Wi78] R.D. Wieting, M.D. Fayer, D.D. Dlott, *J. Chem. Phys.* 69, 1996 (1978).

THEORETICAL CONSIDERATIONS

II.1 Introduction

Triplet state theory has been extensively described in numerous books and papers. In this chapter we want to discuss the theoretical aspects that are relevant to the work described in this thesis.

In section II.2 general properties of molecular triplet states are summarized.

In section II.3 a short description is given of molecular excitons in general. In this section spin angular momentum is not included in the discussion.

In section II.4 special attention is paid to properties of linear chain triplet excitons.

In section II.5 a short discussion on triplet-triplet annihilation is given.

II.2 Molecular triplet states

II.2.1 Zero-field splitting

As mentioned in the first chapter a molecular triplet state arises from the fact that two electrons in the molecule, each possessing a spin angular momentum of $s = \frac{1}{2}$, align their spins parallel. Even in zero magnetic field the three triplet spin components are non-degenerate and the splitting is in most compounds dominated by the magnetic dipole-dipole interaction between the two electrons that make up the triplet state. The Hamiltonian, that describes this dipolar interaction is given by:

$$\mathcal{H}_{SS} = g^2 \beta^2 \sum_{i < j} \left[\frac{\bar{s}_i \cdot \bar{s}_j}{r_{ij}^3} - \frac{3(\bar{s}_i \cdot \bar{r}_{ij})(\bar{s}_j \cdot \bar{r}_{ij})}{r_{ij}^5} \right] \quad (\text{II.1})$$

where g is the electron g factor and β is the Bohr magneton. \bar{s}_i and \bar{s}_j represent the spin angular momentum operators of electrons i and j connected by the vector \bar{r}_{ij} .

Van Vleck in 1951 [V151] , replaced this microscopic Hamiltonian by a phenomenological Hamiltonian, in which only operators of the total spin angular momentum occur. Defining the total spin angular momentum operator as

$$\bar{S} = \sum_i s_i \quad (II.2)$$

one obtains the spin hamiltonian

$$\mathcal{H}_{SS} = \bar{S} \cdot \bar{D} \cdot \bar{S} \quad (II.3)$$

where \bar{D} is the zero-field splitting tensor. The elements of this tensor contain integrals of the operator (II.1) over the electronic wavefunction. In the principal axis system $\bar{x}, \bar{y}, \bar{z}$, \bar{D} is diagonal and \mathcal{H}_{SS} reduces to:

$$\mathcal{H}_{SS} = - [X S_x^2 + Y S_y^2 + Z S_z^2] \quad (II.4)$$

For molecules of C_{2v} symmetry or higher the principal axes of \bar{D} generally coincide with the molecular symmetry axes. The parameters X, Y and Z are the energies of the triplet sublevels in the absence of a magnetic field and their differences lie in the order of 1 - 10 GHz (0,03 - 0,3 cm^{-1}). Only two of the parameters are independent, because the zero-field splitting tensor is traceless ($X + Y + Z = 0$). Very often a different notation for \mathcal{H}_{SS} is used.

$$\mathcal{H}_{SS} = D(S_z^2 - \frac{1}{3} \bar{S}^2) + E(S_x^2 - S_y^2) \quad (II.5)$$

The relation between these zero-field splitting parameters D, E and X, Y, Z is given by:

$$D = \frac{1}{2}(X + Y) - Z = -\frac{3}{2}Z \quad (\text{II.6a})$$

$$E = -\frac{1}{2}(X - Y) \quad (\text{II.6b})$$

The symmetry and structure of the molecule in the triplet state have a strong influence on the D and E values observed. In fact, D is associated with the electron distribution along the z-axis, while E reflects the asymmetry around this axis.

The triplet eigenfunctions are linear combinations of the well-known eigenfunctions of the S_z operator $|+1\rangle$, $|0\rangle$, $|-1\rangle$, corresponding with the magnetic quantum numbers $m_s = +1, 0, -1$.

$$\begin{aligned} |x\rangle &= \frac{1}{\sqrt{2}}(|-1\rangle - |+1\rangle) = \frac{1}{\sqrt{2}}(|\beta\beta\rangle - |\alpha\alpha\rangle) \\ |y\rangle &= \frac{i}{\sqrt{2}}(|-1\rangle + |+1\rangle) = \frac{i}{\sqrt{2}}(|\beta\beta\rangle + |\alpha\alpha\rangle) \\ |z\rangle &= |0\rangle = \frac{1}{\sqrt{2}}(|\alpha\beta\rangle + |\beta\alpha\rangle) \end{aligned} \quad (\text{II.7})$$

A few important properties of these functions should be mentioned:

$$\begin{aligned} S_x|y\rangle &= -S_y|x\rangle = i|z\rangle \text{ et cycl.} \\ S^2|u\rangle &= 2|u\rangle \\ S_u|u\rangle &= 0 \end{aligned} \quad \left. \vphantom{\begin{aligned} S_x|y\rangle &= -S_y|x\rangle = i|z\rangle \text{ et cycl.} \\ S^2|u\rangle &= 2|u\rangle \\ S_u|u\rangle &= 0 \end{aligned}} \right\} \text{ for } u = x, y, z \quad (\text{II.8})$$

The lowest line in eq. (II.8) states that $|u\rangle$ is an eigenfunction of the operator S_u with eigenvalue 0. In other words, the triplet eigenfunctions correspond to situations, where the spin angular momentum vector lies in one of the coordinate planes $x = 0$, $y = 0$ or $z = 0$. It may be also concluded from eq. (II.8) that there is no net magnetic moment associated with any of the triplet substates in zero-field:

$$\langle u|S_v|u\rangle = 0 \quad u = x, y, z; v = x, y, z \quad (\text{II.9})$$

With the aid of eq. (II.8) we can show that magnetic dipole transitions are allowed between the triplet sublevels. In order to account for the interaction with a microwave field a time-dependent term must be added to the spin hamiltonian (II.4)

$$V(t) = g\beta\bar{S} \cdot \bar{B}_1 \cos\omega t \quad (\text{II.10})$$

where B_1 is the amplitude of the alternating magnetic field. According to time-dependent perturbation theory and using eq. (II.8), a time independent transition probability arises, proportional to:

$$| \langle z | \bar{S} \cdot \bar{B}_1 | y \rangle |^2 = B_{1x}^2 \quad (\text{II.11})$$

In this specific example we assumed that the microwave field is resonant with the $|z\rangle \leftrightarrow |y\rangle$ transition. The result shows that transitions between the triplet component in zero-field are linearly polarized, in this example along the x-axis.

II.2.2 Spin-orbit coupling (SOC)

Electric dipole transitions between states of different spin multiplicity are quantummechanically forbidden (selection rule $\Delta S = 0$). Radiative and non-radiative transitions between the triplet and singlet manifold are nevertheless found to occur. The reason is that the lowest triplet state is not a pure triplet state and the ground state is not a pure singlet. Mixing of states with a different spin multiplicity may occur through the spin-orbit interaction. This interaction gives matrix elements between singlet and triplet states and therefore allows electric dipole transitions between the triplet state and the singlet ground state (an extensive review on spin-orbit coupling in aromatic molecules is given by van der Waals and de Groot [Wa67]). The operator for spin-orbit coupling is approximated by:

$$\mathcal{H}_{SO} = \sum_j A_j \bar{S}_j \cdot \bar{L}_j \quad (\text{II.12})$$

where the summation is over all electrons. The coefficient A_j contains the electric field gradients at the nuclei and \bar{S}_j and \bar{L}_j are the operators for electron spin angular momentum and orbital angular momentum, respectively. Then, as a result of SOC, the wave function of the triplet spin component u ($= x, y, z$), and in a similar way the wavefunction of the ground state, must be written:

$${}^3\Psi_u = {}^3\Psi_u^0 + \sum_i \frac{\langle {}^1\Psi_i^0 | \mathcal{H}_{SO} | {}^3\Psi_u^0 \rangle}{E_i^0 - E_u^0} {}^1\Psi_i^0 \quad (\text{II.13})$$

where ${}^3\Psi_u^0$ is the pure triplet component without SOC, the ${}^1\Psi_i^0$ represent the perturbing singlet functions and E_i^0 and E_u^0 are the energies of the perturbing singlet states and the triplet substate, respectively. Only a small amount of singlet character is usually mixed into the triplet manifold, but it allows intersystem crossing (ISC) to occur and it is responsible for the non-zero electric dipole transition moment, $\langle {}^1\Psi_0 | e\vec{r} | {}^3\Psi_u \rangle$, between the triplet state and the singlet ground state. Therefore phosphorescence "steals" its intensity from allowed singlet-singlet and triplet-triplet transitions.

An important side-effect of SOC is the fact that mixing between singlets and triplets occurs in a very selective way. This selectivity arises from the fact that SOC gives only matrix elements between states of the same *total* symmetry. Consequently, the radiative decay rates characterizing the individual triplet sublevels, in a general case are very different. Moreover, since the intersystem crossing from the first excited singlet state to the first excited triplet state is in the same way governed by SOC, the individual populating rates of the triplet spin states can also be very different. In Optically Detected Magnetic Resonance (ODMR) and Microwave Induced Delayed Phosphorescence (MIDP) experiments (see Chapter VI) one takes advantage of the phenomenon that the radiative decay rates are different for the different triplet sublevels. In these experiments one changes the populations in the different sublevels by inducing magnetic dipole transitions between them. Then, as a result of the changed populations the intensity of the emitted phosphorescence will change.

II.2.3 The Zeeman interaction

The effect of an external magnetic field on the energies of the triplet sublevels is described by the Zeeman term, which is added to the Hamiltonian:

$$\mathcal{H} = \mathcal{H}_{SS} + g\beta\bar{B}_0 \cdot \bar{S} \quad (\text{II.14})$$

where \bar{B}_0 is the static external magnetic induction.

The energies of the spin components depend on both the direction and strength of the applied field. If we let l , m and n be the direction cosines of \bar{B}_0 with the spin axes x , y and z respectively, then the matrix of the Hamiltonian in the basis set $|x\rangle$, $|y\rangle$, $|z\rangle$ becomes

$$\begin{array}{l} |x\rangle \\ |y\rangle \\ |z\rangle \end{array} \begin{array}{ccc} |x\rangle & |y\rangle & |z\rangle \\ \left(\begin{array}{ccc} X & -ig\beta B_0 n & ig\beta B_0 m \\ ig\beta B_0 n & Y & -ig\beta B_0 l \\ -ig\beta B_0 m & ig\beta B_0 l & Z \end{array} \right) \end{array} \quad (\text{II.15})$$

One finds the triplet state energies for a given orientation of the magnetic field by solving the secular equation of (II.15). When the field is along the z -axis, for example ($l = m = 0$, $n = 1$) it is immediately clear that $|z\rangle$ remains an eigenfunction of the system, but $|x\rangle$ and $|y\rangle$ are mixed through the off-diagonal elements $\pm ig\beta B_0$. The roots of the secular equation then yield the eigenvalues

$$E_1 = Z, \quad E_{2,3} = \frac{X+Y}{2} \pm \sqrt{\left(\frac{X-Y}{2}\right)^2 + (g\beta B_0)^2} \quad (\text{II.16})$$

The corresponding wavefunctions are readily found to be

$$|+\rangle = -\frac{1}{2} \sqrt{2} (\eta_z^+ |x\rangle + i \eta_z^- |y\rangle)$$

$$|0\rangle = |z\rangle \tag{II.17}$$

$$|-\rangle = \frac{1}{2} \sqrt{2} (\eta_z^- |x\rangle - i \eta_z^+ |y\rangle)$$

with

$$\eta_z^\pm = \sqrt{1 \pm (X - Y)/\alpha_z}$$

$$\alpha_z = 2 \sqrt{\left(\frac{X - Y}{2}\right)^2 + (g\beta B_0)^2} \tag{II.18}$$

In zero magnetic field the states $|+\rangle$, $|0\rangle$ and $|-\rangle$ are equal to $|x\rangle$, $|z\rangle$ and $|y\rangle$, respectively. On the other hand, in an infinitely high field $\parallel z$ we see comparing eq. (II.17) with eq. (II.7) that $|+\rangle$ and $|-\rangle$ approach $|+1\rangle$ and $|-1\rangle$. Physically this means that in a very large magnetic field the electron spin is completely quantized along this field and the magnetic quantum number m becomes a constant of motion.

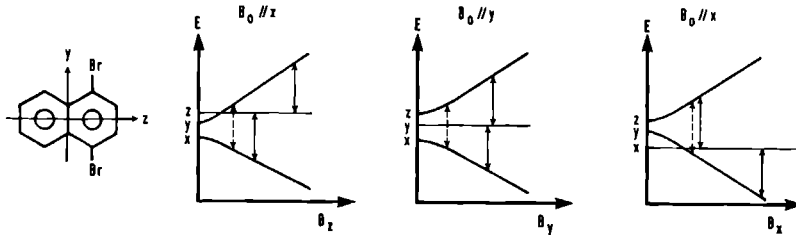


Fig. II.1 Triplet energy levels of 1,4-dibromonaphthalene in a magnetic field. The " $\Delta m = \pm 1$ " transitions are indicated by solid arrows and the " $\Delta m = \pm 2$ " transitions by broken arrows.

Fig. II.1 shows the energy levels of localized states in 1,4-dibromonaphthalene when the magnetic field is applied parallel to x, y and z. The allowed ($\Delta m = \pm 1$) and forbidden ($\Delta m = \pm 2$) ESR transitions have been indicated by means of arrows.

When the magnetic fields that are used are not very large, the level separations resulting from the Zeeman interaction and the zero-field splitting are comparable in the magnitude. The levels can no longer be described by the quantum number m. Transitions may now occur among the three levels wherever they are energetically possible. Nevertheless, it is often useful to retain the high field terminology throughout the range of magnetic fields and to describe the transitions as corresponding to $\Delta m = \pm 1$ or $\Delta m = \pm 2$.

II.3 Excitons in molecular crystals

In the previous section we have described some properties of isolated molecular triplet states. In a pure crystal, though, intermolecular interactions are present and because of these intermolecular interactions the crystal may be excited as a whole. Such collective excitations are called "excitons" and were first described by Frenkel [Fr31]. In the outline, presented here, we follow the work of Davydov [Da62]. Spin angular momentum will not be included in this section, but special properties of linear chain triplet excitons will be discussed in the next section.

Let us consider a large crystal that consists of N identical molecules and the length of the crystal edges is given by $N_i a_i$ ($i = 1, 2, 3$). For simplicity we assume that the unit cell, formed by the basis vectors $\bar{a}_1, \bar{a}_2, \bar{a}_3$, contains only one molecule per unit cell. The position of a molecule in this crystal is given by the vector:

$$\bar{n} = \sum_{i=1}^3 n_i \bar{a}_i \quad (\text{II.19})$$

where n_i are integers. Then, neglecting the presence of phonons, the wavefunctions ϕ and energy levels E of the stationary states of the whole crystal are given by the Schrödinger equation

$$\left(\sum_{\bar{n}} \mathcal{H}_{\bar{n}} + \frac{1}{2} \sum'_{\bar{n}, \bar{m}} V_{\bar{n}\bar{m}} \right) \phi = E \phi \quad (\text{II.20})$$

where $\mathcal{H}_{\bar{n}}$ is the hamiltonian for a molecule at site \bar{n} and $V_{\bar{n}\bar{m}}$ is the interaction operator between the molecules \bar{n} and \bar{m} . The prime in the second summation indicates that the term where $\bar{n} = \bar{m}$ should be omitted. Since the wavefunctions $\varphi_{\bar{n}}^0$ that describe the ground state of the isolated molecules, are known we can write now the wavefunction describing the ground state of the entire crystal in first order by antisymmetrizing the products of $\varphi_{\bar{n}}^0$ with respect to all electrons.

$$\phi_0 = A \Psi_0 \quad (\text{II.21})$$

where

$$\Psi_0 = \prod_{\bar{n}} \varphi_{\bar{n}}^0 \quad (\text{II.22})$$

and A represents the antisymmetrizing operator.

Consider now the situation that one molecule (i.e. molecule \bar{n}) is being excited to state f. When it is first assumed that $V_{\bar{n}\bar{n}} = 0$, an excited state of the crystal can be described by

$$\chi_{\bar{n}}^f = A \Psi_{\bar{n}}^f \quad (\text{II.23})$$

where

$$\Psi_{\bar{n}}^f = \varphi_{\bar{n}}^f \prod_{\bar{m} \neq \bar{n}} \varphi_{\bar{m}}^0 \quad (\text{II.24})$$

Those crystal states (II.23) that differ only in their index \bar{n} (the place of excitation) obviously belong to the same energy of the crystal. Therefore, these states are N-fold degenerate in a first order approximation. It is customary now to make use of the translational symmetry of the crystal and to introduce N new orthonormalized functions

$$\phi^f(\bar{k}) = N^{-\frac{1}{2}} \sum_{\bar{n}} \chi_{\bar{n}}^f e^{i\bar{k} \cdot \bar{n}} \quad (\text{II.25})$$

These so-called Bloch functions depend on the wavevector \bar{k} , which is defined by:

$$\bar{k} = \sum_{i=1}^3 \frac{2\pi}{N_i} \bar{b}_i \nu_i \quad (\text{II.26})$$

The vectors \bar{b}_i are the basis vectors of the reciprocal lattice and are related to the basis vectors of the direct lattice \bar{a}_i by $\bar{b}_i \cdot \bar{a}_j = \delta_{ij}$. The ν_i are integers, satisfying the inequality:

$$-\frac{N_i}{2} < \nu_i < \frac{N_i}{2} \quad i = 1, 2, 3 \quad (\text{II.27})$$

The set of all \bar{k} vectors is often referred to as the first Brillouin zone.

When now $V_{\bar{n}\bar{m}} \neq 0$, the excitation will no longer be localized on the molecule \bar{n} , but due to the intermolecular interaction it can be considered to be transferred from one molecule to another. The N -fold degeneracy of the different \bar{k} -states will now be removed under influence of the interaction $V_{\bar{n}\bar{m}}$. Since in molecular crystals $V_{\bar{n}\bar{m}}$ is small compared with intramolecular interactions, one may still use the function (II.21) in a first-order approximation to calculate the energy of the ground state of the crystal in the presence of $V_{\bar{n}\bar{m}}$. One can calculate the excitation energy by taking the energy difference between the ground state and the excited states (II.25)

$$E^f(\bar{k}) = \Delta\epsilon^f + D^f + L^f(\bar{k}) \quad (\text{II.28})$$

where $\Delta\epsilon^f$ is the excitation energy of a free molecule, D^f determines the difference in the interaction energy between the excited and normal molecule \bar{n} with all the remaining molecules. Thus the excitation energy (II.28) of a crystal differs from the excitation energy of a molecule by the two terms of D^f and $L^f(\bar{k})$. $L^f(\bar{k})$ is given by

$$L^f(\vec{k}) = \sum_{\vec{m}} M_{\vec{n}\vec{m}}^f e^{i\vec{k} \cdot (\vec{n} - \vec{m})} \quad (\text{II.29})$$

where $M_{\vec{n}\vec{m}}^f$ is the matrix element:

$$\begin{aligned} M_{\vec{n}\vec{m}}^f &= \langle \varphi_{\vec{n}}^o(2) \varphi_{\vec{m}}^f(1) | V_{\vec{n}\vec{m}} | \varphi_{\vec{m}}^o(1) \varphi_{\vec{n}}^f(2) \rangle \\ &- \sum_{\mu} \langle \varphi_{\vec{m}}^f(1) \varphi_{\vec{n}}^o(2) | V_{\vec{n}\vec{m}} | \varphi_{\vec{n}}^f(1) \varphi_{\vec{m}}^o(2) \rangle \end{aligned} \quad (\text{II.30})$$

The sum over μ covers all possible permutations of pairs of electrons between the molecules \vec{n} and \vec{m} . This matrix element $M_{\vec{n}\vec{m}}^f$ is responsible for the transfer of the excitation from molecule \vec{n} to \vec{m} . The first term is a Coulomb interaction, which is the dominant interaction for singlet "excitons". The second term describes the exchange interaction and is assumed to be the dominant term in triplet "exciton" transport.

In large crystals, adjacent values of \vec{k} correspond to energies, which differ only little from one another. So the N values of the excitation energy $E^f(\vec{k})$ form a quasi-continuous band of excited states. Each of these excited states, labelled \vec{k} , is a collectively excited state of the entire crystal. These elementary excitations ("excitons") are characterized by the quasi-momentum $\hbar\vec{k}$ and energy $E^f(\vec{k})$.

If we want to determine the selection rule for optical transitions between the ground state Φ_0 and an excited state $\Phi^f(\vec{k})$ we must calculate the matrix element:

$$\langle f | e\vec{r} | 0 \rangle = \langle \Phi^f(\vec{k}) | e\vec{r} | \Phi_0 \rangle \quad (\text{II.31})$$

Assuming that the wavevector \vec{Q} of light may be disregarded ($\vec{Q} \approx 0$), we find:

$$\langle f | e\vec{r} | 0 \rangle = N^{-\frac{1}{2}} \sum_{\vec{n}} e^{i\vec{k} \cdot \vec{n}} \langle \varphi_{\vec{n}}^f | e\vec{r} | \varphi_{\vec{n}}^o \rangle \quad (\text{II.32})$$

The integrals in (II.32) do not depend on \vec{n} . Therefore the transition moment will differ from zero only when

$$\bar{k} = 0 \quad (\text{II.33})$$

This means that optical transitions may occur only to or from the $\bar{k} = 0$ region of an exciton band. If \bar{Q} is not neglected then (II.33) changes to

$$\bar{k} = \bar{Q} \quad (\text{II.33a})$$

II.4 Linear chain triplet excitons

An important difference between singlet and triplet excitons resides in the matrix element for excitation transfer, M_{nm}^f (equation II.30). It involves the intersite interaction operator V_{nm} and contains both Coulomb interaction and the intermolecular exchange interaction, which depends on the overlap of the wavefunctions for adjacent molecules. It can be shown via a multipole expansion of the operator V_{nm} that in first order the Coulomb part of M_{nm}^f is proportional to the product of the spectroscopic transitions dipole moments for the two molecules involved [Cr68]

$$\text{Coul} \propto \langle \varphi_m^o(1) | e\bar{r} | \varphi_m^f(1) \rangle \langle \varphi_n^o(2) | e\bar{r} | \varphi_n^f(2) \rangle \quad (\text{II.34})$$

Since the operator in the matrix elements involved, does not act on spin coordinates it is obvious, that this term gives a zero bandwidth for triplet excitons. Inclusion of a spin-orbit coupling term gives a non-zero bandwidth but this effect is assumed to be small. The exchange terms in equation II.30 are thought to be the most important factor in determining the bandwidth for triplets. Due to the fact that the pure Coulomb dipole-dipole contribution is large for singlet excitons, these excitons usually have a large bandwidth of several hundreds cm^{-1} . For triplet excitons bandwidths no greater than 1 - 50 cm^{-1} are found in aromatic hydrocarbons.

In single crystals of DBN two sublattices can be distinguished, each of a set of four molecules labelled 1, 2, 3 and 4. Due to the fact that we have now four molecules in the unit cell instead of one, the exciton band will be split into four exciton bands, which can be labelled A_g , B_g , A_u and B_u according to the irreducible representations of the unit cell

group C_{2h} . Furthermore, for the triplet exciton bands there is an additional splitting of each of these four bands into three because of the zero-field splitting. Therefore in total we have $4 \times 3 = 12$ triplet exciton bands. The crystal wavefunctions for both sublattices (omitting the spin for now) are given by:

$$\begin{aligned}
 \phi_{A_g}^f &= \frac{1}{2} [\phi_1^f + \phi_2^f + \phi_3^f + \phi_4^f] \\
 \phi_{B_g}^f &= \frac{1}{2} [\phi_1^f - \phi_2^f - \phi_3^f + \phi_4^f] \\
 \phi_{A_u}^f &= \frac{1}{2} [\phi_1^f + \phi_2^f - \phi_3^f - \phi_4^f] \\
 \phi_{B_u}^f &= \frac{1}{2} [\phi_1^f - \phi_2^f + \phi_3^f - \phi_4^f]
 \end{aligned}
 \tag{II.35}$$

For molecules at a general position \bar{x} , \bar{y} , \bar{z} in such a cell the exciton band structure is given by [Er77]

$$\begin{aligned}
 E(\bar{k}) &= 2A_1 \cos \bar{k} \cdot \bar{a}_1 + 2A_2 \cos \bar{k} \cdot \bar{a}_2 + 2A_3 \cos \bar{k} \cdot \bar{a}_3 \\
 \begin{pmatrix} + \\ - \\ + \end{pmatrix} & 2D_{12} \cos \bar{k} \left(\frac{\bar{a}_1}{2} - 2\bar{x} - 2\bar{y} \right) \cos \bar{k} \cdot \frac{\bar{a}_2}{2} \\
 \begin{pmatrix} + \\ - \\ + \end{pmatrix} & 2D_{13} \cos \bar{k} \left(\frac{\bar{a}_2}{2} - 2\bar{y} \right) \cos \bar{k} \cdot \frac{\bar{a}_1}{2} \\
 \begin{pmatrix} + \\ - \\ - \end{pmatrix} & D_{14} \cos \bar{k} (2\bar{x} + 2\bar{y} + 2\bar{z})
 \end{aligned}
 \tag{II.36}$$

The indicated signs are related in the same order to the functions (II.35) above. The terms A_1 , A_2 and A_3 indicate the interaction between translationally equivalent neighbouring molecules in the \bar{a}_1 , \bar{a}_2 , \bar{a}_3 direction of the crystal, whereas \bar{x} , \bar{y} , \bar{z} are vectors of arbitrary magnitude parallel to the \bar{a}_1 , \bar{a}_2 , \bar{a}_3 axes, respectively. The terms D_{12} , D_{13} , and D_{14} correspond to the interactions between molecule 1 and molecules 2, 3, 4 of one sublattice.

Because of symmetry only the A_u and $B_u \bar{k} = 0$ states give transitions to the ground state. The so-called Davydov-splitting is then given by

$$\Delta E_{\text{Davydov}} = E_{A_u}(0) - E_{B_u}(0) = 4(D_{12} - D_{13}) \quad (\text{II.37})$$

Because of the special crystal structure of DBN (Fig. I.2) the exchange interaction in the c-direction is very much larger than the exchange interaction in other directions [Ho72]. Therefore we neglect A_1 and A_2 . Further, it was experimentally proved that the individual D's are all zero [Ho72]. Consequently, exciton transport topology in DBN is (quasi-) one-dimensional. In this case equation (II.36) reduces to

$$E(k) = 2J \cos k a_3 \quad (\text{II.38})$$

where $J \equiv A_3$ is the exchange integral between two neighbouring molecules in the c-direction (In the linear case we omit the vector signs). It is obvious now, that for the linear case the total bandwidth is equal to $4J$. When the band-model description of the linear exciton applies the group velocity for exciton wave-packets is defined as:

$$v_g(k) = \frac{1}{\hbar} \frac{\partial E(k)}{\partial k} = -\frac{1}{\hbar} 2J a_3 \sin k a_3 \quad (\text{II.39})$$

To these wave-packets the uncertainty relation applies

$$\Delta x \Delta k \approx 2\pi \quad (\text{II.40})$$

The larger the region over which the excitation is spread out the better the wavevector k is defined. However, when in a non-ideal crystal the translational symmetry is destroyed by lattice imperfections or lattice vibrations (phonons) the exciton motion may become "incoherent". It was already mentioned in the first chapter that scattering in k -space can be the result of exciton-phonon coupling or of an interaction of excitons with lattice defects. As a result of this scattering, the width of an exciton wave-packet in k -space increases when the scattering processes become more important. Then it follows from the uncertainty relation

(II.40) that the degree of delocalization decreases. When Δx becomes of the order of the lattice constant, exciton motion changes from a coherent process to a random walk. Usually the "hopping" model is applied to this incoherent exciton motion [Bu79]. In this model the average exciton velocity is given by

$$\bar{v}_{\text{incoh}} = \frac{1}{\hbar} J a_3 \quad (\text{II.41})$$

For excitons described in the band model a "density of states" function may be defined:

$$Z(k) = \left| \frac{1}{\partial E / \partial k} \right| = \left| \frac{1}{2J a_3 \sin k a_3} \right| \quad (\text{II.42})$$

in which "van Hove-singularities" are present at the band edges. Fig. II.2 gives a graphical display for $E(k)$, $|V_g(k)|$ and $Z(k)$ in the first Brillouin zone of a linear system.

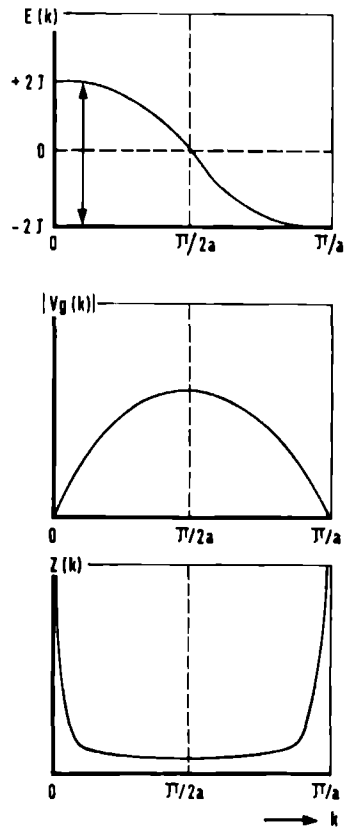


Fig. II.2 $E(k)$, $|V_g(k)|$ and $Z(k)$ in the first Brillouin zone.

In a magnetic field, in addition to the zero-field splitting which splits the triplet exciton band into three bands, also a Zeeman splitting will occur. When the strength of the magnetic field is large (>1 Tesla) the Zeeman term completely dominates the zero-field splitting term and the triplet exciton band will split into three separate bands according to $m_S = +1, 0, -1$. The optical properties of the three bands will be determined by the $k = 0$ states present in each sublevel band. In Fig. II.3 the Zeeman effect on a linear triplet exciton band is illustrated. The $k = 0$ state is indicated at the bottom of each band, according to the situation in DBN. Note that due to the large triplet exciton bandwidth in DBN ($\sim 30 \text{ cm}^{-1}$) the magnetic sublevel bands will be overlapping until a field of ~ 30 Tesla.

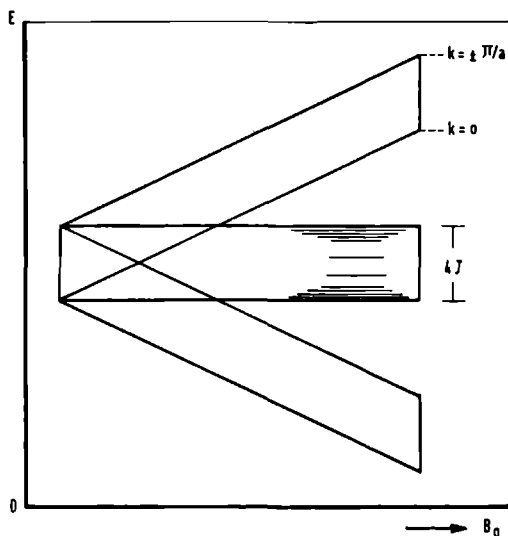


Fig. II.3
The Zeeman effect on a linear triplet exciton band.

II.5 Annihilation of triplet excitons

Triplet excitons usually live long enough to sample many molecular sites. When two triplet excitons meet, they may interact with one another. This interaction can lead to their annihilation, while a singlet exciton is formed. This is possible when the two triplets together have more excitation energy than the excitation energy of the singlet exciton. The singlet exciton eventually disappears, for instance, by emitting a photon. This phenomenon is called "delayed fluorescence".

It has been demonstrated by Johnson, Merrifield and Avakian [Jo67] that the intensity of the delayed fluorescence can be changed by applying a magnetic field. These magnetic field effects, which are due to a field dependent triplet-triplet annihilation rate, occur at rather low fields (0 - 1 Tesla) where the Zeeman interaction is of the same order of magnitude as the zero-field splitting.

In Chapter VII it is shown how much larger fields (0 - 14 Tesla) in DBN also change the triplet-triplet annihilation rate. Merrifield developed a theory for the phenomenon of triplet-triplet annihilation [Me71]. In this chapter we extend this theory to the case of very high magnetic fields in order to explain our experimental results of Chapter VII. In Merrifield's theory the annihilation process starts with the encounter of two triplets (assumed to be identical). The two triplets then form, for a short time, an intermediate complex and subsequently dissociate without change of the individual spin states or annihilate with change of spin states



where S_0 is a singlet ground state and S^* a singlet exciton. The overall bimolecular annihilation rate γ_S can be defined by



The singlet exciton can then decay to the ground state via the emission of (delayed) fluorescence. Of course, intersystem crossing to a triplet exciton is in principle also possible, but not very likely for DBN and therefore neglected. Also it is assumed here that the only outcome of an annihilation process is a singlet exciton. As we shall see (*vide infra*) two triplets may also combine to one triplet and a ground state or to a quintet state and a ground state. These possibilities will be neglected.

To see why γ_S is magnetic field dependent we consider the nine possible spin states of the intermediate complex (TT). The Hamiltonian of the complex can be represented by:

$$\begin{aligned}
\mathcal{H}_{\text{TT}} &= \mathcal{H}_e(1) + \mathcal{H}_{\text{SS}}(1) + \mathcal{H}_z(1) \\
&+ \mathcal{H}_e(2) + \mathcal{H}_{\text{SS}}(2) + \mathcal{H}_z(2) \\
&+ \mathcal{H}_{\text{int}}
\end{aligned} \tag{II.45}$$

$\mathcal{H}_e(1)$, $\mathcal{H}_e(2)$ are the electrostatic Hamiltonians for exciton 1 and 2; \mathcal{H}_{SS} and \mathcal{H}_z are likewise the zero-field spin-spin and Zeeman interaction terms. The intermolecular interaction term \mathcal{H}_{int} is made up of an electrostatic and a spin-spin dipolar interaction term. Following Merrifield we assume that \mathcal{H}_{int} is not zero but so small that there is no effect on the eigenfunctions of \mathcal{H}_{TT} . This approximation is valid as long as $|\tau\mathcal{H}_{\text{int}}| \ll 1$ where τ is the lifetime of the complex. The product wavefunctions $|m_S(1), m_S(2)\rangle$ or $|u(1), u(2)\rangle$ (in high magnetic field or zero magnetic field, respectively) then are eigenfunctions of \mathcal{H}_{TT} but not of $(\vec{S}_1 + \vec{S}_2)^2$ because

$$[(\mathcal{H}_{\text{SS}}(1) + \mathcal{H}_z(1) + \mathcal{H}_{\text{SS}}(2) + \mathcal{H}_z(2)), (S_1 + S_2)^2] \neq 0 \tag{II.46}$$

The above product wavefunctions, now denoted as $\psi_\lambda, \lambda = 1 - 9$, are therefore mixtures of pure singlet, triplet and quintet wavefunctions:

$$\psi_\lambda = C_S^\lambda |S\rangle + \sum_{i=1}^3 C_T^{\lambda,i} |T_i\rangle + \sum_{i=1}^5 C_Q^{\lambda,i} |Q_i\rangle \tag{II.47}$$

The pure singlet, triplet and quintet pair states are shown in Table II.1A. The functions ψ_λ are given in Table II.1B. From this table the coefficients C can be readily obtained.

In the high temperature limit, when kT is greater than the splitting between the components of the individual triplets, each of the nine states ψ_λ is formed with equal probability $\frac{1}{9} k_1 n^2$, where n is the concentration of triplet excitons. The result of the collision may be either scattering at a rate k_{-1} , or annihilation yielding a singlet exciton. The rate constant for the latter process for pair state ψ_λ is:

$$k_2 \{C_S^\lambda\}^2 \tag{II.48}$$

Table II.1

A) Pure singlet triplet and quintet pair states for homointeraction of two triplet states in zero magnetic field [Me71].

$$|S\rangle = \frac{1}{\sqrt{3}} (|xx\rangle + |yy\rangle + |zz\rangle)$$

$$|T_1\rangle = \frac{1}{\sqrt{2}} (|yz\rangle - |zy\rangle)$$

$$|T_2\rangle = \frac{1}{\sqrt{2}} (|zx\rangle - |xz\rangle)$$

$$|T_3\rangle = \frac{1}{\sqrt{2}} (|xy\rangle - |yx\rangle)$$

$$|Q_1\rangle = \frac{1}{\sqrt{2}} (|xx\rangle - |yy\rangle)$$

$$|Q_2\rangle = \frac{1}{\sqrt{6}} (|xx\rangle + |yy\rangle - 2|zz\rangle)$$

$$|Q_3\rangle = \frac{1}{\sqrt{2}} (|yz\rangle + |zy\rangle)$$

$$|Q_4\rangle = \frac{1}{\sqrt{2}} (|zx\rangle + |xz\rangle)$$

$$|Q_5\rangle = \frac{1}{\sqrt{2}} (|xy\rangle + |yx\rangle)$$

B) Singlet, triplet and quintet character of the pair states in zero magnetic field [Me71].

$$|xx\rangle = \frac{1}{\sqrt{3}}|S\rangle + \frac{1}{\sqrt{2}}|Q_1\rangle + \frac{1}{\sqrt{6}}|Q_2\rangle$$

$$|xy\rangle = \frac{1}{\sqrt{2}}|T_3\rangle + \frac{1}{\sqrt{2}}|Q_5\rangle$$

$$|xz\rangle = \frac{1}{\sqrt{2}}|Q_4\rangle - \frac{1}{\sqrt{2}}|T_2\rangle$$

$$|yx\rangle = \frac{1}{\sqrt{2}}|Q_5\rangle - \frac{1}{\sqrt{2}}|T_3\rangle$$

$$|yy\rangle = \frac{1}{\sqrt{3}}|S\rangle - \frac{1}{\sqrt{2}}|Q_1\rangle + \frac{1}{\sqrt{6}}|Q_2\rangle$$

$$|yz\rangle = \frac{1}{\sqrt{2}}|T_1\rangle + \frac{1}{\sqrt{2}}|Q_3\rangle$$

$$|zx\rangle = \frac{1}{\sqrt{2}}|T_2\rangle + \frac{1}{\sqrt{2}}|Q_4\rangle$$

$$|zy\rangle = \frac{1}{\sqrt{2}}|Q_3\rangle - \frac{1}{\sqrt{2}}|T_1\rangle$$

$$|zz\rangle = \frac{1}{\sqrt{3}}|S\rangle - \frac{1}{\sqrt{3}}\sqrt{6}|Q_2\rangle$$

where $C_S^\ell = \langle S | \psi_\ell \rangle$ represents the singlet amplitude in ψ_ℓ . Because $\sum \{C_S^\ell\}^2 = 1$ the total rate constant is k_2 . The annihilation constant γ_S can then be written as

$$\gamma_S = k_1 \sum_{\ell=1}^9 \frac{k_2 \{C_S^\ell\}^2}{k_{-1} + k_2 \{C_S^\ell\}^2} P_\ell \quad (\text{II.49})$$

where P_ℓ is the relative population of ψ_ℓ after formation of the (TT) complex. In the high temperature limit $P_\ell = \frac{1}{9}$. γ_S depends on how many pair states have singlet character. As an extreme example consider the case where all nine pair states have an equal amount of singlet character, then $(C_S^\ell)^2 = \frac{1}{9}$ for all ℓ and

$$\gamma_S = P_\ell k_1 \left(\frac{k_2}{k_{-1} + \frac{1}{9}k_2} \right) \quad (\text{II.50})$$

In the other extreme, only one state, with all singlet character, $(C_S^\ell)^2 = 0$ for all ℓ except for ℓ' , then $(C_S^{\ell'})^2 = 1$, the delayed fluorescence intensity is smaller because

$$\gamma_S = P_{\ell'} k_1 \frac{k_2}{k_{-1} + k_2} \quad (\text{II.51})$$

In general one can say that the more pair states have singlet character, the larger γ_S .

In the absence of a magnetic field the spin functions $|x\rangle$, $|y\rangle$, $|z\rangle$ are the eigenfunctions of the individual spin Hamiltonians and the singlet pair state is

$$\frac{1}{\sqrt{3}} (|x(1)x(2)\rangle + |y(1)y(2)\rangle + |z(1)z(2)\rangle) \quad (\text{II.52})$$

At zero field only three ($|x(1)x(2)\rangle$, $|y(1)y(2)\rangle$, $|z(1)z(2)\rangle$) out of nine states have a singlet component (Table II.1). With the aid of Table II.1

it can easily be derived that

$$\gamma_S(B = 0) = \frac{1}{9} k_1 \frac{k_2}{k_{-1} + \frac{1}{3}k_2} \quad (\text{II.53})$$

When a magnetic field is turned on in an arbitrary direction, the Zeeman interaction starts to mix the zero-field states and more pair states acquire singlet character, thereby increasing γ_S and the delayed fluorescence intensity. At intermediate magnetic fields, where the Zeeman interaction is large compared to the zero-field splitting (Merrifield's high field limit, for DBN at fields $> \sim 1$ Tesla), the spins are quantized along the field. In the case of homoannihilation, where the two triplets are equivalent, the pair states $|+1, -1\rangle$ and $|-1, +1\rangle$ are degenerate. The inter-triplet interaction \mathcal{H}_{int} causes that the new eigenfunctions of \mathcal{H}_{TT} are

$$\frac{1}{\sqrt{2}} (|+1, -1\rangle \pm |-1, +1\rangle) \quad (\text{II.54})$$

Only the symmetric combination has singlet character, and the pair state $|00\rangle$. Therefore at intermediate field strengths the delayed fluorescence should be smaller than at zero-field (see Fig. II.4).

When the magnetic field strength increases further, the Zeeman splittings become so large that at the temperatures where we work, the high temperature approximation is no longer valid. This means that creating a pair state $|-1, -1\rangle$ has a much higher probability than say $|+1, +1\rangle$. In the expression for γ_S (II.49) the coefficients C_S^l have become constant but now the population factors P_l are going to change. In the limit of extreme high fields, where only $|-1, -1\rangle$ is populated, Table II.2 shows that γ_S has become zero and so the delayed fluorescence (Fig. II.4). At somewhat lower fields B the populations of the three components of a triplet are given by

$$\begin{aligned}
 | +1 \rangle &\rightarrow \frac{\alpha^2}{z} n \\
 | 0 \rangle &\rightarrow \frac{\alpha}{z} n \\
 | -1 \rangle &\rightarrow \frac{1}{z} n
 \end{aligned}
 \tag{II.55}$$

where n again is the number of triplets, $\alpha = \exp(-g\beta B/kT)$ and $z = 1 + \alpha + \alpha^2$. With the aid of Table II.2 one can then easily derive that

$$\gamma_S(B) = \frac{\alpha^2}{z^2} k_1 \left[\frac{\frac{1}{3}k_2}{k_{-1} + \frac{1}{3}k_2} + \frac{\frac{2}{3}k_2}{k_{-1} + \frac{2}{3}k_2} \right]
 \tag{II.56}$$

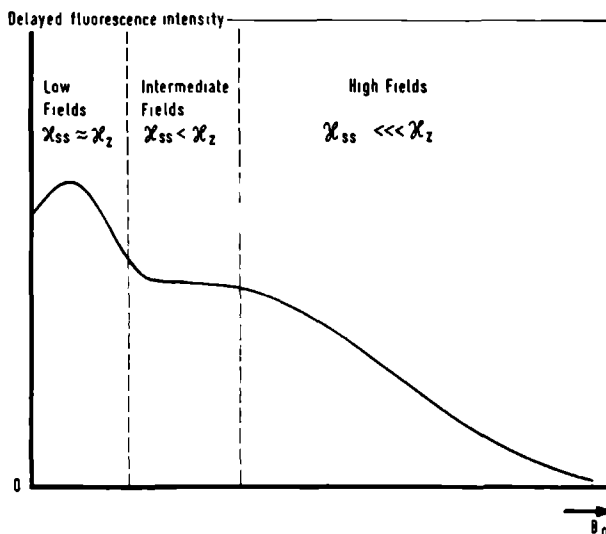


Fig. II.4 The behaviour of the delayed fluorescence in a magnetic field.

Table II.2

A) *Pure singlet, triplet and quintet pair states for homointeraction of two triplet states in high magnetic field [Me71,Wh71] .*

$$|S_0\rangle = \frac{1}{\sqrt{3}} (|-1,1\rangle + |1,-1\rangle - |0,0\rangle)$$

$$|T_1\rangle = \frac{1}{\sqrt{2}} (|0,1\rangle - |1,0\rangle)$$

$$|T_0\rangle = \frac{1}{\sqrt{2}} (|-1,1\rangle - |1,-1\rangle)$$

$$|T_{-1}\rangle = \frac{1}{\sqrt{2}} (|0,-1\rangle - |-1,0\rangle)$$

$$|Q_2\rangle = |1,1\rangle$$

$$|Q_1\rangle = \frac{1}{\sqrt{2}} (|0,1\rangle + |1,0\rangle)$$

$$|Q_0\rangle = \frac{1}{\sqrt{6}} (|-1,1\rangle + |1,-1\rangle + 2|0,0\rangle)$$

$$|Q_{-1}\rangle = \frac{1}{\sqrt{2}} (|0,-1\rangle + |-1,0\rangle)$$

$$|Q_{-2}\rangle = |-1,-1\rangle$$

B) *Singlet, triplet and quintet character of the pair states in high magnetic field [Me71,Wh71] .*

$$|1,1\rangle = |Q_2\rangle$$

$$|1,0\rangle = \frac{1}{\sqrt{2}} (|Q_1\rangle - |T_1\rangle)$$

$$|1,-1\rangle = \frac{1}{\sqrt{6}} |Q_0\rangle + \frac{1}{\sqrt{3}} |S_0\rangle - \frac{1}{\sqrt{2}} |T_0\rangle$$

$$|0,1\rangle = \frac{1}{\sqrt{2}} (|Q_1\rangle + |T_1\rangle)$$

$$|0,0\rangle = \frac{1}{3} \sqrt{6} |Q_0\rangle - \frac{1}{\sqrt{3}} |S_0\rangle$$

$$|0,-1\rangle = \frac{1}{\sqrt{2}} (|Q_{-1}\rangle + |T_{-1}\rangle)$$

$$|-1,1\rangle = \frac{1}{\sqrt{6}} |Q_0\rangle + \frac{1}{\sqrt{3}} |S_0\rangle + \frac{1}{\sqrt{2}} |T_0\rangle$$

$$|-1,0\rangle = \frac{1}{\sqrt{2}} (|Q_{-1}\rangle - |T_{-1}\rangle)$$

$$|-1,-1\rangle = |Q_{-2}\rangle$$

11.6 References

- [Bu79] D.M. Burland, A.H. Zewail, in Adv. Chem. Phys. XL, 369 (1979).
- [Cr68] D.P. Craig, S.H. Walmsley, "Excitons in molecular crystals",
W.A. Benjamin (1968).
- [Da62] A.S. Davydov, "Theory of molecular excitons", McGraw-Hill (1962).
- [Er77] V. Ern, Chem. Phys. 25, 307 (1977).
- [Fr31] J. Frenkel, Phys. Rev. 37, 1276 (1931).
- [Ho72] R.M. Hochstrasser, J.D. Whiteman, J. Chem. Phys. 56, 5945 (1972).
- [Jo67] R.C. Johnson, R.E. Merrifield, P. Avakian, R.B. Flippen, Phys.
Rev. Lett. 19, 285 (1967).
- [Me71] R.E. Merrifield, Pure and Appl. Chem. 27, 481 (1971).
- [V151] J.H. van Vleck, Rev. Mod. Phys. 23, 213 (1951).
- [Wa67] J.H. v.d. Waals, M.S. de Groot, in "The triplet state", p. 101,
edited by A.B. Zahlan, Cambridge University Press (1967).
- [Wh71] J.D. Whiteman, Ph.D. Thesis, University of Pennsylvania (1971).

EXPERIMENTAL CONDITIONS

III.1 Sample preparation

The undeuterated compound 1,4-dibromonaphthalene (DBN-h₆) was purchased from Eastman Kodak (Nr. 7595). An Al₂O₃ column with n-pentane as the eluent was used as a first step in the purification of the crude material. Subsequently, the material was vacuum sublimed and then zone-melted extensively (150 passes). The material in the central part of the zone-refining tube was isolated and zone-melted for another 75 passes. Depending on the crystal growing technique (*vide infra*) the resulting material was either directly used for crystal preparation or subjected to a subsequent refinement step, viz. zone-sublimation at 35°C (10 cycles). In this case the temperature was kept far below the melting point (83°C) to slow down possible decomposition.

The fully deuterated system (DBN-d₆) was obtained from Merck, Sharp and Dohme (Montreal). The compound was not purified any further, because of the very limited amount of material available. From mass spectral analysis it appeared that except from the d₆-isomer also a relatively large amount (~10%) of the d₅-isomer and a small amount (~1%) of the d₄-isomer are present.

The dibromonaphthalene isomers 1,5-DBN and 1,8-DBN were kindly synthesized for us in the Organic Chemistry Department of this University. The isomers were synthesized from the corresponding amine by diazotation and bromination (Sandmeyer reaction). 1,5-diaminonaphthalene and 1,8-diaminonaphthalene were obtained from Aldrich Europe. Due to the limited amount of 1,5-DBN and 1,8-DBN available, the compounds were only recrystallized (2×) and sublimed (3×).

The system 1,2,4,5-tetrachlorobenzene (TCB) was obtained from Aldrich Europe, vacuum sublimed (2×) and zone-melted extensively. A few single crystals of zone-refined TCB were kindly made available to us by Dr. A. van Strien, from the University of Leiden.

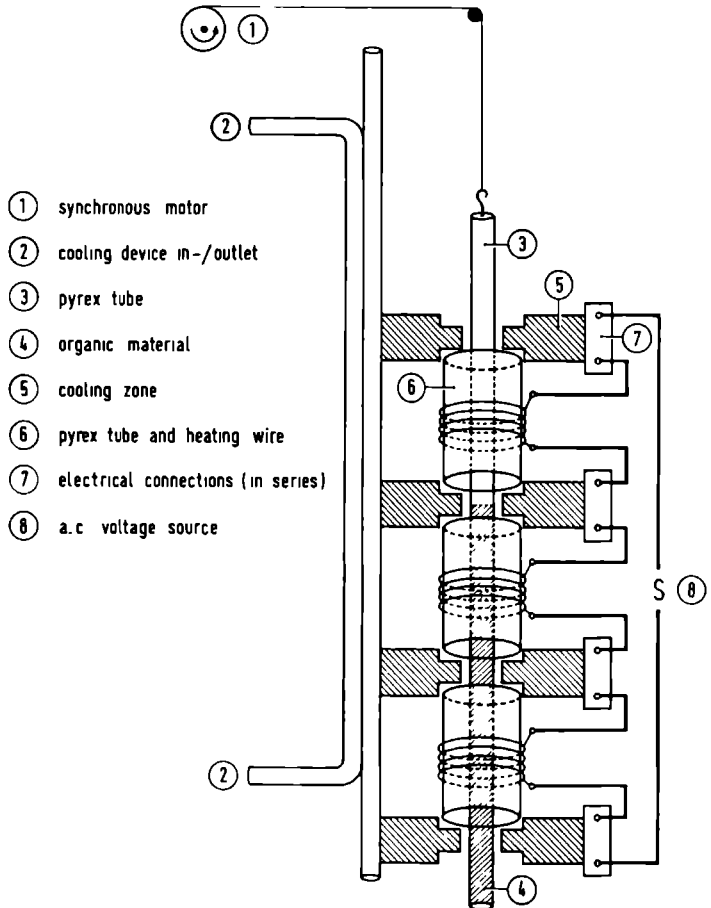
III.2 Zone-refining

III.2.1 Zone-melting

Zone-melting is a purification technique to obtain ultrapure materials [He63, PF66, Sc64]. The method is especially convenient for organic compounds because of their relatively low melting points. In the semi-conductor industry the method is used to obtain ultrapure silicon, notwithstanding the fact that this compound has a high melting point.

For this technique a long, narrow tube is filled with the solid material to be purified and then raised vertically through a narrow region ("zone") of high temperature (Fig. III.1). The temperature in this zone is higher than the melting point. When the tube is raised the molten zone moves through the tube.

Fig. III.1
Schematic diagram
of the zone-
melting equipment.



In principle this technique is based on the fact, that most impurities have a different solubility in the liquid and solid phase of the material to be purified. Consequently, the impurities present in the molten zone start to diffuse to both ends of the tube. When the tube has been moved a sufficient number of times through the hot zone, the impurities may be collected at both ends of the tube. After a sufficient number of passes the contents of the center part of the tube are used for growing crystals.

The final degree of purification depends on a number of factors like the type of impurity, length of the tube, the number of passes of the molten zone through the tube and the velocity with which the molten zone moves [He63]. For optimal results [He63] the length of the tube L should be at least 10 times the length of the zone z and the number of passes at least L/z . A schematic drawing of the zone-refiner is shown in Fig. III.1.

III.2.2 Zone-sublimation

Zone-sublimation is an analogous technique developed for organic materials with high vapour pressures at or just below the melting point. Zone-melting usually does not work satisfactory for these compounds. Furthermore many organic compounds decompose at or near their melting point.

To overcome the problem of decomposition one could in principle add a solvent to the material to be purified. One obtains a gel-like structure that can be used for the zone-melting procedure but a serious problem, which implicitly arises, is that of contamination of the pure material by solvent molecules.

Another technique, which may be used, is zone-sublimation. A schematic drawing of the zone-sublimation apparatus is given in Fig. III.2. The instrument is quite similar to the one described by Dugacheva [Du76]. The organic material is placed between two concentric tubes, the outer one made of pyrex with a length of 800 mm and an inner diameter of 13 mm, the inner one is a glass capillary with an outer diameter of 6 mm and an inner diameter of 1.7 mm. Around the outer tube a heater is placed and above it a cooler. The heater consists of thermocoax wire (Philips) and the cooler of two turns of thin copper tubing cooled by water. In the glass capillary an iron-constantan thermo-couple is placed that measures the temperature at the center of the heater.

- ① groundplate
- ② rods
- ③ pyrex glasstube
- ④ attachment for glasstube
- ⑤ evacuation outlet
- ⑥ synchronous motor
- ⑦ glider unit
- ⑧ cooling unit
- ⑨ heater unit
- ⑩ attachment for thermocouple
- ⑪ teflon plugs
- ⑫ glider cable, attached to motor

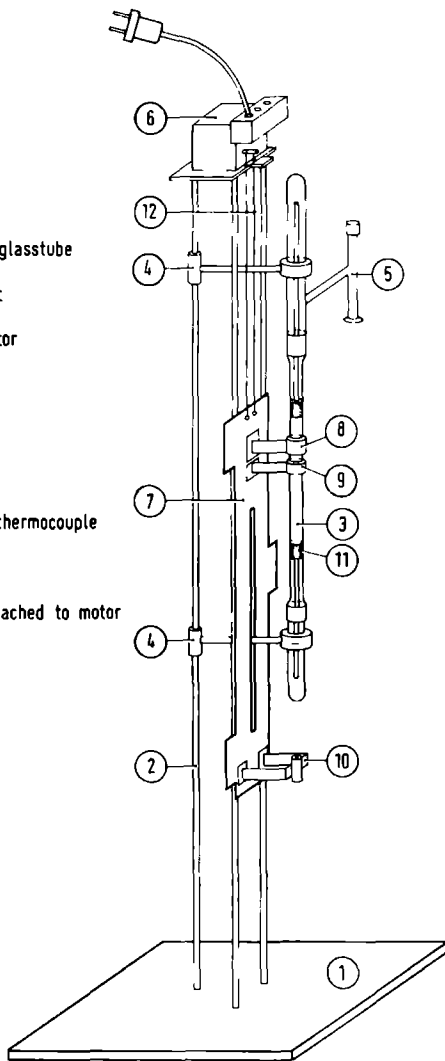


Fig. III.2
*Schematic diagram of
 the zone-sublimation
 apparatus.*

The heater, the cooler and the thermocouple move together and can be lowered at a constant rate (1 mm/hr) over the length of the evacuated tube filled with material. The material is enclosed between two, movable, teflon plugs. The heater temperature is adjusted so that the material can sublime without melting.

Before starting the zone sublimation procedure, the lower teflon plug is pressed against the material to be purified and the upper teflon piston

is moved up so that there is a gap between the plug and the material. Due to the heater, sublimation takes place and the material sublimates, first on the upper teflon plug and later, when the heater-cooler unit moves down, on the material already sublimated. When one pass has been made a gap is created between the material and the lower teflon piston so that for the next pass the lower piston has to be pressed against the material again and the upper teflon plug raised one zone-length. Again, after a sufficient number of passes, the center part of the tube is taken and used for crystal growing.

As the zone-melting technique uses the difference in solubility of an impurity in the liquid and solid phase of the main component, zone sublimation is based on the difference in sublimation rate of an impurity and the main component.

III.3 Crystal growing techniques

For the experiments described in this thesis single crystals have been used, which were grown via different methods. The first method is the Bridgman-Stockbarger technique [Br23]. Basically this technique is a variant of the zone-melting procedure.

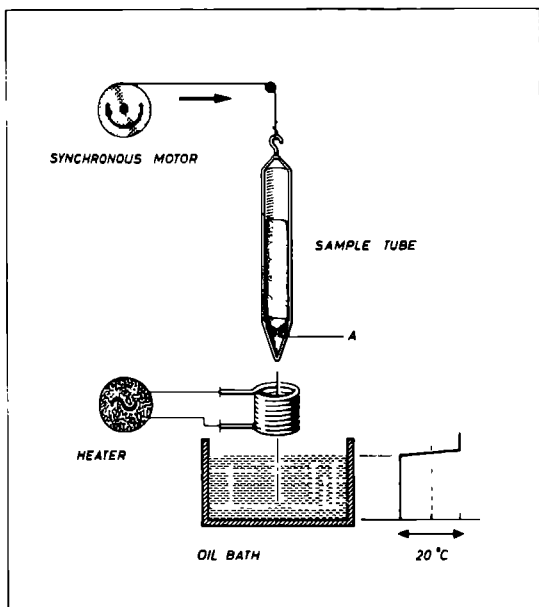


Fig. III.3
Crystal growth apparatus.
The diagram on the right represents the temperature gradient through which the sample tube is passed.

A sharp negative temperature gradient, centered at the melting point of the material, moves through the sample. The experimental set-up is schematically shown in Fig. III.3. The furnace was constructed by winding Nichrome wire inside a pyrex tube. A tapered cylindrical sample tube is lowered with a rate of 1 ~ 5 mm/hr into an oil bath, which is kept at temperatures, slightly below the melting point of the material.

The crystal growing tube contains two compartments as shown in Fig. III.3. The procedure for growing a crystal is as follows: first the tube is heated above the melting point, subsequently crystal growth is initiated in the lower compartment, by placing the point in the oil bath. Then as the temperature gradient moves up in this compartment, a number of crystalline regions with different growing directions will develop. When the temperature gradient reaches A, only one growing direction will occur in the upper compartment, giving in most cases a large single crystal of good quality. After the crystal was grown, it was sometimes annealed in a constant temperature environment (10°C below the melting point) for one or two days. Finally the crystals were examined under a polarizing microscope.

The second method that we used to obtain single crystals, was solution growing. Basically two variants were used. Crystals were obtained by either slow evaporation of the solvent (dichloromethane, ethanol, n-hexane) or by cooling down a supersaturated solution in a period of several weeks. This was done in co-operation with the Crystal Growing Group (Solid State Chemistry) of this University.

The third method was the vapour-growing technique. Small amounts of material that was first zone-melted and zone sublimed, were placed in vacuo in the zone sublimation equipment. By adjusting the temperature one can vary the growing time from several days to several weeks. Crystals are formed in this way on the upper teflon piston and on the pyrex wall.

III.4 The spectrometer

III.4.1 Zero magnetic field

The experiments to be described in the next chapters have been performed in the absence as well as in the presence of an external magnetic field. Fig. III.4 shows the experimental arrangement as was used

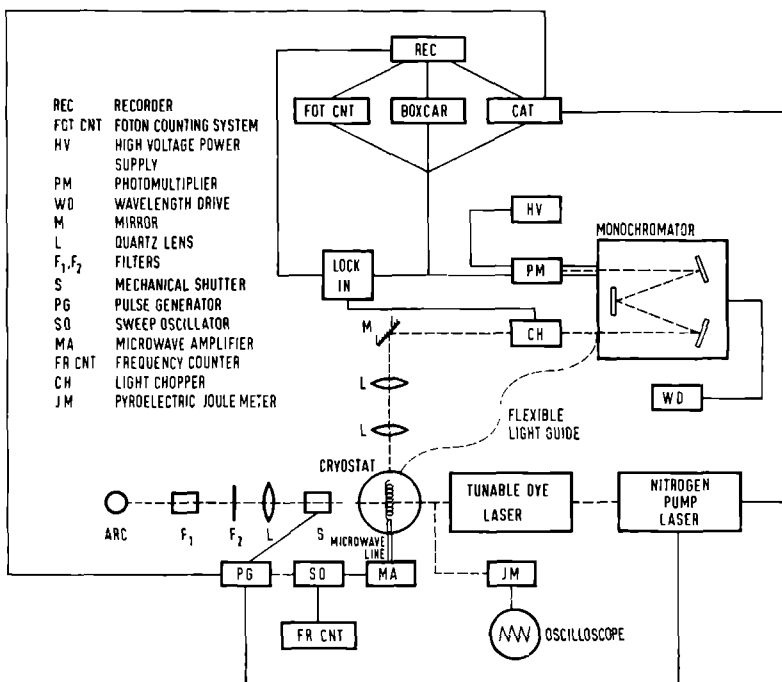


Fig. III.4 Schematic diagram of the zero-field spectrometer.

for the zero-field experiments. The sample is mounted inside a four-window Leybold-Heraeus stainless steel cryostat. Excitation can be performed by UV light from an Osram HBO 200 W/2 high pressure mercury arc in an Oriel lamp housing via an appropriate set of filters. The crystals may also be irradiated by means of a Molectron UV 12 nitrogen laser (337.1 nm, pulses of 10 ns) with or without a Molectron DL14P dye laser (linewidth 0.3 cm^{-1} , operating in 6th order). For the experiments on 1,4-dibromonaphthalene Coumarin 307 in ethanol was used as the dye (Fig. III.5). The output of the dye laser can be measured by a pyroelectric Molectron J3-05DW joulemeter. In the dye laser the dye is dissolved in an appropriate solvent (Table III.1) and contained in two quartz cuvetts. Each dye exhibits a relatively broad band of emission (Table III.1) and a grating present in the dye laser performs the wavelength selection for the laser beam.

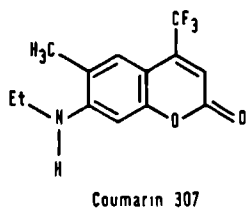


Fig. III.5

Table III.1 *Some commercially available dyes.*

Name	Solvent	Emission wavelength (nm)	Max. emission (nm)
PBD	Toluene	355 - 386	365,380
Stilbene 1	Ethyleneglycol	390 - 450	413
Coumarin 47	Ethanol	445 - 490	460
Coumarin 307	Ethanol	473 - 547	500
Rhodamine 6G	Ethanol	568 - 615	580
DCM	DMSO	615 - 705	666

After excitation, the resulting emission from the sample is detected at a right angle to the excitation by a 0.85 m Spex double monochromator 14018 (2400 grooves/mm holographic gratings, resolution in first order 0.4 cm^{-1}) and a Peltier cooled photomultiplier RCA C31034. For some experiments also a EMI 9524 B photomultiplier has been used. As indicated in Fig. III.4 the output of the photomultiplier can be guided to a recorder, to an Ortec Brookdael photon counting system 5C1, to a PAR Boxcar integrator, model 162 or to a Nicolet 1170 signal averager. Occasionally, an Ortec Brookdael phase-sensitive detector type 411 was used in combination with an Ortec Brookdeal light chopper, model 9479.

For optically detected magnetic resonance (ODMR) and microwave induced delayed phosphorescence (MIDP) experiments, the sample has to be irradiated with microwaves. In that case the sample is placed in a microwave helix, acting as a low Q, broadband, resonator connected to a variable frequency

microwave source. The microwave source consists of a Hewlett Packard (HP) sweep oscillator (HP 8620 C) plus various plug-ins for the frequency range 100 - 9000 MHz. The microwaves are amplified to 1 Watt by microwave power amplifiers for frequencies between 1000 and 6500 MHz. The frequency is measured by a HP frequency counter. A home-built pulse generator controls the Vincent Ass. Uniblitz model 3100 shutter, the microwave sweep and the recording device.

All experiments, presented in this thesis, have been carried out at liquid helium temperatures (1.2 - 4.2 K). The sample is therefore placed in liquid helium in an optical, stainless steel cryostat. It is assumed that the temperature of the sample is equal to that of the surrounding liquid. The temperature of the liquid helium can be lowered from 4.2 K to 1.2 K by pumping on the helium bath by means of a Leybold-Heraeus vacuum pump, model D30A. The liquid helium temperature is determined via measurement of the helium vapour pressure.

III.4.2 Magnetic field experiments

Only a limited number of experiments has been performed in a low magnetic field (0 - 10 kG). In this case an optical helium cryostat was used which fitted between the poles of a Varian 9-inch electromagnet. The magnetic field could be rotated around a vertical axis, the sample around a horizontal axis, so that every orientation of the magnetic field relative to the molecular axes could be reached. Most of the experiments in a magnetic field were performed in a Bitter-coil of the Nijmegen High Magnetic Field Laboratory. A Bitter magnet consists of a stack of copper discs with a radial slit of a few mm, separated by isolation discs. These isolation discs, made of mica, have a radial slit of a few cm and isolate the copper discs electrically from each other, except for the area where no isolating material is present. The stacking of the conducting and isolating discs is performed in such a way that the effective path of the current is a loop. The whole stack is tightly pressed between a top and bottom flange through a set of bolts. The cooling water is pumped through axial channels, which are formed by holes in both the isolation and copper discs. The number and spatial distribution of the holes has been calculated to balance heat generation and cooling capacity throughout the stack.

To generate high magnetic fields in a Bitter magnet huge currents (20 kA), which due to the dissipation in the copper discs lead to huge heat generation (6 MW) that has to be carried away by the cooling, are necessary. Therefore, the energising and cooling system are much larger than the magnet itself. Fig. III.6 shows the schematic outline of the experimental set-up in the Nijmegen High Magnetic Field Laboratory. The power supply consists of 2 units, each of 3 MW. Both can be operated together or separately and have a 100% overload capacity for one minute. The current through the magnet and consequently the magnetic field is controlled by an external voltage which can be supplied by either a set of voltage dividers or with an external voltage from a sweep generator. Specifications of the energy system and the magnet used are given in Table III.2.

Table III.2 *Specifications of the Bitter-magnet system.*

Power supply (one unit)

Primary voltage	10 kV (ac)
Secondary voltage	0 - 300 V (dc)
Secondary current	0 - 10 kA
Short term current stability	0,01% of setting
Speed of control	30 V/s
Current error for constant $\frac{dI}{dt}$	$< 0,1\%$ at $\frac{dI}{dt} < 110$ A/s i.e. $\frac{dB}{dt} < 0.15$ T/s

Magnet

Maximum field strength	15 T
Homogeneity	0,1% in 1 cm sphere
Height	54 cm
Diameter	65 cm
Number of copper discs	190
Bore	60 mm
Field factor	B = 0 0.727 T/kA B = 15 T 0.723 T/kA
Waterflow	250 m ³ /hr

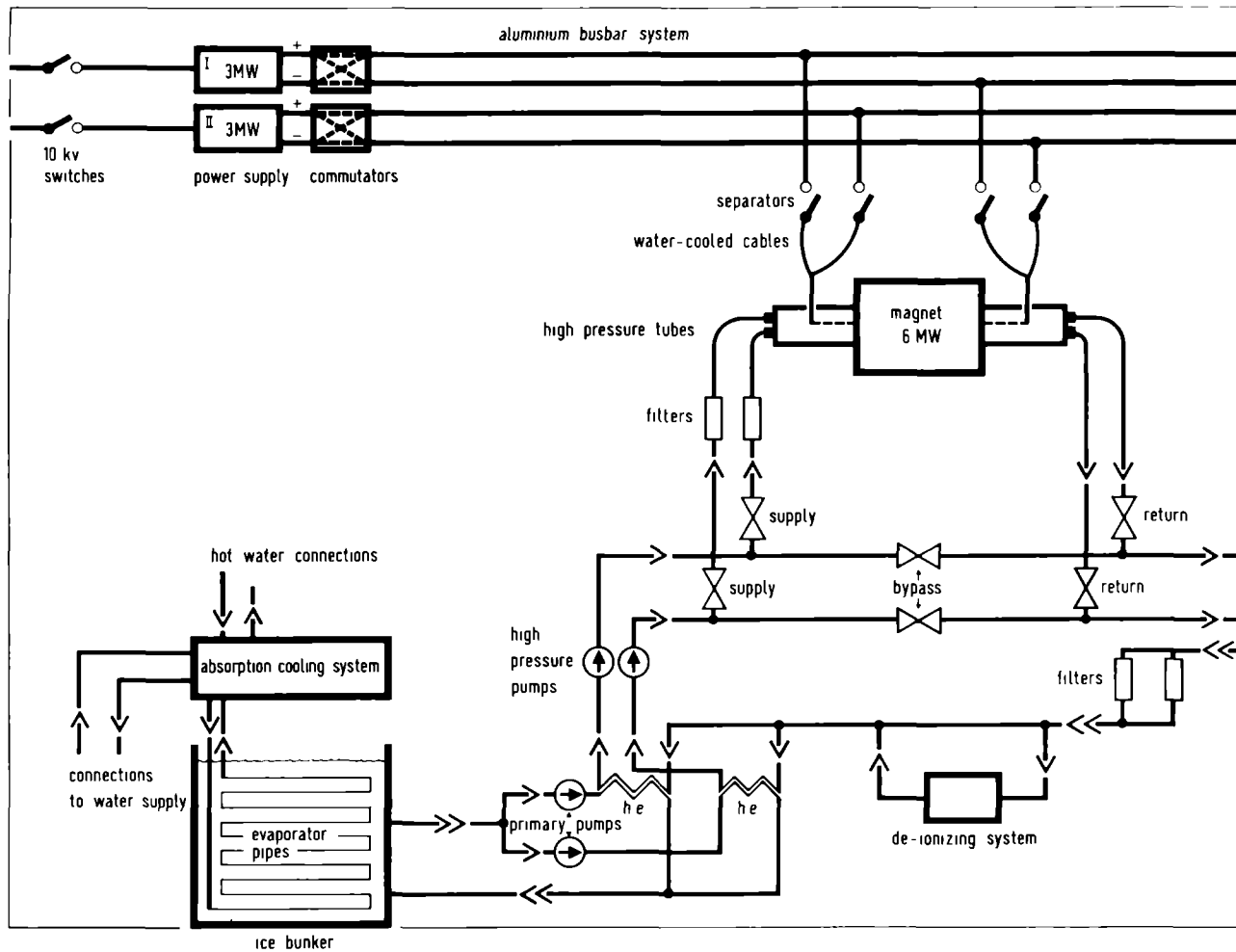


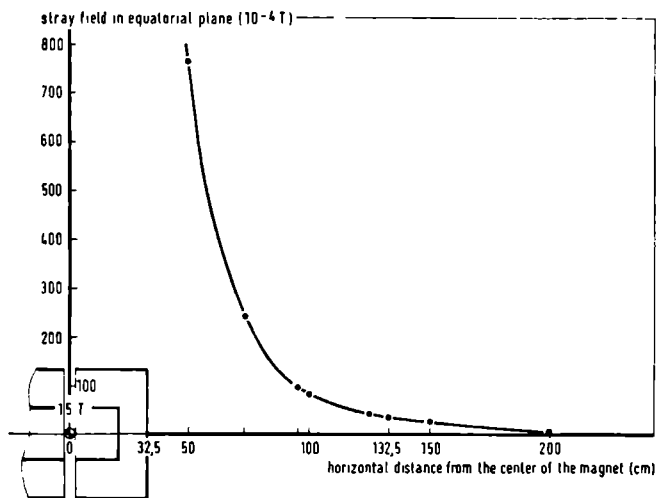
Fig. III.6 Schematic diagram of the experimental set-up in the Wijmegen High Magnetic Field Laboratory.

The cooling system consists of a primary circuit containing de-ionised water, which is pressed through the magnet with pumps, and a secondary circuit, which cools the water from the primary circuit in heat exchangers to the desired temperature. The water in this secondary circuit is in turn cooled by ice, which is created in an ice bunker through an absorption cooling machine. The capacity of this ice bunker is 150 tons of ice which allows three hours continuous operation at full power. The capacity of the absorption cooling machine implies that it takes 16 hours to make a new supply of 150 tons of ice.

For the experiments in the Bitter-magnet system a stainless steel optical cryostat was used with the tail adjusted to fit the 60 mm bore of the magnet. Excitation is performed from below the magnet system via lenses and a mirror mounted on an optical Micro Control bench. The bench is 3 m long to minimize the effects of the stray magnetic field on the excitation source. Fig. III.7 gives an impression of the strength of the stray magnetic field.

Fig. III.7

The stray magnetic field of the Bitter coil, measured in a horizontal plane.



The crystal is mounted inside the cryostat in a home-built mechanical 4π -rotator, especially fit for optical experiments (Fig. III.8). In this way every orientation of the crystal can be obtained with respect to the fixed magnetic field. Bridgman grown crystals of 1,4-DBN are very difficult to orient. Approximate orientation was performed by means of conoscopical techniques [Wa79]. Bridgman grown crystals appear to have the short crystallographic axis parallel to the growing direction.

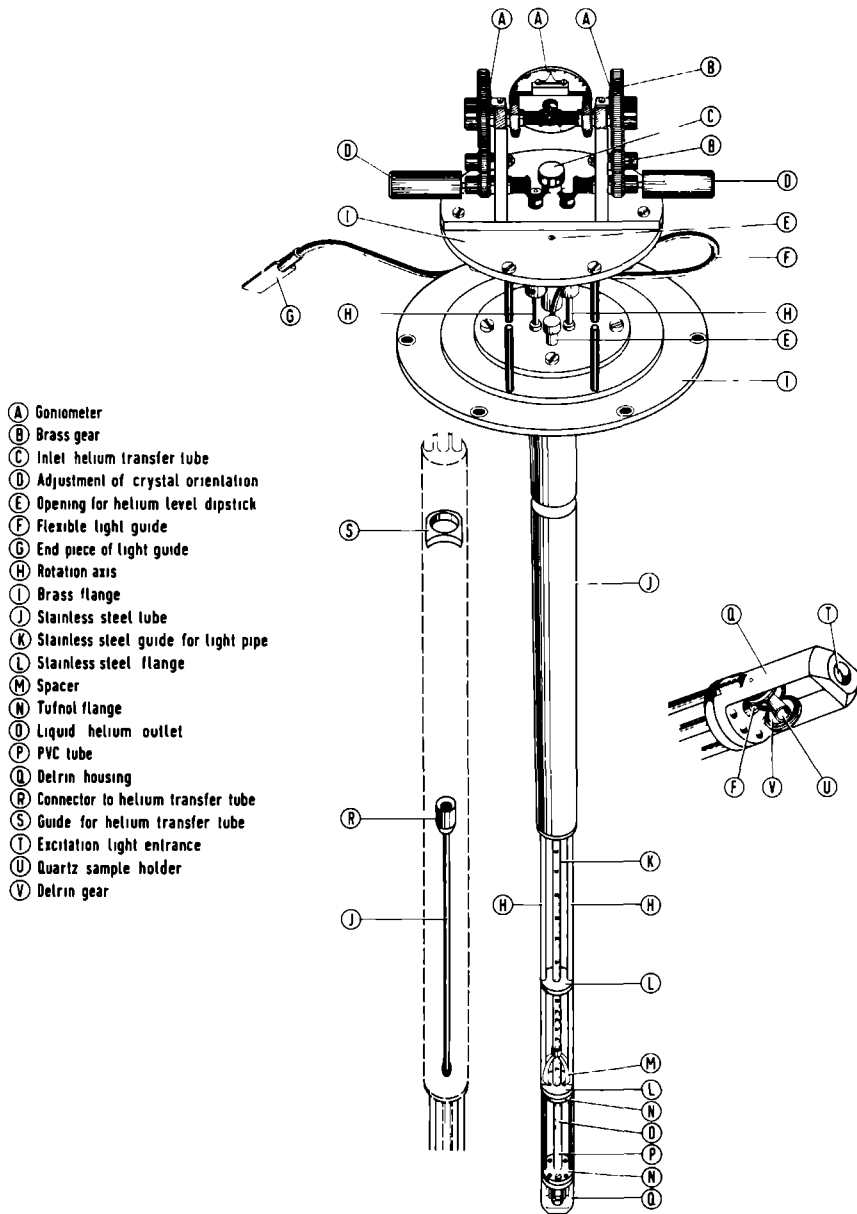


Fig. III.8 *The home-built mechanical 4π-rotator. The orientation of the crystal is changed by rotating the knobs D.*

The emission from the sample is guided through a Volpi flexible multi-wire glass light guide to the entrance-slit of the Spex double monochromator. At the entrance the wires are collimated in a rectangular shape of 10×0.3 mm so that the entrance slit is always completely illuminated. The light guide is 3 meters long to reduce the effect of the stray magnetic field on the photomultiplier, which in addition was covered by several layers of μ -metal foil. For residual effects of the magnetic field on the photomultiplier gain, corrections were made.

III.5 Typical experiments

III.5.1 Emission experiments

In emission experiments the sample can be irradiated by the mercury arc via appropriate filters or by the nitrogen laser (10 ns pulses at 337.1 nm) or by the nitrogen laser-dye laser combination (10 ns pulses at variable wavelength). The resulting emission is detected by the monochromator and photomultiplier. In case the mercury arc is used for excitation, the output of the photomultiplier can be fed directly to a recorder. For weak emissions the photon counting system or phase-sensitive detector and light chopper combinations give improved signal to noise ratio.

When the laser is the excitation source, the resulting emission is time-dependent and the photomultiplier output cannot be directly fed into the recorder. Then the Boxcar integrator can be used which yields an output voltage proportional to the emission intensity integrated from time t_1 to t_2 after the laser pulse (see Fig. III.9). t_1 and t_2 can be adjusted in accordance to the desire of the experimentalist. When the monochromator is swept slowly, the Boxcar integrator output varies according to the emission spectrum.

III.5.2 Time-resolved experiments

In time-resolved experiments the 10 ns pulses of the nitrogen laser or dye laser excite the sample. The photomultiplier output is then fed into a Nicolet signal averager (CAT). When the monochromator slits and wavelength are set for a specific emission, the time-dependence of this

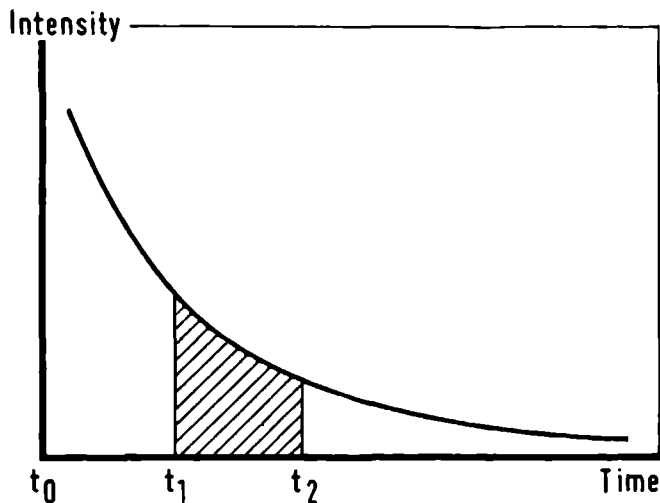


Fig. III.9 *The integration of a time-dependent signal by a Boxcar integrator. The output voltage is proportional to the shaded area.*

emission is digitized and stored in a maximum of 4096 data points with a maximum time resolution of $1 \mu\text{s}/\text{point}$. By repeating the experiment, the signal to noise ratio can be improved by averaging. In order not to damage the photomultiplier the wavelength of the monochromator should not coincide with the laser excitation wavelength.

III.5.3 Excitation spectroscopy

In these experiments one uses the pulsed nitrogen/dye-laser combination, the monochromator and the Boxcar integrator. Since it is an absorption experiment the wavelength of the laser beam is swept. The detection occurs via the *emission* at a different fixed wavelength, where the energy, that was absorbed, has been transferred to via molecular processes. Therefore the experiment differs from a normal absorption experiment in which the amount of absorbed radiation is measured directly

via the transmission through the sample. In an excitation experiment the *emission increase* at one wavelength corresponds to an *increase of absorption* at another wavelength. A direct correlation between the two frequencies is implicitly established by such an experiment.

III.6 References

- [Br23] P.W. Bridgman, Proc. Amer. Acad. Arts Sci. 58, 165 (1923).
- [Du76] G.M. Dugacheva, N.V. Avramenko, Russ. J. Phys. Chem. 50, 1350 (1976).
- [He63] E.F.G. Herington, "Zone melting of organic compounds", J. Wiley and Sons (1963).
- [Pf66] W.G. Pfann, "Zone melting", J. Wiley and Sons (1966).
- [Sc64] H. Schildknecht, "Zonenschmelzen", Verlag Chemie (1964).
- [Wa79] E.E. Wahlström, "Optical Crystallography", J. Wiley and Sons (1979).

OPTICAL PROPERTIES OF THE LOWEST TRIPLET STATE
OF 1,4-DIBROMONAPHTHALENE CRYSTALS

IV.1 Phosphorescence emission

By irradiation of single crystals of DBN individual molecules (traps) or arrays of molecules (excitons) can become excited. Phosphorescence emission is one of the ways the crystal can decay to the ground state. The phosphorescence emission spectrum may show many lines. First, a distinction can be made between exciton emission and trap emission. Many trap emission lines from traps with different trap depths may be present. Further, each excited state (exciton or trap) may give rise to several phosphorescence lines due to the presence of molecular or crystal vibrations. Transitions between the vibrationally lowest state of the excited triplet and the vibrationally excited ground state are denoted as o-n transitions, where n indicates the number of vibrational quanta; n = 0 corresponds to the purely electronic transition.

In the experiments of this paragraph the crystal is excited with the mercury arc set up (Chapter III). Fig. IV.1 shows the phosphorescence emission spectra of a melt-grown and a vapour grown single crystal of DBN. For both crystals the same starting material is used, except that for the vapour-grown crystal additional zone-sublimation was applied. It is immediately obvious from the spectra presented in Fig. IV.1 that phosphorescence emission in DBN is very sensitive to the way of crystal preparation.

The spectrum of the vapour grown crystal is almost temperature independent between 1.2 K and 4.2 K and only shows two deep traps at 20056.1 and 20006.1 cm^{-1} with their vibration bands (Fig. IV.1A). The difference in trap depth of 50 cm^{-1} suggests that the two traps are the same in nature but belong to the two crystallographically inequivalent sublattices. The intersublattice energy spacing for the lowest triplet state is known to be $\sim 50 \text{ cm}^{-1}$ (Fig. I.3). Dye laser experiments, though, cannot confirm this unambiguously, since the experiments show that excitation in the $k \approx 0$ state of either sublattice results in the population of both traps. More details

on the effects of different crystal growing techniques of DBN single crystals will be presented in Chapter VIII of this thesis.

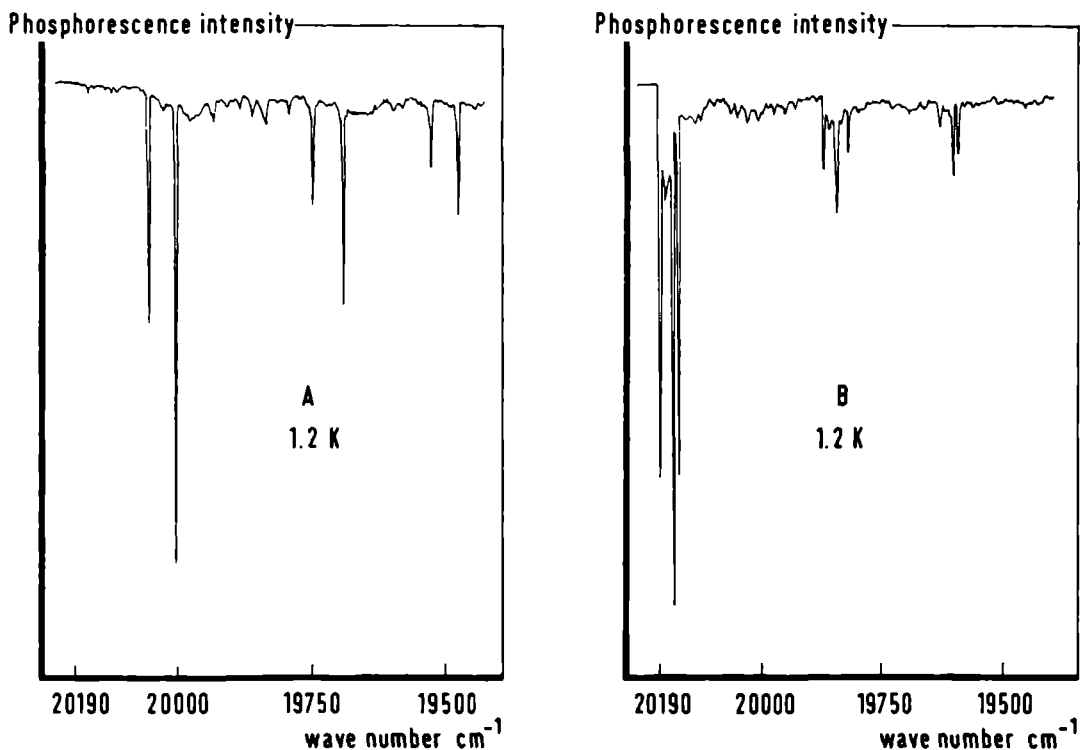


Fig. IV.1

- A) Phosphorescence emission spectrum of a vapour grown crystal of DBN at 1.2 K. Emission from shallow traps is extremely weak.
- B) Phosphorescence emission spectrum of a DBN crystal grown by means of the Bridgman technique. At 1.2 K only shallow trap emission is observed.

The spectrum of the melt-grown crystals (Bridgman technique) shows several emissions relatively close to the exciton origin (exciton 0-0 transition) and is strongly temperature dependent. At 4.2 K, besides a deep trap at 20029 cm^{-1} , two overlapping lines are found at 20193.2 cm^{-1} (EM1) and 20191.1 cm^{-1} (EM2) (Fig. IV.2A), very close to the value reported for the exciton 0-0 band (20192.4 cm^{-1} [Ho72]). By lowering the temperature, more emissions show up. At 3.5 K a strong emission line is found at 20157.4 cm^{-1}

(EM4), at 3.0 K another line becomes apparent at 20166.7 cm^{-1} (EM3). Finally, at the lowest temperature we can reach, 1.2 K, the spectrum shown in Fig. IV.1B is found. At 1.2 K the relative intensities of the two overlapping emissions at 20193.2 and 20191.1 cm^{-1} are different from those at 4.2 K (Fig. IV.2B); the emission at 20191.1 cm^{-1} has become much stronger and the peak position has shifted to somewhat lower energy (20190.6 cm^{-1}) which we, nevertheless, will also denote by EM2. In this thesis the states giving rise to the four emissions EM1 to EM4 of the melt grown crystal play a dominating part. EM3 and EM4 clearly are "deep" traps (the EM notation will be used not only to denote the emissions but also the states from which they result).

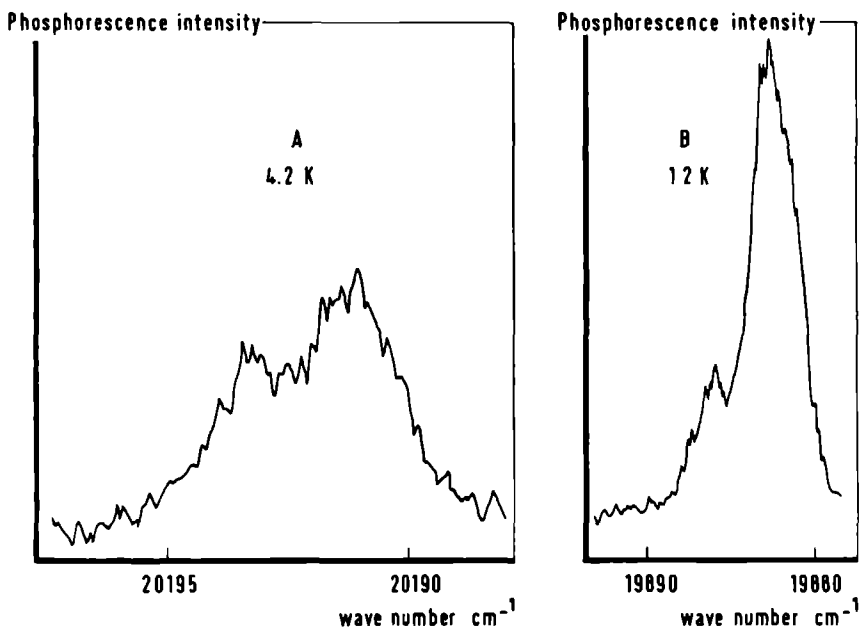


Fig. IV.2

- A) Emission around the origin at 4.2 K. The spectrum was recorded by means of a photon counting system and with a setting of monochromator slits of $50 \mu\text{m}$.
- B) The emission of the first vibration ($\sim 310 \text{ cm}^{-1}$) of the "origin", monitored after dye laser pulses into the $k = 0$ state of the lowest triplet exciton band using a Boxcar integrator.

The spectra of Fig. IV.1 and IV.2 show two remarkable facts. First, the emission line of the melt-grown crystal in Fig. IV.1 at a wavelength very near the reported exciton wavelength, consists of two components^{*} (EM1 and EM2) (Fig. IV.2) with, as discussed in the next chapter, very different lifetimes. Secondly, the above mentioned emissions at about the exciton wavelength are completely absent in the vapour grown crystals. This in spite of the fact that vapour crystal growth is believed to be superior to growth from the melt. This is evidenced by the fact that in our crystals both triplet absorption and emission lines in the Bridgman grown crystals are more than twice as broad as in the vapour grown crystals.

The two components of Fig. IV.2 correspond to two physically distinct states: exciton states and trap-like states very close to the exciton origin. Such quasi-local states may be pushed out of the exciton band by small distortions of the crystal lattice [Cr66,Me63] and form an intermediate kind of state between a fully delocalized exciton and a fully localized trap which arises when the trap depth is much larger than the exciton bandwidth. The existence of trap-like states in DBN is not reported earlier in the literature. Only a short suggestion for the presence of a small amount of such states in Bridgman grown crystals doped with the fully deuterated 1,4-DBN-d₆ analog was given [Sm79]. The spectra presented in Fig. IV.2 were taken with a setting of monochromator slits of 50 μm and were recorded via a photon counting system to improve the poor S/N-level, the consequence of such a narrow slit setting. When the monochromator slits are opened further to obtain a higher light intensity, only one broadened

* Similar lineshapes as presented in Fig. IV.2 may be obtained as a result of self-reversal effects [Ma76]. Self-reversal is a case of self-absorption when an emission line is self-absorbed to such an extent that the peak or central wavelength intensity is less than at the wings or non-central wavelengths. CW-laser experiments on thick DBN crystals showed that this may happen and furthermore the results of these experiments showed that small differences between emission and absorption wavelengths may occur in DBN [Ma76]. The results discussed in this thesis, however, make clear that the lineshapes shown in Fig. IV.2 are not due to self-reversal effects.

emission line is observed. At low temperatures ($T < 2$ K) this line in good approximation represents the emission of the trap-like states alone, because their emission intensity is then much stronger than the excitonic intensity. It is obvious, that at first glance this emission may easily be confused with excitonic emission because of the similar emission wavelength and similar lifetime (*vide infra*).

At first sight we found it surprising that Bridgman grown crystals do exhibit excitonic emission, while the more perfect vapour grown crystals do not exhibit excitonic emission. In fact this was one of the first observations, that led us to the assumption, which will be defended throughout this thesis, that some crystal *imperfections* are required to observe emission from excitons in linear systems. A special property of such imperfections must be that they act as scattering centers rather than as traps, in other words their triplet energy must be higher than that of DBN. As a result the stacks of DBN molecules will be interrupted and linear cages are formed. An excitation that is generated within such a cage may either be trapped instantaneously, when a trap is present within or near by the cage, or be reflected several times by the scattering barriers at the end of the cage, when no trap is present. The energy transport from cage to cage possibly occurs via an incoherent hopping process. It is obvious that short molecular chains confined by high energy scattering centers are most likely to be found in Bridgman grown crystals rather than in vapour grown crystals, where the quasi-1D-cages will be larger.

The probability of finding a trap in or near a short cage is smaller than for a long cage. *Therefore in a more perfect crystal trapping of excitons is expected to be more probable than in a less perfect crystal.*

A special imperfection that one can deliberately introduce in the crystal is the perdeuterated molecule DBN-d₆. Fig. IV.3 shows the absorption spectrum of the lowest triplet state in a Bridgman grown crystal of "pure" DBN-d₆. This triplet state has an energy which is 65 cm⁻¹ higher than the corresponding triplet state in DBN-h₆ (The absorptions to lower energy are caused by not fully deuterated DBN isomers like DBN-d₅ and DBN-d₄, which are also present). Experiments on Bridgman grown crystals of DBN-h₆ doped with DBN-d₆ were described in the literature [Ho72] and it has been known that the intensity of the exciton phosphorescence emission, which is present in the Bridgman grown crystals, increases on doping with DBN-d₆. A first

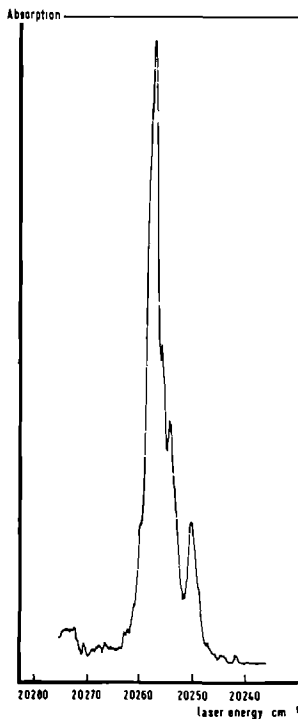


Fig. IV.3 *The absorption spectrum of the lowest triplet state in a Bridgman grown crystal of "pure" DBN-d₆. The absorptions to lower energy are caused by not fully deuterated DBN-isomers.*

stringent test for the applicability of the cage model in DBN therefore was to try and grow crystals from *the vapour* with well defined short molecular chains, rather than with longer chains as was supposed to be the case in neat vapour grown h₆-crystals. For this reason we doped the vapour grown crystals with 15% DBN-d₆. Fig. IV.4 shows the phosphorescence emission spectrum of such doped vapour grown crystals at 1.2 K. Now, in contrast to the neat specimens where no exciton emission was observed, excitonic emission is observed almost exclusively. Traps are reduced to a minor intensity. Even at the lowest temperature the line is purely excitonic in nature and no trap-like states can be detected at around 20190.6 cm⁻¹ as was the case in Bridgman grown neat-h₆ crystals.

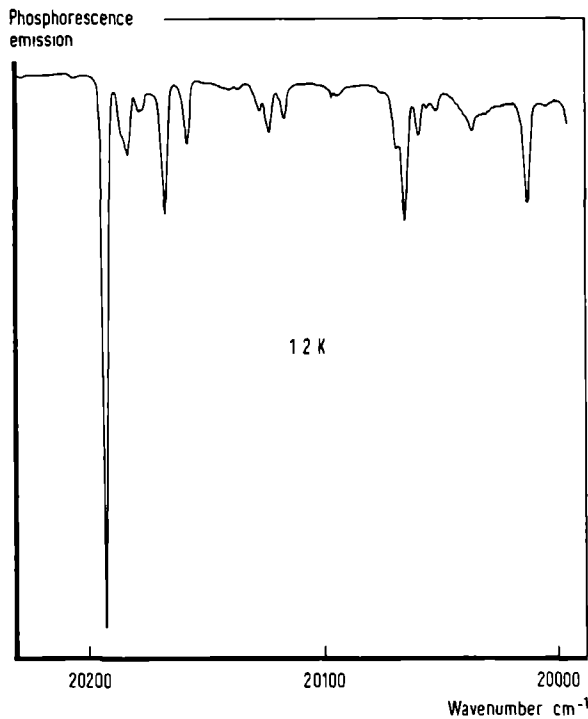
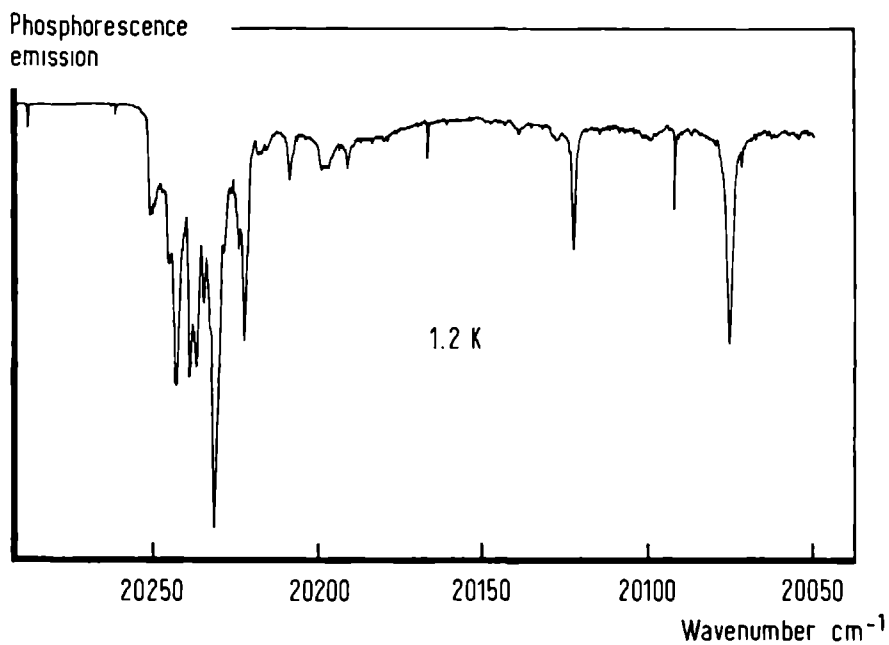


Fig. IV.4

Phosphorescence emission spectrum of a vapour grown crystal of 85% DBN- h_6 /15% DBN- d_6 at 1.2 K.

Fig. IV.5

Phosphorescence emission spectrum of neat DBN- d_6 .



A point of less importance is that several weak emissions can be observed to higher energy in these doped crystals. The same emissions are found much stronger in crystals of neat DBN-d₆ (Fig. IV.5). Most of these lines have been reported before [Ho72] except for the emissions at 20250 cm⁻¹ and 20230 cm⁻¹. The origin of these emissions could not be identified conclusively. These emission lines are not observed in Bridgman grown crystals of the same composition. On the other hand a very small amount of trap-like states close to the exciton can be detected in these Bridgman grown crystals.

A conclusion at this point is that introducing barriers (DBN-d₆) in the DBN crystals grown from vapour indeed has the effect predicted by the cage model. In the Bridgman grown, non-doped crystals it is very unlikely that DBN-d₆ molecules are present to act as barriers. However, in the next part of this chapter and in Chapter VIII it will be unambiguously shown that in Bridgman grown DBN crystals an isomer, 1,5-dibromonaphthalene, is present with the same triplet state energy as DBN-d₆. This isomer, therefore, can act as a barrier to form linear cages in Bridgman grown DBN crystals. On the other hand, the above mentioned isomer *cannot* be responsible for *all* barriers in Bridgman grown DBN crystals. Therefore, physical imperfections in these crystals also can and must create barriers.

As a conclusion of this paragraph it can be stated, that emission experiments have revealed the existence of four emitting states in melt-grown DBN crystals (Two deep traps, one shallow trap and an exciton state, the latter distinction to be proved by time-resolved experiments in Chapter V). In vapour grown DBN crystals only two deep traps are detected, no excitons.

IV.2 Delayed fluorescence

IV.2.1 General aspects

One of the most remarkable properties of triplet excitons is that of mutual annihilation of a pair of triplets. Theoretical aspects of such a collision have shortly been treated in Chapter II. The result of such annihilation may be either a vibrationally excited singlet exciton, or a vibrationally excited triplet exciton. Schematically the results of annihilation of two triplets can be summarized as follows:

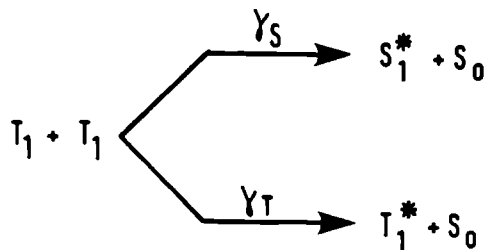


Fig. IV.6 *Schematic representation of triplet-triplet annihilation.*

In principle also an excited quintet molecule could result from such a collision of triplets. In general, however, the total energy of the two colliding triplets is not enough to make such a quintet state accessible.

When a singlet exciton is produced, the radiative decay of this exciton to the ground state is termed "Delayed Fluorescence". This delayed fluorescence has the same spectral distribution as the normal UV-excited prompt fluorescence, but it has a lifetime, which is several orders of magnitude longer than that of the prompt fluorescence. At high temperatures ($-100^{\circ}\text{C}/+25^{\circ}\text{C}$) the triplet-triplet annihilation rate does not appear to be affected much by crystal purity. The annihilation results from two identical mobile triplet excitons and is called "homo-annihilation". Room temperature studies of homo-annihilation processes in DBN have been presented in the literature [Er74,Bo78]. At low temperatures, however, triplet-triplet annihilation between free and trapped triplets ("hetero-annihilation") becomes important [Sm68]. In fact, from the low temperature experiments on DBN to be discussed (Chapter V) it follows that the delayed fluorescence in DBN is caused by hetero-annihilation.

In the case of homo-annihilation the concentration N_{EX} of triplet excitons at time t is governed by the simplified rate equation:

$$\frac{\partial N_{\text{EX}}}{\partial t} = \alpha i - \beta N_{\text{EX}} - \gamma N_{\text{EX}}^2 + \delta \nabla^2 N_{\text{EX}} \quad (\text{IV.1})$$

where ∇ is the nabla operator, α is the singlet-triplet absorption coefficient for the incident photon flux i , β is the monomolecular decay rate constant, γ the over-all bimolecular annihilation rate constant and δ the diffusion constant. The intensity of the emitted delayed fluorescence is given by:

$$I_{\text{del.fl.}} = \frac{1}{2} f \gamma N_{\text{EX}}^2 \quad (\text{IV.2})$$

where f is the fraction of triplet-triplet annihilations that lead to delayed fluorescence. For steady-state conditions under continuous ($\frac{\partial N_{\text{EX}}}{\partial t} = 0$) and uniform illumination of the crystal ($\nabla^2 N_{\text{EX}} = 0$) one can derive for low enough exciting light intensity ($\beta N_{\text{EX}} \gg \gamma N_{\text{EX}}^2$):

$$I_{\text{del.fl.}} = \frac{1}{2} f \gamma \frac{\alpha^2}{\beta^2} i^2 \quad (\text{IV.3})$$

and one expects a quadratic dependence of $I_{\text{del.fl.}}$ on the exciting light intensity i . On the other hand at high intensities ($\gamma N_{\text{EX}}^2 \gg \beta N_{\text{EX}}$) we have

$$I_{\text{del.fl.}} = \frac{1}{2} f \alpha i \quad (\text{IV.4})$$

and one predicts a linear dependence. Similar relations between the delayed fluorescence intensity and the exciting light intensity can be derived for hetero-annihilation.

IV.2.2 The DBN case

The occurrence of triplet-triplet annihilative processes at low temperatures ($1.2 \text{ K} < T < 4.2 \text{ K}$) in DBN is easily demonstrated by measuring the delayed fluorescence spectrum. Vapour grown crystals of DBN do not exhibit delayed fluorescence and neither do DBN crystals doped with 15% DBN- d_6 . Fig. IV.7 shows the delayed fluorescence spectrum of Bridgman grown neat DBN- h_6 crystals after dye laser excitation into the $k = 0$ state of the lowest triplet exciton band. Because of the pulsed excitation a Boxcar integrator has to be used (see Chapter III). The delay of the Boxcar

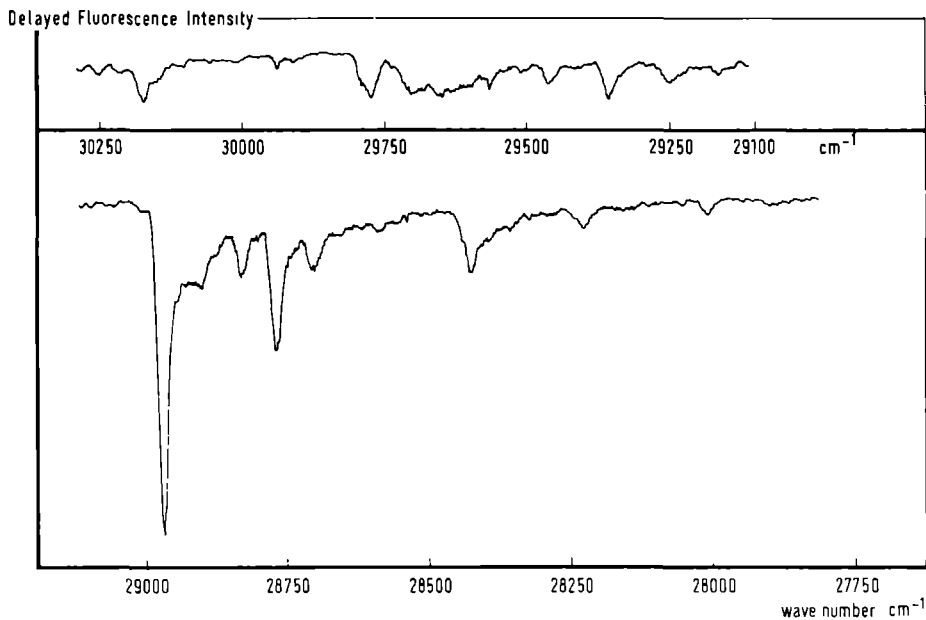


Fig. IV.7 *Delayed fluorescence spectrum of a Bridgman-grown DBN-h₆ crystal. The spectrum was recorded by means of a Boxcar integrator after dye-laser pulses into the lowest triplet exciton band.*

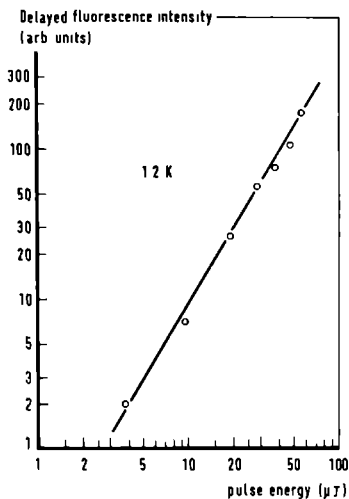


Fig. IV.8 *The intensity of the delayed fluorescence (28969 cm⁻¹) as a function of the energy of the exciting laser beam.*

is chosen to be 5 μ s in this experiment. The delayed fluorescence spectrum starts at $\sim 30290 \text{ cm}^{-1}$ with a region of weak emission. Intense emission commences at 28969 cm^{-1} with a strong vibration at 210 cm^{-1} . Since this vibration is not a characteristic DBN vibration [Ho72] it is obvious that the strong part of the fluorescence originates from an impurity. In fact, in Chapter VIII it will be shown that this particular impurity is the isomer 1,5-dibromonaphthalene. Apparently, the 1,5-DBN isomer acts as a very effective singlet trap for 1,4-DBN singlet excitons.

In Fig. IV.8 the intensity of the delayed fluorescence (28969 cm^{-1}) as a function of the exciting laser intensity is displayed in a double logarithmic plot. The slope of this curve ($n \approx 1.7$) shows that a nearly quadratic dependence is observed, which makes clear that the lifetime of the triplet excitons is determined by trapping rather than by annihilation.

The absence of delayed fluorescence in crystals doped with 15% DBN-d₆ together with the observation (section IV.1) that no trap-like state EM2 is observed in the phosphorescence emission from these doped crystals, give a first indication that the EM2-state is involved in triplet-triplet annihilation. The same conclusion will be obtained from time-resolved measurements in the next chapter.

IV.3 $S_0 \rightarrow T_1$ Absorption

The first absorption experiments on DBN have been presented in the literature some 10 years ago [Ca67, Ho72]. At that time it was already noticed, that direct excitation of the first triplet state produced much more phosphorescence than did singlet excitation. This phenomenon may find its explanation in the fact that very effective singlet traps like the 1,5-DBN isomer are present. When the singlet trapping process is faster than the intersystem crossing rate, it is obvious that phosphorescence will be largely quenched.

Our experimental set-up was not suited for direct absorption measurements, i.e. irradiating a sample and measuring how much of the incident irradiation is absorbed by the sample. Instead, an indirect detection is used. In this way the intensity of an emission line (e.g. trap phosphorescence, exciton phosphorescence or delayed fluorescence) is used as a measure for the absorption, while the wavelength of the excitation

light is varied. The disadvantage but at the same time the advantage of this excitation technique, compared to directly detected absorption, is illustrated by the following example. Of a crystal with excitons and traps the absorption around the exciton wavelength is measured by irradiating with light of variable wavelength while monitoring the emission intensity of one of the traps (say trap A). The observed absorption line, in principle, does not represent the absorption of all excitons but only of those excitons which have a chance to be trapped at trap A. The disadvantage of such an indirect detection of absorption therefore is, that in principle it will only give part of the total absorption. At the same time this is an advantage because one can discriminate between different excitons.

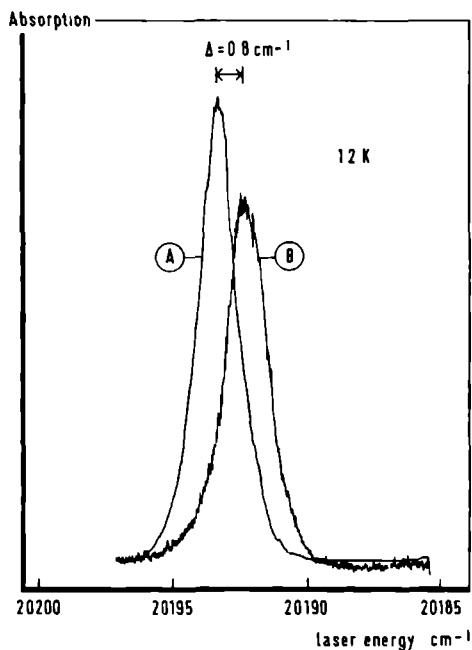


Fig. IV.9

- A) Lowest triplet absorption for melt-grown DBN- h_6 crystals detected at the delayed fluorescence.
 B) Ibid. The detection is performed at the phosphorescence from trap EM4.

Figs. IV.9 show the absorption curves for melt-grown crystals of DBN with detection at a delayed fluorescence line (Fig. IV.9A) and at the phosphorescence from trap EM4 (Fig. IV.9B). We monitored the intensity of the delayed fluorescence at 28969 cm^{-1} by means of the Boxcar integrator, while the excitation wavelength of the pulsed dye-laser was swept through an energy region covering the triplet absorption of the first sublattice (Fig. IV.9A). the absorption maximum was determined at 20193.2 cm^{-1} , coinciding with one component in the phosphorescence emission (EM1). When the same experiment is repeated using the phosphorescence at 20157.4 cm^{-1} (EM4) as the monitor (Fig. IV.9B) a different absorption maximum is found, 0.8 cm^{-1} to lower energy, coinciding with the reported value for the exciton absorption (20192.4 cm^{-1} [Ho72]).

Thus, excitons responsible for delayed fluorescence absorb at a different wavelength than excitons responsible for populating trap EM4. Therefore, it may be concluded that different excitons exist in DBN, one type responsible for delayed fluorescence, the other responsible for populating trap EM4. The excitons causing delayed fluorescence can be further discriminated with respect to lifetime.

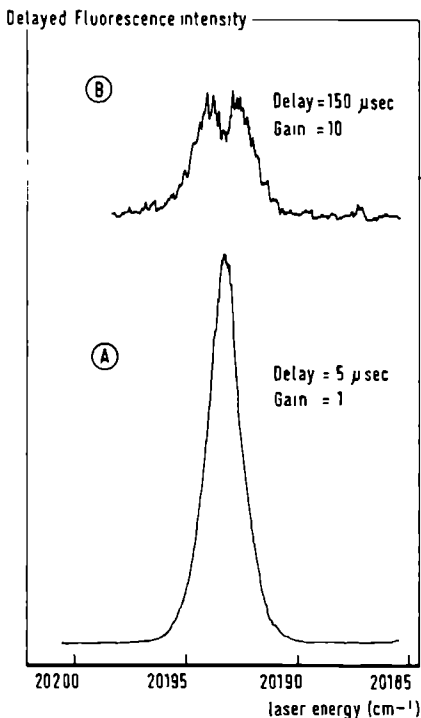


Fig. IV.10

- A) The absorption spectrum of the lowest DBN- h_0 triplet state by monitoring the delayed fluorescence after dye-laser pulses of indicated energy. The boxcar delay after the pulse is set at $5 \mu\text{s}$.
- B) As in Fig. A; now the Boxcar delay is increased up to $150 \mu\text{s}$.

Fig. IV.10A shows the absorption spectrum of the lowest triplet exciton band, when the delayed fluorescence is monitored, while the dye-laser is swept through a region around 20192 cm^{-1} . The delay of the Boxcar is set to be $5 \mu\text{s}$. Fig. IV.10B shows the effect on the absorption spectrum when the Boxcar delay is increased from $5 \mu\text{s}$ to $150 \mu\text{s}$ (The recorder gain has been increased a factor 10). The absorption of excitons with a relative short lifetime is removed from the spectrum due to the long Boxcar delay and two new absorption maxima are apparent now (20193.8 cm^{-1} respectively 20192.6 cm^{-1}) at an equal distance of 0.6 cm^{-1} from the central line. These two lines are visible until the Boxcar delay has increased up to $800 \mu\text{s}$. The delayed fluorescence arising from these two absorptions, apparently is connected with excitons appearing in the wings of the main absorption line. Their lifetime is relatively long compared with that of the excitons giving rise to the main part of the delayed fluorescence.

These absorption experiments unambiguously show the existence of several types of excitons. In the next chapter time-resolved experiments will be reported which enabled us to measure the lifetimes of these different excitons. It will become clear that these lifetimes are so completely different that the different excitons have to exist in different regions (cages!) of the crystal and are well-shielded from each other. The importance of the occurrence of cages in molecular crystals was recognized by Wieting et al. [Wi78].

The reason that the different excitons have different absorption energies can be found in the fact that cages or chains of different lengths have different excitation frequencies. According to Hochstrasser and Whiteman [Ho72] one can write for the absorption energy of an exciton restricted to a chain of length z :

$$E(z) = \epsilon + 2 J \cos \frac{\pi}{1+z} \quad (\text{IV.5})$$

where J is the intrachain intermolecular exchange interaction and ϵ is a constant energy term. The larger the chains, the smaller $E(z)$. Therefore when cages of different lengths are present, this causes an inhomogeneous broadening of the absorption line. Burland [Bu73, Bu76, Bu77] in a study on exciton scattering in DBN claimed a width of 0.3 cm^{-1} for the absorption line of the triplet exciton band. This is substantially narrower than the

observed linewidth in our Bridgman grown crystals ($\sim 2 \text{ cm}^{-1}$ at a laser linewidth of $\sim 0.3 \text{ cm}^{-1}$) and Burland assumed his absorption line to be homogeneous. In a theoretical paper Klafter and Jortner claim that the lowest triplet absorption in DBN is *inhomogeneously* broadened by structural disorder [K178]. All Bridgman grown crystals studied in this thesis exhibited inhomogeneous broadening of the lowest triplet absorption.

IV.4 Concluding remarks

Experiments on phosphorescence emission, delayed fluorescence and triplet absorption in the quasi-linear system 1,4-dibromonaphthalene show that excitons in our DBN crystals should not be considered as collectively excited states of the crystal as a whole. The experimental observations can be explained by a model that assumes that crystals of DBN should be considered to consist of a large amount of cages, each cage being bordered by high-energy scattering barriers. The length of the different cages is determined by the concentration of the randomly distributed barriers. Slight differences in absorption energy accompany the difference in chain length. A very important feature that follows directly from the absorption experiments is the strong isolation of the cages from one another. This isolation condition can be concluded from the fact that it is possible to discriminate between different excitons on the basis of their lifetime. When this stringent isolation would not hold, the excitons could be described as one bath in internal equilibrium. All the excitons would have the same lifetime then.

Furthermore it appears that *crystal imperfections* are required in order to observe exciton phosphorescence emission in DBN. In fact, the more perfect the crystals, the weaker the phosphorescence emission from exciton states. In vapour grown crystals, which in the absence of high-energy barriers do not show any exciton emission, doping with such barriers (DBN-d₆) causes a strong exciton emission to appear.

More details on the dynamics of this complicated set of different excitons will be discussed in the next chapter on time-resolved measurements.

IV.5 References

- [Bo78] H. Bouchriha, V. Ern, J.L. Fave, C. Guthmann, M. Schott, Chem. Phys. Lett. 53, 288 (1978).
- [Bu73] D.M. Burland, J. Chem. Phys. 59, 4283 (1973).
- [Bu76] D.M. Burland, R.M. MacFarlane, J. Lum. 12/13, 213 (1976).
- [Bu77] D.M. Burland, U. Konzelmann, R.M. MacFarlane, J. Chem. Phys. 67, 1926 (1977).
- [Ca67] G. Castro, R.M. Hochstrasser, J. Chem. Phys. 47, 2241 (1967).
- [Cr66] D.P. Craig, M.R. Philpott, Proc. Roy. Soc. A290, 583 (1966).
D.P. Craig, M.R. Philpott, Proc. Roy. Soc. A290, 602 (1966).
D.P. Craig, M.R. Philpott, Proc. Roy. Soc. A293, 213 (1966).
- [Er74] V. Ern, H. Bouchriha, M. Schott, G. Castro, Chem. Phys. Lett. 29, 453 (1974).
- [Ho72] R.M. Hochstrasser, J.D. Whiteman, J. Chem. Phys. 56, 5945 (1972).
- [Kl78] J. Klafter, J. Jortner, J. Chem. Phys. 68, 1513 (1978).
- [Ma76] R.M. MacFarlane, U. Konzelmann, D.M. Burland, J. Chem. Phys. 65, 1022 (1976).
- [Me63] R.E. Merrifield, J. Chem. Phys. 38, 920 (1963).
- [Sm68] G.C. Smith, Phys. Rev. 166, 839 (1968).
- [Sm79] D.D. Smith, A.H. Zewail, J. Chem. Phys. 71, 3533 (1979).
- [Wi78] R.D. Wieting, M.D. Fayer, D.D. Dlott, J. Chem. Phys. 69, 1996 (1978).

TIME-RESOLVED MEASUREMENTS

V.1 Introduction

In this chapter we will present the results of time-resolved measurements on the phosphorescence and delayed fluorescence which were performed in zero magnetic field. Corresponding measurements performed in a magnetic field will be presented in Chapter VII. In this kind of experiments the system is excited by means of short laser pulses (10 ns) and the response of the system is studied at various emission wavelengths.

First we will introduce a kinetic model for the case of a linear triplet exciton band coupled to one single trap. Of course DBN is, as we saw before, a system with many separate exciton species and several traps and at first sight it seems that one has to use a more sophisticated model including all excited states. Such a model, however, would in general result in cubic or higher order equations for the decay constants, which are very difficult if not impossible to solve analytically. Fortunately, it will appear that each of the different traps observed in our crystals is almost selectively coupled to one kind of excitonic species hidden under the inhomogeneously broadened lowest triplet absorption. Therefore this simple kinetic model turns out to be valuable for the DBN system. The same model has been used to describe the trapping dynamics of the linear system 1,2,4,5-tetrachlorobenzene, which exhibits phosphorescence emission from only one trap state [Sh76].

V.2 A kinetic model for an exciton-trap system

Fig. V.1 shows a schematical representation of the dynamics of a coupled exciton-trap system. Exciton and trap population are coupled by the trapping rate constant k_1 and the detrapping rate k_0 . The decay to the ground state is characterized by the rate constants k_e and k_t . Triplet-triplet annihilation between exciton and trap occurs at a rate γ_S . In the description here, however, it is assumed that this process is negligible compared to the trapping process (a first order approximation).

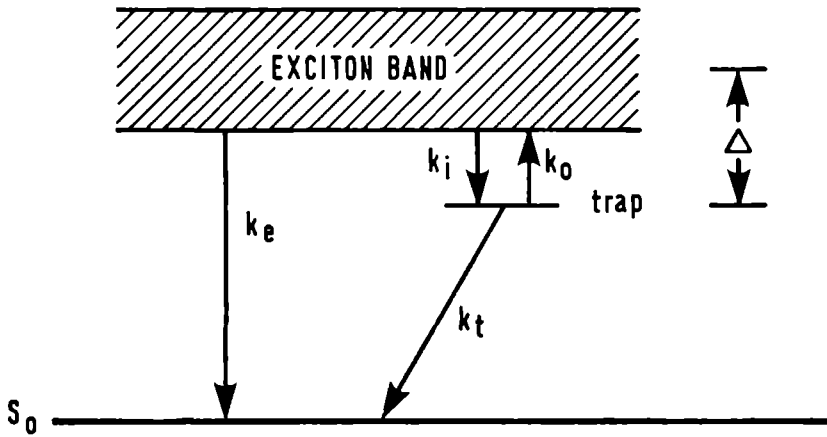


Fig. V.1 Schematical representation of the dynamics of a coupled exciton trap system.

The population in the exciton and trap levels after pulse excitation is described by the set of coupled differential equations:

$$\frac{\partial N_{EX}(t)}{\partial t} = - (k_i + k_e) N_{EX}(t) + k_o N_t(t) \quad (V.1)$$

$$\frac{\partial N_t(t)}{\partial t} = - (k_t + k_o) N_t(t) + k_i N_{EX}(t) \quad (V.2)$$

These equations may be solved by standard procedures. The solutions take the form

$$N_{EX}(t) = c_1 \exp(\alpha_+ t) + c_2 \exp(\alpha_- t) \quad (V.3)$$

$$N_{\pm}(t) = c_3 \exp(\alpha_+ t) + c_4 \exp(\alpha_- t) \quad (V.4)$$

where

$$2\alpha_{\pm} = -(k_i + k_e + k_t + k_0) \pm \sqrt{(k_i + k_e + k_t + k_0)^2 - 4\{(k_i + k_e)(k_t + k_0) - k_0 k_i\}} \quad (V.5)$$

$$= -(k_i + k_e + k_t + k_0) \pm \sqrt{(k_i + k_e + k_t + k_0)^2 - 4(k_i k_t + k_e k_t + k_0 k_e)}$$

The coefficients c_1 , c_2 , c_3 and c_4 are determined from the initial conditions: $N_{EX}(t = 0) = N_0$ and $N_t(t = 0) = 0$. This implies that the trap cannot be excited directly by absorption of a photon. This is in agreement with all experimental observations of this thesis and of related studies by others. Then the following time dependence results for the population in the exciton and trap levels.

$$N_{EX}(t) = N_0 \left\{ \left[\frac{(\alpha_- + k_i + k_e)}{(\alpha_- - \alpha_+)} \right] \exp(\alpha_+ t) \right. \quad (V.6)$$

$$\left. + \left[\frac{(\alpha_+ + k_i + k_e)}{(\alpha_+ - \alpha_-)} \right] \exp(\alpha_- t) \right\}$$

$$N_t(t) = \left[\frac{k_i N_0}{(\alpha_+ - \alpha_-)} \right] [\exp(\alpha_+ t) - \exp(\alpha_- t)] \quad (V.7)$$

where α_+ and α_- are experimental observables.

We will consider now two important limiting cases: the *slow detrapping regime*, where $k_0 \ll k_i, k_t$ and the *fast detrapping regime*, where $k_0 \gg k_i, k_t$. To obtain some more insight in the observables α_{\pm} , we will approximate equation (V.5) with aid of equation (V.8)

$$\sqrt{a + \epsilon} \approx \sqrt{a} + \frac{\epsilon}{2\sqrt{a}} \quad (\epsilon \ll a) \quad (V.8)$$

Using this approximation we find with $a = (k_i + k_e + k_t + k_0)^2$ and $\epsilon = -4(k_i k_t + k_e k_t + k_0 k_e)$

$$\alpha_+ = - \frac{k_i k_t + k_e k_t + k_0 k_e}{k_i + k_e + k_t + k_0} \quad (V.9)$$

$$\alpha_- = - (k_i + k_e + k_t + k_0) + \frac{k_i k_t + k_e k_t + k_0 k_e}{k_i + k_e + k_t + k_0} \quad (\text{V.10})$$

In the *slow detrapping regime*, where $k_0 < k_t \ll k_i$, equations (V.9) and (V.10) reduce to

$$\alpha_+ = - \frac{(k_i + k_e)k_t}{k_i + k_e + k_t} = - k_t \quad (\text{V.11})$$

$$\alpha_- = - (k_i + k_e + k_t) + k_t = - (k_i + k_e) \quad (\text{V.12})$$

The exciton population decays as a biexponential. It is dominated by the fast [$\alpha_- \approx - (k_i + k_e)$] component due to the combined effects of trapping and decay to the ground state, but still exhibits a long tail ($\alpha_+ \approx - k_t$) of less magnitude, which is caused by detrapping. It is important to note, that in this regime the trap builds up with the same rate as the exciton decays and then decays with its characteristic decay constant k_t .

In the other limit (*fast detrapping*) the equations (V.9) and (V.10) reduce to:

$$\alpha_+ = - k_e \quad (\text{V.13})$$

$$\alpha_- = - k_0 \quad (\text{V.14})$$

Because of the fast detrapping the population spends little time in the trap and the decay of the exciton is dominated by the slow component ($\alpha_+ \approx - k_e$), which characterizes the exciton decay to the ground state. The population in the trap is minimal. It builds up very fast ($\alpha_- \approx - k_0$) and then decays with a rate equal to that of the exciton, owing to the rapid communication with the exciton band. In Fig. V.2 we illustrate this by hypothetical time resolved curves, describing the exciton and trap population in a coupled exciton trap system in the slow and fast detrapping regime. Note that, in agreement with the experiment (the photomultiplier output is a negative voltage), decreasing intensity is indicated *upwards*.

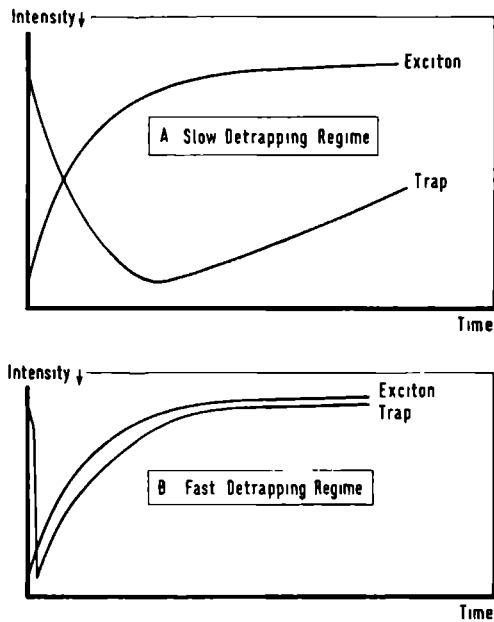


Fig. V.2

- A) Slow detrapping regime: the trap population builds up with the same rate as the exciton decays, and then decays with its total decay constant.
- B) Fast detrapping regime: trap population appears very quickly and decays with the same time constant as the exciton, owing to the rapid communication with the exciton band.

In this model it is implicitly assumed that each exciton has the same probability of encountering a trap. This is a consequence of the assumption, that the trapping process can be described by a trapping rate constant k_i . On the other hand it is obvious that not each exciton-trap encounter must necessarily lead to an actual localization of the excitation. If we characterize the chance of actual trapping by a parameter κ then, in the coherent limit, where the exciton propagation can be described with an average group velocity $\langle V_g \rangle$, the trapping rate constant is given by [Sh76]

$$k_i = \kappa \left(\frac{\langle V_g \rangle}{d} \right) \quad (V.15)$$

where d is the average distance between traps. It is obvious, that the value of the parameter κ will be rather uncertain since it depends on physical quantities like the duration of the exciton-trap interaction, appropriate phonon density at the exciton-trap energy difference to dissipate the released energy and the exact form of the exciton wave vector. When incoherent hopping characterizes the exciton transport, the trapping rate is inversely related to the average time for reaching a trap [Sh76],

$$k_i = \frac{a^2}{\tau d^2} \quad (V.16)$$

where a is the step length (the intermolecular spacing). In the coherent limit k_i will be weakly temperature dependent since the average group velocity is dependent on the thermal equilibrium over the exciton band. In the incoherent limit the trapping rate is temperature independent since the exciton hops with an average step time $t = \frac{\hbar}{4J}$, where J is the intermolecular interaction matrix element. Fayer and Harris developed a model [Fa74] in which they derive an expression for the temperature dependence of the phonon assisted detrapping rate k_0 :

$$k_0 = c\rho_{EX}(E_i)\exp\left(-\frac{E_i}{kT}\right) \quad (V.17)$$

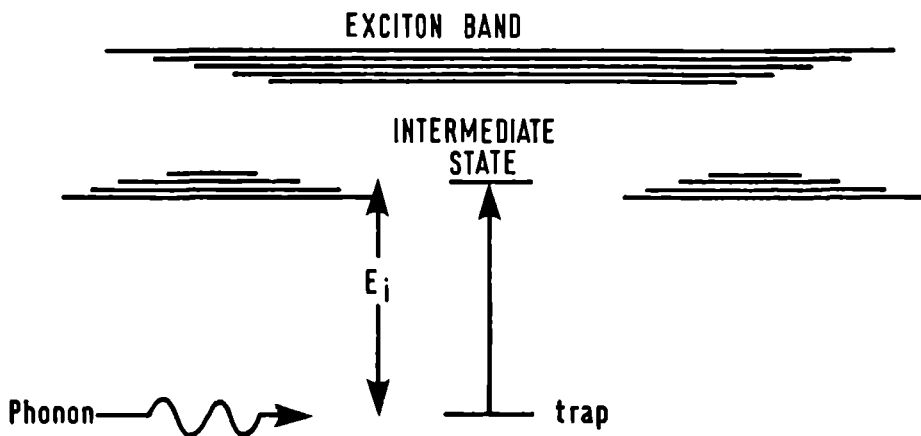


Fig. V.3 Schematical representation of phonon assisted detrapping.

where c is a temperature independent constant, $\rho_{EX}(E_1)$ is the exciton density of states at an energy E_1 of the phonon-trap coupled intermediate state which can subsequently decay into some linear combination of delocalized exciton band states (Fig. V.3). The energy E_1 is taken relative to the trap energy, which is assumed at zero energy. From this equation it can be seen, that temperature will have a drastic effect on k_0 in the range that can be covered by liquid helium experiments for trap depths in the order of tens of cm^{-1} . Therefore one expects a clear effect of temperature on the phosphorescence response of such traps on short laser pulses.

V.3 Experimental results

V.3.1 Phosphorescence emission

The response of DBN phosphorescence emission after short (10 ns) laser pulses has been studied for different temperatures and different emission wavelengths. Both dye-laser and nitrogen laser excitation (337 nm) have been used. Table V.1 shows the results for dye-laser excitation into the triplet exciton band. In the left part of this table the time constants for the population build-up of the various emissions are indicated. The percentages given in parentheses indicate the relative intensity corresponding to the particular time constant. In the right part of the table the decay constants are given.

Data obtained with N_2 -laser excitation differ only in the relative intensities of the slow build-up components presented in the left part of Table V.1. For EM3 N_2 -laser excitation reduces the intensity of the slow build-up component from 80% to 30% (Fig. V.4), whereas for EM4 no slow build-up component can be detected at any temperature (Fig. V.5). The 10% slow build-up component presented for EM4 at 1.2 K in Table V.1 could not be detected in all the crystals studied with dye-laser excitation.

Confining ourselves to the results obtained with dye laser excitation, we can immediately draw conclusions from the data in Table V.1. First, we see that the lifetimes of the two traps EM3 and EM4 are much longer than those of the two emissions around the exciton origin. Therefore, it may be assumed that for these traps the slow detrapping regime is appropriate and

Table V.1 *Build-up and decay times of the various emissions after a dye laser pulse at 20192.3 cm⁻¹ except for the data of EM1 where excitation in the second sublattice was used.*

T(K)	Build-up time (μs)				Decay time (μs)			
	EM1 20193.2 cm ⁻¹	EM2 20190.6 [*] cm ⁻¹	EM3 20166.7 cm ⁻¹	EM4 20157.4 cm ⁻¹	EM1 20193.2 cm ⁻¹	EM2 20190.6 [*] cm ⁻¹	EM3 20166.7 cm ⁻¹	EM4 20157.4 cm ⁻¹
4.2	< 1	(10%) < 1 (90%) 10	-	-	150	150	-	-
3.0	< 1	(10%) < 1 (90%) 10	(100%) < 1	(100%) < 1	150	150	1400	6400
2.0	< 1	(10%) < 1 (90%) 17	(20%) < 1 (80%) 150	(100%) < 1	150	160	4700	6500
1.2	< 1	(10%) < 1 (90%) 20-40 [☆]	(20%) < 1 (80%) 150	(90%) < 1 (10%) 300	biexp. 150/350	300-500 [☆]	4700	7000

^{*}EM2 position at 1.2 K, at 4.2 K shifted to 20191.1 cm⁻¹.

[☆]Dependent on crystal.

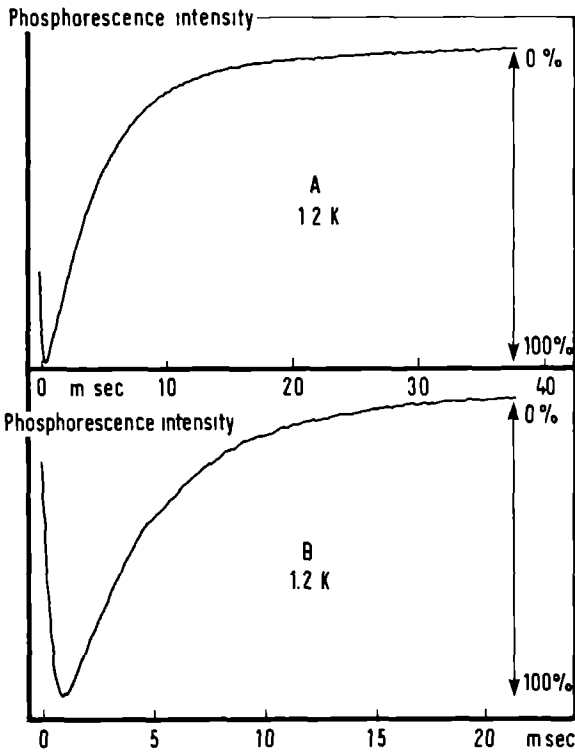
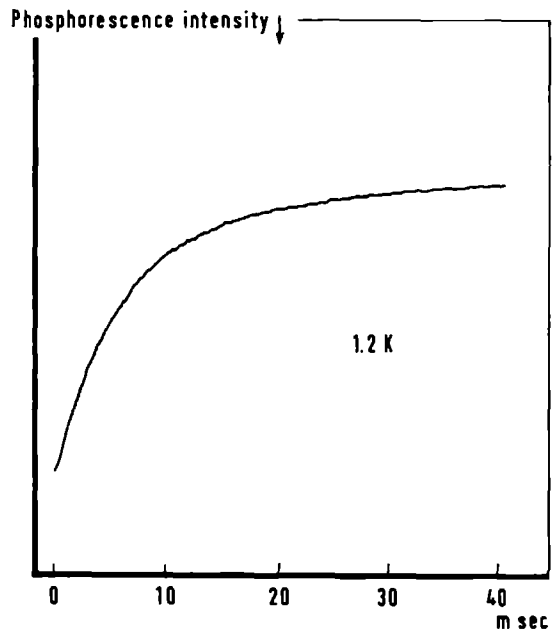


Fig. V.4

The difference in behaviour of trap EM3 population build-up after a nitrogen-laser pulse (A) and a dye-laser pulse exactly into the $k = 0$ state of the lowest triplet-exciton band (B). The intensity of the slow build-up component increases considerably when dye-laser excitation is used instead of nitrogen-laser excitation.

Fig. V.5

The response of the EM4 population after a nitrogen laser pulse. The population build-up is complete within 1 μ s.



the trap build-up rate should then correspond to the lifetime of the states from where they are populated. For the trap at 20157.4 cm^{-1} (EM4) the build-up is very fast ($< 1 \mu\text{s}$), much faster than the lifetimes of the emissions at 20193.2 cm^{-1} (EM1) and 20190.6 cm^{-1} (EM2). So clearly, the trap EM4 is not populated from the states causing the emissions around the exciton origin. At the same time the build-up rate of 80% of the EM3 population equals the EM1 decay rate. However, 20% of the EM3 population is present in a time $< 1 \mu\text{s}$ after the excitation pulse. When we exclude direct excitation of these traps and when we recall the results of Chapter IV, this means that states must exist at $\sim 20192 \text{ cm}^{-1}$ with a lifetime $< 1 \mu\text{s}$ and a strong absorption coefficient. No emission is observed from these states but they are responsible for populating the trap at 20157.4 cm^{-1} (EM4) and partly the trap at 20166.7 cm^{-1} (EM3). Because of their strong absorption these states most likely are exciton states. No emission is found from these excitons because they are trapped in a very short time ($< 1 \mu\text{s}$).

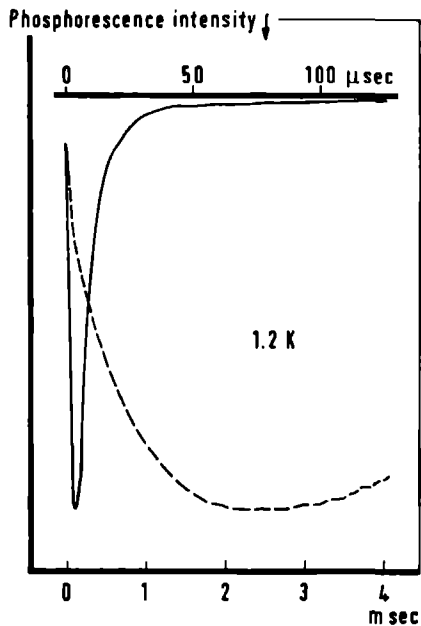


Fig. V.6

The response of the EM2 population after a dye-laser pulse. Only 10% of the population is present within 1 μs . The upper timescale corresponds to the dotted line representing the expanded population build-up.

Further, Table V.1 shows that after a laser flash the emission of EM2 is *not* present immediately but builds up with a characteristic time of 10 - 40 μs depending on temperature and crystal. Fig. V.6 shows a typical example of the build-up and subsequent decay of the emission at 20190.6 cm^{-1} .

Because of the slow population build-up and because of the fact that this state hardly shows any direct absorption, we conclude that EM2 is not an exciton but a trap-like state.

The emission at 20193.2 cm^{-1} (EM1), on the other hand, is considered to be excitonic emission because of three reasons: first, the emission coincides with the absorption, second, the emission is present within $1 \mu\text{s}$ after the laser pulse and third, the trap EM3 build-up time equals the EM1 lifetime, which is indeed predicted by the kinetic model presented in section V.2.

Therefore at this point we have already established the simultaneous presence of two types of excitons with extremely different lifetimes: $< 1 \mu\text{s}$ and $150 \mu\text{s}$. No emission is observed from the excitons with the lifetime $< 1 \mu\text{s}$ but their absorption energy was determined in the previous chapter to be 20192.4 cm^{-1} .

However, in the previous chapter it was also shown that a third type of excitons with a different lifetime may be created by exciting in the wings of the main absorption line. The same phenomenon can be demonstrated as well in the time-resolved phosphorescence emission of the trap at 20166.7 cm^{-1} (EM3). Tuning the laser frequency away to the wings of the inhomogeneously broadened absorption line reduces the relative intensity of the slow build-up component of EM3 (rate = $150 \mu\text{s}$) from 80% to less than 25%, whereas the time constant of this build-up increases from $150 \mu\text{s}$ to $300 \mu\text{s}$. The increased time constant demonstrates that excitons exist with a 0-0 transition frequency, only slightly differing from the main absorption, but with a lifetime differing by a factor two. In fact, the same time constant ($300 \mu\text{s}$) was observed (Table V.1) for 10% of the EM4 population build-up at 1.2 K. Trapping of this third kind of excitons which absorb in the wings of the main absorption line, is therefore thought to be responsible for the 10% EM4 population build-up.

The properties of the EM2 state will be discussed in more detail in the next section on the delayed fluorescence.

V.3.2 Delayed fluorescence

Triplet-triplet annihilative processes in DBN were demonstrated in Chapter IV by measuring the delayed fluorescence spectrum. The most intense

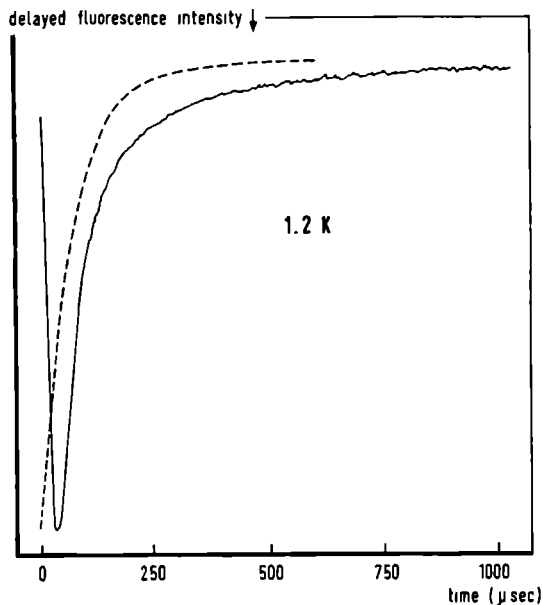


Fig. V.7

The response of the delayed fluorescence after a dye-laser pulse at 20193.2 cm^{-1} . The dotted line represents the calculated time dependence of the delayed fluorescence for homo-annihilation of EMI triplet excitons.

emission line in this spectrum originates from an impurity and appears at 28969 cm^{-1} . We chose this line for the study of the time dependence of the delayed fluorescence. The fact that the fluorescence originates from an impurity does not complicate the underlying study since all rate processes within the singlet system are several orders of magnitude faster than within the triplet system. Therefore the time-dependent behaviour on microsecond timescale can be ascribed completely to processes within the triplet manifold.

The response of the delayed fluorescence at 1.2 K on a dye-laser pulse at 20193.2 cm^{-1} is displayed in Fig. V.7 (solid line). A striking feature of the presented curve is the fact that the intensity builds up almost exponentially with a time constant of 8 - 10 μs . The decay is biexponential with decay times $\tau_1 = 40 \mu\text{s}$ and $\tau_2 = 150 - 250 \mu\text{s}$ (dependent on the crystal under study). Fig. V.7 also shows the calculated behaviour of the delayed fluorescence for pure homo-annihilation of EMI triplet excitons (dotted line). Obviously, pure homo-annihilation of the triplet excitons cannot explain the data since an intensity build-up of $\approx 10 \mu\text{s}$ will never be observed in such a case. This relative slow build-up suggests that one of the states involved in the annihilation is not populated right after the laser pulse but becomes populated in a time of the order of tens

of microseconds. The only state we have detected, which displays such build-up is EM2 at 20190.6 cm^{-1} . Delayed fluorescence is then assumed to be due to hetero-annihilation between excitons and this trap. We tried to obtain a computer fit of the time dependence of the delayed fluorescence by means of the kinetic model presented in section V.2. It was assumed that the effects of bimolecular annihilation are small compared to the effects of trapping and consequently the terms describing the annihilation were omitted from the rate equations. The expressions obtained for the exciton population $N_{EX}(t)$ and trap population $N_{EM2}(t)$ are:

$$N_{EX}(t) = N_0 \left\{ \left[\frac{(\alpha_- + k_i + k_e)}{(\alpha_- - \alpha_+)} \right] \exp(\alpha_+ t) + \left[\frac{(\alpha_+ + k_i + k_e)}{(\alpha_+ - \alpha_-)} \right] \exp(\alpha_- t) \right\} \quad (V.6)$$

$$N_{EM2}(t) = \left[\frac{k_i N_0}{(\alpha_+ - \alpha_-)} \right] [\exp(\alpha_+ t) - \exp(\alpha_- t)] \quad (V.7)$$

where the symbols used were defined in section V.2. It will turn out in Chapter VII that annihilation does not determine the exciton lifetime but it probably does determine to some extent the lifetime of the trap EM2. In a first order approximation, though, we will disregard this decay process in the rate equations and write for the intensity of the delayed fluorescence:

$$I_{del.fl.}(t) \propto N_{EX}(t)N_{EM2}(t) \quad (V.8)$$

By fitting $I_{del.fl.}(t)$ to the observed time dependence, only the following combinations of rate constants can be determined $(k_i + k_e)^{-1} = 40 \mu\text{s}$, $(k_t + k_0)^{-1} = 250 \mu\text{s}$ and $k_0 k_i = 0.000045 \mu\text{s}^{-2}$. Further it can be shown that $k_i > k_0$.

Since the phosphorescence build-up of EM2 (for this particular sample $\tau = 40 \mu\text{s}$) equals the fitted value for $(k_i + k_e)^{-1}$ it follows from the model that in such a case we are clearly in the slow detrapping regime.

In this regime the exciton lifetime is dominated by $(k_i + k_e)$ and therefore the value of $(k_i + k_e)^{-1} = 40 \mu\text{s}$, obtained both from fitting $I_{\text{del.fl.}}(t)$ and from the phosphorescence build-up of EM2, should agree with the observed EM1 lifetime (150 μs). Since this is not true it is probable, that excitons responsible for the largest part of the phosphorescence (lifetime 150 μs) are not the same excitons responsible for delayed fluorescence and for the phosphorescence build-up of EM2 (lifetime 40 μs).

V.4 Discussion and conclusions

Summarizing at this point our findings presented in Chapters IV and V of this thesis, we have shown that the absorption of the first triplet state in DBN is inhomogeneously broadened and can be deconvoluted into separate absorptions of excitons with different excitation frequencies and different lifetimes. At least four different kinds of excitons have been observed and all these excitons contribute to the total optical absorption line.

The fact that these excitons have strongly different lifetimes can only be reconciled with strongly shielded regions in the crystals. In the earlier discussed cage model, scattering impurities or defects cause that the exciton motion along the linear chains is blocked and molecular chains of different length will result. Short chains have absorption spectra which differ from longer chains. Very short chains, though, will have a relatively small chance to contain a trap in contrast to longer chains. When a unit contains a trap, trapping is instantaneous on our time scale. Then traps will derive part of their population within 1 μs after the laser pulse. This may also be the reason that in vapour grown crystals neither exciton phosphorescence nor delayed fluorescence is detected, in spite of the apparent better quality compared to Bridgman grown crystals. In vapour grown crystals the quasi-1D-cages may be larger, thereby increasing the trapping rate.

Several types of excitons have been detected with a lifetime much longer than 1 μs . Excitons with a lifetime of $\sim 40 \mu\text{s}$ are responsible for the main part of the delayed fluorescence. Excitons with a lifetime of $\sim 150 \mu\text{s}$ are detected via their strong phosphorescence, while excitons with a lifetime of $\sim 300 \mu\text{s}$ can be excited by irradiating in the wings of

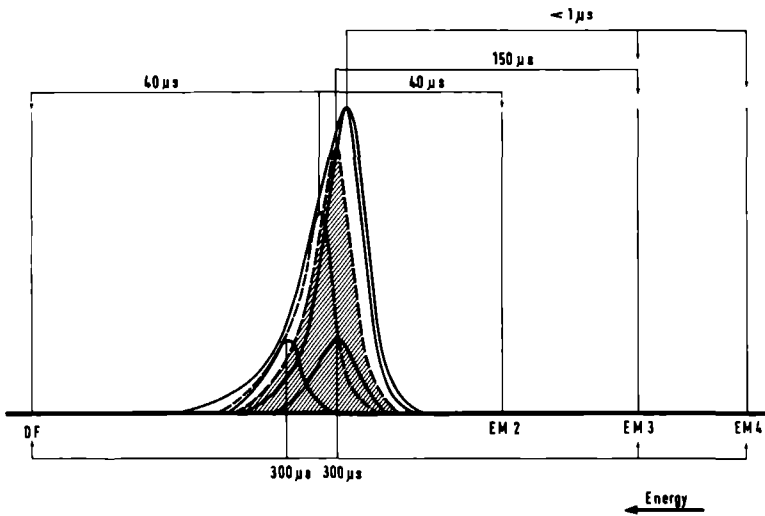


Fig. V.8 Schematic survey of the various states in our Bridgman grown DBN- h_6 crystals. Part of the dynamics is indicated by means of arrows.

of the absorption line (Fig. V.8). Considering this scala of different excitons it is obvious that $k \rightarrow k'$ scattering times determined from optical absorption measurements (for DBN 60 ps [Bk77]) may differ greatly from the scattering times determined from ESR experiments in the microwave region. Such a discrepancy has been reported for a similar linear system, 1,2,4,5-tetrachlorobenzene (TCB). Optical experiments [Bu77] show an exciton dephasing time of 20 ps, while ESR experiments yield a $k \rightarrow k'$ scattering time of $\sim 2 \mu s$ for $k = 0$ excitons [Bo78]. Of course, one cannot compare these figures, obtained in the optical regime and in the microwave region, directly as noticed by van Strien and Schmidt [St80]. A change in microwave frequency $\nu \rightarrow \nu'$ resulting from a scattering of the exciton from state $|k\rangle$ to $|k'\rangle$ in the exciton band in a few ps, only causes an observable change of the spin states after a time of the order of $\frac{1}{\Delta\nu}$, where $\Delta\nu = |\nu - \nu'|$. Therefore the homogeneous width of an exciton microwave spin packet is related to the homogeneous optical wave packet by a factor of the order of the reduction factor f [Fr71] relating the exciton bandwidth to the inhomogeneous microwave line. Van Strien and Schmidt then arrive at an optical scattering time of 500 - 1000 ps, still

much longer than the observed value of 20 ps. The reason may be that in TCB several, independent, species of excitons exist. Some of them may be mainly responsible for the optical absorption, while others cause emission, analogous to the situation in DBN. In a time-resolved experiment on trap emission in the TCB system we found that $\sim 40\%$ of the trap population is present within 1 μs after the laser pulse. This experiment makes it very likely that also in the TCB system excitons exist with an extremely short lifetime simultaneously with excitons having a much longer lifetime. For these long living excitons a coherence length of ~ 200 molecules has been determined [Sh76,Ko82]. This finding qualitatively confirms our conclusions in DBN that short molecular chains are necessary to observe excitonic emission.

Delayed fluorescence in DBN is caused by hetero-annihilation between excitons with a lifetime of 40 μs and EM2 states. The slow population build-up of EM2 after pulse excitation and the fact that this state hardly shows any direct absorption allow the conclusion that EM2 is a trap-like state. From a fitting procedure of the time-dependence of the delayed fluorescence it follows that the detrapping rate from EM2 is smaller than the trapping rate of 40 μs excitons at EM2.

V.5 References

- [Bk77] D.M. Burland, U. Konzelmann, R.M. MacFarlane, J. Chem. Phys. 67, 1926 (1977).
- [Bo78] B.J. Botter, A.I.M. Dicker, J. Schmidt, Mol. Phys. 36, 129 (1978).
- [Bu77] D.M. Burland, D.E. Cooper, M.D. Fayer, C.R. Gochanour, Chem. Phys. Lett. 52, 279 (1977).
- [Fa74] M.D. Fayer, C.B. Harris, Phys. Rev. B9, 748 (1974).
- [Fr71] A.H. Francis, C.B. Harris, Chem. Phys. Lett. 9, 181 (1971).
A.H. Francis, C.B. Harris, Chem. Phys. Lett. 9, 188 (1971).
- [Ko82] J.F.C. v. Kooten, A.J. v. Strien, J. Schmidt, Chem. Phys. Lett. 90, 337 (1982).
- [Sh76] R.M. Shelby, A.H. Zewail, C.B. Harris, J. Chem. Phys. 64, 3192 (1976).
- [St80] A.J. v. Strien, J.F.C. v. Kooten, J. Schmidt, Chem. Phys. Lett. 76, 7 (1980).

**MAGNETIC RESONANCE ON LOCALIZED EXCITED TRIPLET STATES
IN 1,4-DIBROMONAPHTHALENE**

VI.1 Introduction

It was shown in Chapter II, that one can induce magnetic dipole transitions between the non-degenerate triplet spin components of an excited molecule in the absence of a steady external magnetic field. The zero-field splitting parameters that characterize these transitions, correspond to frequencies in the microwave region and usually have values between 0.5 and 12 GHz. A simple method to measure these parameters would be the zero-field analog of a normal ESR experiment: one varies the microwave frequency and detects the changes in microwave power transmission due to resonant absorption in the sample. In practice, however, there appear to be extreme technical difficulties in this approach. An elegant way out of this problem is provided by the ODMR technique (optical detection of magnetic resonance).

VI.2 Optically detected magnetic resonance (ODMR)

Fig. VI.1 gives a schematical representation of an ODMR experiment. We have seen in Chapter II that spin-orbit coupling causes a selective mixing of singlet states with triplet states. Consequently, the three triplet sublevels will generally have a different lifetime and a different population. We now consider the case of magnetic dipole transitions between for example the $|z\rangle$ and $|y\rangle$ triplet sublevels. These sublevels are characterized by the radiative decay constants k_z^r respectively k_y^r and the total decay constants (radiative + radiationless) k_z and k_y . Under steady state conditions with continuous irradiation the observed emission intensity, I , from these two sublevels is:

$$I = k_z^r N_z + k_y^r N_y \quad (\text{VI.1})$$

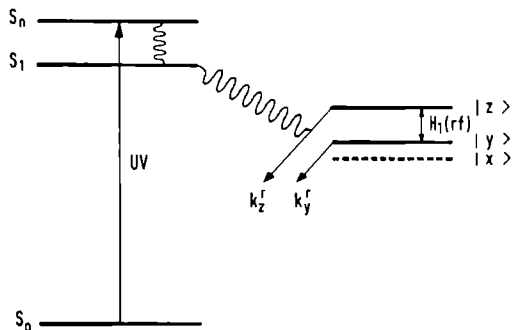


Fig. VI.1
Schematic diagram of an
ODMR experiment.

where N_z and N_y are the steady-state populations of the states $|z\rangle$ and $|y\rangle$. If now a microwave field is switched on resonant with the energy difference between the $|z\rangle$ and $|y\rangle$ level, the populations in both levels will be redistributed. Assuming that the total number of triplet state molecules is not influenced by the microwave field, the corresponding change in phosphorescence intensity is given by:

$$\Delta I = \delta N_z k_z^r + \delta N_y k_y^r = \delta N(k_z^r - k_y^r) \quad (\text{VI.2})$$

where $\delta N_z = -\delta N_y = +\delta N$ indicate the changes in population for the two sublevels induced by the microwave field. This means that the total observed phosphorescence emission intensity changes under a resonant microwave field when $k_z^r \neq k_y^r$ and $\delta N \neq 0$. In this way one can optically detect zero-field transitions.

To improve the experimental signal/noise ratio one should make δN as large as possible. This may be done by both saturating the microwave transition and by lowering the temperature. When the transition is saturated one obtains:

$$\delta N = \frac{1}{2}(N_y - N_z) \quad (\text{VI.3})$$

* When the total number of triplet state molecules is not assumed to be constant, this condition changes to $k_z^r/k_z \neq k_y^r/k_y$.

By lowering the temperature one affects spin-lattice relaxation processes. When spin-lattice relaxation is faster than the sublevel lifetimes, a Boltzmann equilibrium will be reached over the triplet sublevels:

$$\frac{N_z}{N_y} = e^{-\Delta E_{zy}/kT} \quad (\text{VI.4})$$

Therefore, at higher temperatures the population differences will be rather small. At low temperatures, though, spin-lattice relaxation processes will become much slower, usually so slow that the triplet sublevels may be considered to decay independently from one another. For negligible spin-lattice relaxation one can write:

$$\frac{dN_u}{dt} = P_u - k_u N_u \quad u = x, y, z \quad (\text{VI.5})$$

where it is assumed that the number of ground state molecules is so large that it is essentially constant. In this equation the P's are the populating rates. Under steady-state conditions we have:

$$N_u = \frac{P_u}{k_u} \quad (\text{VI.6})$$

Due to selective spin-orbit coupling $|N_z - N_y|$ may be one order of magnitude larger than the difference at higher temperature (spin polarization). For this reason ODMR experiments are usually performed at a temperature as low as possible, usually 1.2 K.

VI.3 Microwave induced delayed phosphorescence (MIDP)

MIDP is a technique, developed by Schmidt, Antheunis, Veeman and Van der Waals [Sc69, Sc71] for measuring the populating and depopulating rates of the individual triplet spin components. The experiments must be performed in a temperature region where spin-lattice relaxation is negligible during the triplet lifetimes and again one makes use of the

different decay constants of the various triplet sublevels. In a MIDP-experiment, however, the dynamics are studied in a time-resolved fashion.

VI.3.1 Determination of the absolute decay rates k_U

To start one creates a steady-state situation by irradiating the sample with a continuous light source. A fast shutter is then used to cut off the exciting beam at time $t = 0$. The phosphorescence intensity, which is monitored e.g. with a signal averager, decays rapidly due to the quick disappearance of the population from the short living radiative levels ($|z\rangle$ and $|y\rangle$ in the case of DBN). The remaining intensity on a longer timescale comes from the "non-radiative" level $|x\rangle$, which has still a large population. Then at a time $t = t_1$ long compared with the decay times k_z^{-1} and k_y^{-1} (e.g. $t = 5 k_z^{-1}$) the population of the radiative levels is considered to be (approximately) zero and a microwave field is suddenly switched on resonant with for example the Z-X transition. As a result population will be transferred from $|x\rangle$ to $|z\rangle$ and a sharp increase of the phosphorescence intensity will be observed (Fig. VI.2). The leading edge of this "delayed signal" is given by

$$\begin{aligned}
 h_{xz}(t_1) &= c \cdot f_{xz} \cdot \{N_x(t_1) - N_z(t_1)\} (k_z^r - k_x^r) \\
 &\approx c \cdot f_{xz} \cdot N_x(t_1) (k_z^r - k_x^r) \\
 &= c \cdot f_{xz} \cdot N_x(0) e^{-k_x^r t_1} (k_z^r - k_x^r)
 \end{aligned}
 \tag{VI.7}$$

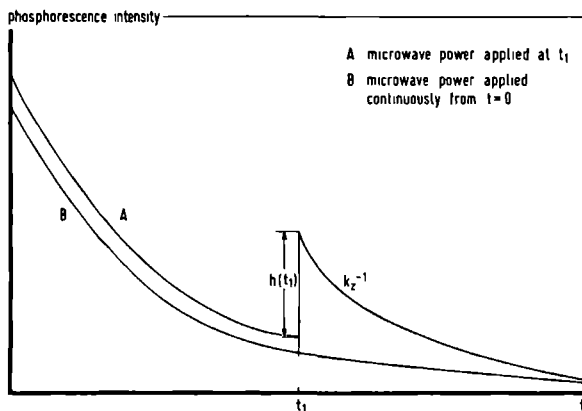


Fig. VI.2
Schematic diagram of a MIDP experiment.

c is an instrumental constant and f_{xz} is a transfer factor representing the number of molecules transferred from $|x\rangle$ to $|z\rangle$. f_{xz} strongly depends on the microwave power. If $f_{xz} = 0$ no molecules are transferred, if $f_{xz} = 1$ all molecules are transferred. One can obtain k_x by repeating the experiment for different values of t_1 and plotting $\log h_{xz}(t_1)$ against t_1 , for $t_1 > 5 k_z^{-1}$.

After the microwave pulse the $|z\rangle$ level is the only radiative level that is populated. Therefore the value of k_z can be determined from the tail of the delayed signal (Fig. VI.2). In a similar way one determines k_y .

VI.3.2 Determination of the relative decay rates k_i^r

To obtain the relative values of the radiative decay constants, first the transfer factors must be known. These are easily obtained by modifying the experiment displayed in Fig. VI.2 in such a way that two consecutive microwave pulses are given at times t_1 and t_2 , such that $t_2 - t_1 \geq 5 k_z^{-1}$.

Then, the population in the non-radiative level $|x\rangle$ just before t_2 is given by

$$N_x(t_2) = (1 - f_{xz})N_x(t_1)e^{-(t_2-t_1)k_x} \quad (\text{VI.8})$$

and consequently the leading edge of the delayed signal at t_2 is given by

$$h_{xz}(t_2) = c.f_{xz} \cdot (1 - f_{xz})N_x(t_1)e^{-(t_2-t_1)k_x}(k_z^r - k_x^r) \quad (\text{VI.9})$$

The transfer coefficient is now obtained from the ratio of $h_{xz}(t_2)$ and $h_{xz}(t_1)$

$$(1 - f_{xz}) = \frac{h_{xz}(t_2)}{h_{xz}(t_1)} e^{(t_2-t_1)k_x} \quad (\text{VI.10})$$

To determine k_x^r one continuously saturates the Z-X transition. Due to the leak via the radiative $|z\rangle$ level also the non-radiative $|x\rangle$ level will be empty in a time $\sim 5 k_z^{-1}$ (curve B in Fig. VI.2). The intensity difference

between the curves A and B in Fig. VI.2 just before the delayed signal, is caused by the fact that in curve B the $|x\rangle$ level is empty, while this is not true for curve A. Therefore:

$$A(t_1) - B(t_1) = c \cdot N_x(t_1) k_x^r \quad (\text{VI.11})$$

By combining equations (VI.7) and (VI.11) one can determine k_x^r/k_z^r . In a similar way one obtains k_x^r/k_y^r . Unfortunately, absolute values for k_u^r cannot be determined with this technique.

VI.3.3 Determination of the relative steady state populations $N_u(0)$

A general expression, which contains the relative magnitudes of $N_x(0)$, $N_y(0)$ and $N_z(0)$ can be obtained with the aid of the total phosphorescence intensity at time $t = 0$, $I(0)$:

$$I(0) = c(N_x(0)k_x^r + N_y(0)k_y^r + N_z(0)k_z^r) \quad (\text{VI.12})$$

The ratio of equations (VI.12) and (VI.7) subsequently gives

$$\frac{I(0)}{h_{xz}} = \frac{1}{f_{xz}} \cdot \frac{\frac{k_x^r}{k_z^r} + \frac{N_y(0)k_y^r}{N_x(0)k_z^r} + \frac{N_z(0)}{N_x(0)}}{e^{-k_x t_1} \left(1 - \frac{k_x^r}{k_z^r}\right)} \quad (\text{VI.13})$$

In contrast to the systems studied by Schmidt et al. the DBN system has two radiative levels ($|z\rangle$ and $|y\rangle$) instead of one. Therefore one cannot determine $N_x(0)/N_y(0)$ from the MIDP-signals taken from the X-Z and Y-Z transitions, as is the case for two non-radiative levels, $|x\rangle$ and $|y\rangle$. A sweep through the X-Z and X-Y resonances in our case yields the same information on the population of the one non-radiative level. Therefore we need an extra experiment to determine the relative magnitude of $N_x(0)$, $N_y(0)$ and $N_z(0)$. To do this we first create a steady-state situation by continuous

illumination. Then during the illumination a microwave pulse is given. At the moment of the microwave pulse we have a steady-state population over the triplet sublevels. The change in phosphorescence intensity immediately after the pulse is given by:

$$\Delta_{xz} = d.f. \frac{d}{dx} [k_z^r - k_x^r] [N_x(0) - N_z(0)] \quad (\text{VI.14a})$$

$$\Delta_{xy} = d.f. \frac{d}{dy} [k_y^r - k_x^r] [N_x(0) - N_y(0)] \quad (\text{VI.14b})$$

for the X-Z and X-Y transition, respectively; d is an instrumental constant. Combining equation (VI.13) with the ratio of Δ_{xz} and Δ_{xy} gives the relative steady-state populations. Again, the absolute populations cannot be determined with this technique.

VI.3.4 Determination of the relative populating rates $P_u(0)$

In equation (VI.6) the relation was given between the steady-state populations $N_u(0)$, the absolute decay constants k_u , and the relative populating rates $P_u(0)$:

$$N_u = \frac{P_u}{k_u} \quad (u = x, y, z) \quad (\text{VI.6})$$

Since we know the values for the parameters $N_u(0)$ and k_u we can calculate the relative populating rates $P_u(0)$.

VI.4 The DBN case

Electron spin resonance (ESR) and optically detected magnetic resonance (ODMR) techniques have been used to study triplet excitons [Sc74] and traps [Ni75] in the DBN system. In contrast to the finding in TCB, triplet exciton ODMR spectra of DBN, remarkably, can only be obtained in a magnetic field [Sc72]. Whether or not the presence of various different excitons and trap-like states very close to the exciton origin play a crucial role in this peculiar behaviour, is not immediately clear.

In addition to zero-field ODMR work on localized states by other authors [Ni75] we want to present in this chapter zero-field ODMR and MIDP data on DBN traps, that provide extra proof for the existence of excitons with an extremely short lifetime ($\ll 1 \mu\text{s}$). It will be shown, that the relative trap populating rates, P_u , for all deep traps are very different for the different triplet sublevels. Since the fine structure tensor axes of traps and exciton are almost coincident, these populating rates depend solely on the relative populations in the exciton sublevels at the moment of trapping. Therefore it will be concluded that the excitons live so short that the population in the exciton sublevels cannot reach a Boltzmann equilibrium during their lifetime.

VI.5 Results and discussion

ODMR and MIDP experiments were performed on the trap states at 20056.1 cm^{-1} , 20006.1 cm^{-1} and 20166.7 cm^{-1} , 20157.4 cm^{-1} in the vapour grown and Bridgman grown crystals respectively (see Fig. IV.1). No zero-field ODMR signals could be obtained from the trap-like states at 20190.6 cm^{-1} in the Bridgman grown crystals. ODMR experiments on these states in a low magnetic field were also unsuccessful, probably due to experimental difficulties causing a too weak intensity of the exciting beam.

Table VI.1 gives the zero-field splitting parameters at 1.4 K (in MHz) observed for the four traps mentioned above.

Table VI.1 *Zero-field splitting parameters (in MHz) for several DBN traps in neat crystals at 1.4 K.*

O-O band cm^{-1}	20056.1	20006.1	20166.7	20157.4
$ D + E $	2856	2839	2816	2994
$ D - E $	2764	2761	2704	2686
$ D $	2810	2800	2760	2840
$ E $	46	39	56	154

Table VI.2 *Kinetic parameters for different DBN traps at 1.4 K.*

<i>0-0 band, cm⁻¹</i>	<i>20056.1</i>	<i>20006.1</i>	<i>20166.7</i>	<i>20157.4</i>
k_z, s^{-1}	288	315	340	238
k_y, s^{-1} ($\pm 10\%$)	320	410	355	214
k_x, s^{-1}	10.8	13.9	10.8	7.3
k_z^r	110	8	70	6
k_y^r ($\pm 20\%$)	80	27	71	8
k_x^r	1	1	1	1
$N_z(0)$	0.3	0.1	0.5	0.8
$N_y(0)$ ($\pm 20\%$)	0.4	0.8	0.7	1
$N_x(0)$	1	1	1	1
P_z	8	10	15	25
P_y ($\pm 20\%$)	12	23	22	29
P_x	1	1	1	1

The data presented in this table qualitatively agree with the values obtained by other authors [Ni75,La80] for similar traps in DBN. Except for the trap at 20157.4 cm^{-1} a very small $|E|$ value is observed (46 - 56 MHz). By means of the MIDP method we determined the total decay rate constants (k_u), the relative radiative rate constants (k_u^r), the relative populations ($N_u(0)$) and the relative populating rates (P_u) of the triplet sublevels at 1.4 K. These are listed in Table VI.2. The labels of the triplet sublevels are chosen according to Mulliken's notation for C_{2v} -symmetry. The out-of-plane molecular axis is therefore taken to be the x-axis whereas the z-axis is the C_2 -symmetry axis. The DBN molecule in the ground state is known to be absolutely planar [Be78]. If the molecule in the excited state would retain C_{2v} -symmetry, then simple symmetry and spin-orbit coupling considerations would predict only $|z\rangle$ to be radiative. However, it is found that also k_y^r is not negligible, which shows that the molecule in the excited state is distorted. The values for the radiative decay constants vary drastically for the different traps. This is not unexpected when

structural distortions in the excited state play such an important role. The most interesting conclusions may be drawn from the values for the relative populating rates, P_u . The spin population in a particular triplet exciton sublevel is transferred to the different sublevels in a trap at a rate, which is proportional to the squared direction cosines relating the fine structure axes of the exciton to the axes of the trap, when the trapping process occurs randomly with respect to the Larmor precession [Br78]. In DBN the trap fine structure axes are almost coincident with those of the exciton [Sb74]. Our trap populating rates, P_u , were defined, as usual [Sm71], as the product of the trap steady-state population $N_u(0)$ and the trap total decay rate k_u . With this definition the relative trap populating rates P_u in DBN are proportional to the relative steady-state populations in the exciton sublevels. Table VI.2 shows that for all traps $P_z \sim P_y$ but very different from P_x . Therefore we may conclude that the triplet sublevels populations of the excitons, which are trapped at these traps, are about equal for the $|z\rangle$ and $|y\rangle$ sublevels but very different from the population of sublevel $|x\rangle$. Consequently, no Boltzmann equilibrium can exist between the exciton spin levels, proving that the lifetime of these levels is shorter than the spin-lattice relaxation time for transitions between them (The exciton T_1 in DBN was measured to be $15 \mu\text{s}$ in a magnetic field at 1.3 K [Sb74]). In fact, the relative populating rates of the trap are very much like what is expected for the populating rates of the exciton sublevels on the basis of selective spin-orbit coupling, assuming that also in the exciton state C_{2v} -symmetry no longer describes the molecule. On the other hand, it was concluded from magnetic field experiments on the triplet exciton phosphorescence emission [Sb74] that a Boltzmann equilibrium does exist over the magnetic sublevels in a magnetic field. This apparent contradiction can be explained by our finding that in DBN different triplet excitons exist simultaneously with very different lifetimes. Long-lived excitons are responsible for the phosphorescence emission. A Boltzmann distribution exists between the triplet sublevels of these excitons. As shown in the previous chapters, also triplet excitons exist with an extremely short lifetime ($< 1 \mu\text{s}$). It was proved that the latter species are mainly responsible for populating the traps studied here. Therefore these findings are completely in agreement with the conclusions obtained now from the values of the relative populating

rates, showing that these excitons are trapped so quickly, that no Boltzmann equilibrium over the triplet sublevels can be reached within their lifetime. These experiments therefore support our previous conclusion that excitons exist in DBN with an extremely short lifetime.

VI.6 References

- [Be78] J.C. Bellows, E.D. Stevens, P.N. Prasad, Acta Cryst. B34, 3256 (1978).
- [Br78] H.C. Brenner, J.C. Brock, C.B. Harris, Chem. Phys. 31, 137 (1978).
- [La80] K.J. Latas, J. Simons, A.M. Nishimura, J. Photochem. 12, 161 (1980).
- [Ni75] A.M. Nishimura, A.H. Zewail, C.B. Harris, J. Chem. Phys. 63, 1919 (1975).
- [Sb74] R. Schmidberger, Ph.D. Thesis, University of Stuttgart (1974).
- [Sc69] J. Schmidt, W.S. Veeman, J.H. v.d. Waals, Chem. Phys. Lett. 4, 341 (1969).
- [Sc71] J. Schmidt, D.A. Antheunis, J.H. v.d. Waals, Mol. Phys. 22, 1 (1971).
- [Sc72] R. Schmidberger, H.C. Wolf, Chem. Phys. Lett. 16, 402 (1972).
- [Sc74] R. Schmidberger, H.C. Wolf, Chem. Phys. Lett. 25, 185 (1974).
- [Sm71] J. Schmidt, Ph.D. Thesis, University of Leiden (1971).

**MAGNETIC FIELD EFFECTS ON 1,4-DIBROMONAPHTHALENE
PHOSPHORESCENCE EMISSION**

VII.1 Introduction

Experiments on the phosphorescence emission of DBN have been performed in a 6 MW Bitter coil of the Nijmegen High Magnetic Field Laboratory. In the experiments to be described in this chapter we will neglect the influence of the zero-field splitting since the Zeeman splitting dominates in the large fields that were used. In fact, the value of the Zeeman energy, $g\beta B$, increases approximately 1 cm^{-1} for every 1 Tesla ($= 10 \text{ kG}$) magnetic field increase. This implies, that the upper ($|+1\rangle$) and lower ($|-1\rangle$) Zeeman component of a triplet state molecule will be split $\sim 30 \text{ cm}^{-1}$ in energy in a field of 15 Tesla! Consequently, in a field where the Zeeman splitting is larger than the optical linewidth of the three components, one may observe the emission from the three Zeeman components separately, provided that enough population is present in the different levels (Fig. VII.1).

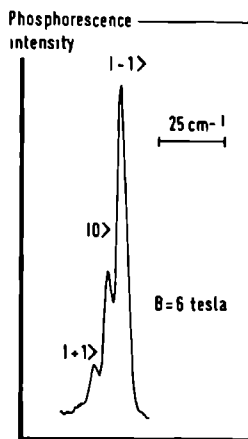


Fig. VII.1

Phosphorescence emission spectrum of the first vibration of the trap at 20006.1 cm^{-1} (vapour-grown crystal) in a field of 6 Tesla.

Our first goal was to make use of the possibility to shift the triplet energy levels over relatively large energy regions. In particular we wanted to study the effect on the trapping dynamics when the $|+1\rangle$ Zeeman component

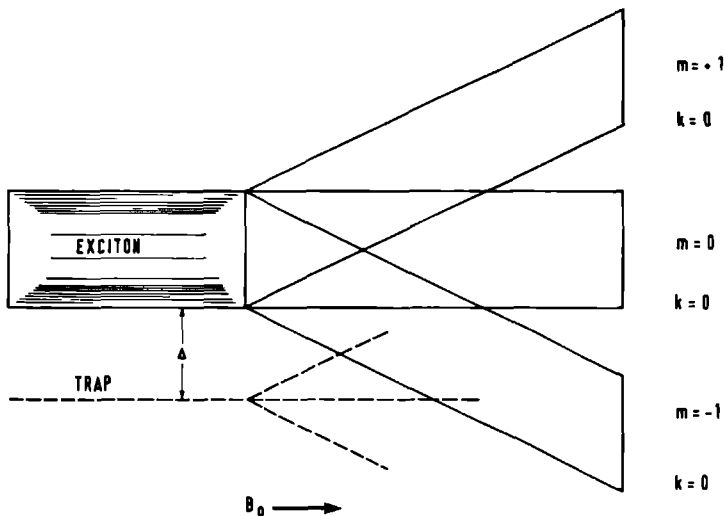


Fig. VII.2 The crossing of energy levels from exciton and a trap due to the Zeeman effect. For different trap depths Δ , these crossings will occur at different values of B_0 .

of the trap at 20166.7 cm^{-1} (EM3) was made to cross the $| -1 \rangle$ Zeeman component of the exciton band (Fig. VII.2). The energy distance between the two approaching levels decreases with $\sim 2 \text{ cm}^{-1}$ per Tesla field and as a result the crossing would occur at ~ 13 Tesla. It is known, that in a normal situation spin angular momentum is conserved in the trapping of triplet excitons [Sh71]. The question was if in this case there would be a spin-dependent interaction which mixes the lowest Zeeman component of the exciton band with different Zeeman components of a trap. If such an interaction would be relatively strong, a change in trapping probability could occur as the result of a level anticrossing effect (LAC), somewhat related to the level anticrossing effect between different Zeeman levels of one triplet state [Ve70]. This would then result in an observable increase in phosphorescence intensity of the trap.

However, these experiments were unsuccessful and no such LAC effect could be detected. Nevertheless, a strong field dependent increase of the emission intensity of the trap-like state (EM2) at 20190.6 cm^{-1} was observed. It appears that triplet-triplet annihilative processes are strongly affected

Phosphorescence intensity

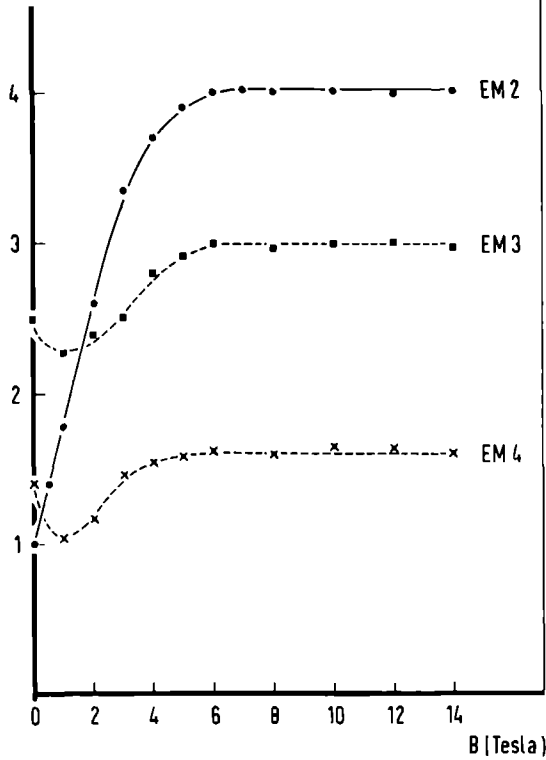
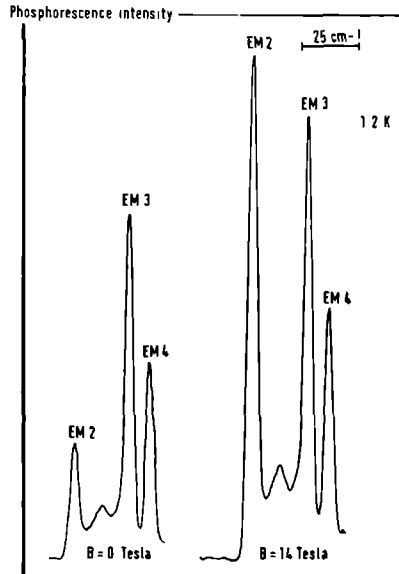


Fig. VII.3

The behaviour of the relative steady state $DBN-h_6$ phosphorescence emission intensity, ϕ_{rel} , in a static magnetic field for an arbitrary orientation of the crystal. Excitation is performed by means of a mercury arc.

Fig. VII.4

The increase of EM2-phosphorescence emission intensity when a large magnetic field is applied.



by the large fields and influence the EM2-emission intensity. Furthermore magnetic field effects were observed in time-resolved experiments.

VII.2 Steady state experiments

In Fig. VII.3 the magnetic field dependent changes in the total phosphorescence intensity of the traps at 20166.7 cm^{-1} (EM3), 20157.4 cm^{-1} (EM4) and the emission of the trap-like states near the origin (EM2) are indicated. Continuous irradiation with a mercury arc was used. In these experiments the monochromator slits were opened to $200 \text{ }\mu\text{m}$ to increase the light intensity at the photomultiplier. Therefore the emission of the excitons (EM1) and the trap-like states (EM2) could not be observed separately. However, the total emission at low temperature ($T < 2 \text{ K}$) in good approximation represents the emission of the trap-like states, because their emission intensity is then much stronger than the excitonic intensity. This was confirmed by high field time-resolved experiments. The magnetic field effect is also present at 4.2 K but the magnitude of the effect is strongly reduced.

Fig. VII.3 is typical for an arbitrary orientation of the crystal. The graph shows a very strong field dependent increase of the EM2 emission intensity. This increase is also illustrated in Fig. VII.4. For most crystals the maximum value is reached around 8 Tesla. The magnitude at maximum field may be as much as 400 to 500% of the zero-field value. When the crystal is rotated in this field an anisotropy is observed, the size of which corresponds to changes in the radiative rate constants caused by the magnetic field.

No such magnetic field effects are observed in crystals doped with 15% perdeuterodibromonaphthalene (DBN-d₆). This doping, however, strongly increases the intensity of the exciton emission in zero-field, as was discussed in Chapter IV. Another difference with pure crystals is the absence of delayed fluorescence in doped crystals, in spite of the increased exciton emission. As mentioned in Chapter IV Bridgman grown *aoped* crystals show only very weak emission from shallow trap-like states, whereas in vapour grown doped crystals these states are completely absent. This explains the absence of delayed fluorescence in doped crystals, because delayed fluorescence in our crystals occurs from annihilation of excitons and shallow trap-like states.

The absence of magnetic field effects in doped crystals, together with the observation that in doped crystals no delayed fluorescence occurs, makes it very likely, that the magnetic field dependent EM2-emission intensity finds its explanation in a magnetic field dependent triplet-triplet annihilation. In an attempt to describe the consequence of this field dependent annihilation for the EM2 phosphorescence intensity, we assume that spin-lattice relaxation is fast enough to obtain a Boltzmann distribution over the three Zeeman levels of both the triplet exciton and the trap EM2. In the limit of fast enough spin-lattice relaxation the triplet decay in zero-field is described by a single total decay constant, which is the average of the three constants,

$$k_T = \frac{(k_x + k_y + k_z)}{3} \quad (\text{VII.1})$$

Then, for the concentration $[T^*]$ of the shallow trap-like states EM2 we can write in zero-field:

$$\frac{d[T^*]}{dt} = k_i [E] - (k_T + k_0) [T^*] - \gamma_B (B = 0) [T^*][E] \quad (\text{VII.2})$$

where k_i and k_0 represent the trapping and detrapping rate constant, respectively; $[E]$ gives the total concentration of those excitons (lifetime 40 μ s) that may populate the EM2 state and are responsible for delayed fluorescence, γ_S is the rate (equation II.53) describing the annihilation via the singlet channel. In principle triplet-triplet annihilation can lead to an excited singlet molecule, an excited triplet molecule or an excited quintet molecule. Excited quintet molecules require the simultaneous presence of two excited electrons on one molecule and are energetically inaccessible. Annihilation via the triplet channel is most likely to generate a vibrationally excited EM2 triplet state [Sw73] and is not expected to influence the EM2 phosphorescence intensity. Thus, only annihilation via the singlet channel, leading to delayed fluorescence, is considered. For steady-state conditions the zero-field phosphorescence yield of the EM2 state is given by

$$\phi_T(0) = k_T^r [T^*] = \frac{k_T^r k_i [E]}{k_T + k_0 + \gamma_S(B=0) [E]} \quad (\text{VII.3})$$

In a magnetic field we can write a similar rate equation for the EM2 state:

$$\begin{aligned} \frac{d[T^*]}{dt} = & k_i [E] - k_0 [T^*] - \left(\frac{\alpha^2}{z} k^+ + \frac{\alpha}{z} k^0 + \frac{1}{z} k^- \right) [T^*] \\ & - \gamma_S(B) [T^*] [E] \end{aligned} \quad (\text{VII.4})$$

where

$$\alpha = \exp\left(-\frac{g\beta B}{kT}\right) \quad (\text{VII.5})$$

$$[T_{+1}^*] = \frac{\alpha^2}{z} [T^*] \quad (\text{VII.6})$$

$$[T_0^*] = \frac{\alpha}{z} [T^*] \quad (\text{VII.7})$$

$$[T_{-1}^*] = \frac{1}{z} [T^*] \quad (\text{VII.8})$$

$$z = 1 + \alpha + \alpha^2 \quad (\text{VII.9})$$

As discussed in Chapter II γ_S is field-dependent, starting from zero-field γ_S first increases, then decreases and levels off at intermediate fields (~ 1 Tesla). At higher fields γ_S decreases to zero, see Fig. II.4.

According to equation II.56 above intermediate fields $\gamma_S(B)$ is given by:

$$\gamma_S(B) = \frac{\alpha^2}{z} k_1 \left(\frac{\frac{1}{3} k_2}{k_{-1} + \frac{1}{3} k_2} + \frac{\frac{2}{3} k_2}{k_{-1} + \frac{2}{3} k_2} \right) = \frac{\alpha^2}{z^2} k_S \quad (\text{VII.10})$$

By using this expression which was derived in Chapter II for homofusion, we assume that the triplets involved in the annihilation process, EM2 and excitons with a 40 μ s lifetime, are equivalent with respect to zero-field splitting. In order to keep the description simple we assume for both the total (k^i) and radiative constants (k_T^i), that for a general orientation of

the crystal with respect to the magnetic field:

$$k_{(r)}^+ \approx k_{(r)}^0 \approx k_{(r)}^- = k_B^{(r)} \quad (\text{VII.11})$$

An expression can be derived now for the total phosphorescence yield in a magnetic field in steady-state:

$$\phi_T(B) = k_B^r [T^*] = \frac{k_B^r k_i [E]}{k_B + k_0 + \frac{\alpha}{2} k_S [E]} \quad (\text{VII.12})$$

The relative phosphorescence yield is given by:

$$\phi_{\text{rel}} = \frac{\phi_T(B)}{\phi_T(0)} = \frac{1}{P_1 + P_2 \frac{\alpha}{2}} \quad (\text{VII.13})$$

where

$$P_1 = \frac{k_T^r (k_B + k_0)}{k_B^r (k_T + k_0 + \gamma_S (B=0) [E])} \quad (\text{VII.14})$$

$$P_2 = \frac{k_T^r k_S [E]}{k_B^r (k_T + k_0 + \gamma_S (B=0) [E])} \quad (\text{VII.15})$$

The total steady-state exciton concentration is not very much magnetic field dependent. In our situation triplet-triplet annihilation does not largely influence the steady-state exciton concentration, because the exciton lifetime is determined almost exclusively by trapping. We therefore take $[E]$ to be magnetic field independent. For the EM2 state this is different. Annihilation cannot be neglected compared to other EM2 decay channels, since the lifetime of EM2 is much longer than the exciton lifetime.

The parameter P_1 determines the magnitude of the magnetic field effect at an infinitely high field ($B \rightarrow \infty$, $\alpha \rightarrow 0$). The parameter P_2 determines the shape of the curve presented for the EM2 states in Fig. VII.3. Adjustment of the unknown parameters P_1 and P_2 by means of a fitting procedure gives quantitative agreement with the experimental curve. It is obvious from equations VII.13 - VII.15 that the curve should be sensitive to the orientation of the field and to the intensity of the exciting beam. Both facts were experimentally observed.

Whiteman [Wh71] has reported results very similar to those of Fig. VII.3. He claimed that the exciton emission increases with the field, but in view of the experiments described previously in this thesis, it seems very likely, that Whiteman's excitons correspond to states similar to our EM2. Whiteman also tried to explain the magnetic field dependent emission intensity as the result of a magnetic field dependent triplet-triplet annihilation but the outcome was not very satisfying. A numerical calculation of the field dependence did not show any correspondence with the experimental results and reliable fits could not be obtained.

All our experiments can be explained quantitatively on the basis of the simple kinetic model presented above. Fitting the results for EM2 in Fig. VII.3 with equation VII.13 results in parameter values of $P_1 = 0.25$ and $P_2 = 1.04$. From these values it can be extracted that $k_S[E]/(k_B + k_0) \approx 4$, showing that annihilation is a major competing process in the decay of the EM2 state. In simple words, the increase of the EM2 phosphorescence intensity at high magnetic field is caused by the decrease of delayed fluorescence. Delayed fluorescence removes not only EM2 traps but also excitons capable of populating EM2 at a later time. A decrease of delayed fluorescence therefore causes a strong increase of EM2 phosphorescence.

VII.3 Time-resolved experiments

The above discussed steady-state experiments showed that in a magnetic field more quasi-local states EM2 become available for phosphorescence. The large increment of EM2 phosphorescence intensity in a magnetic field also influences the trapping dynamics. Fig. VII.5 shows for the trap at 20157.4 cm^{-1} (EM4) the effect of a large magnetic field on the build-up rate of the population after a nitrogen laser pulse at 1.5 K. At zero

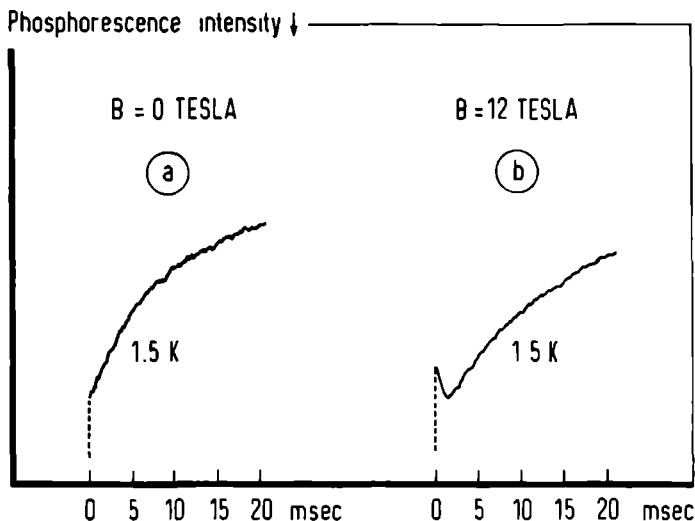


Fig. VII.5
The effect of a large magnetic field on the build-up rate of the EM4-population after a nitrogen-laser pulse at 1.5 K.

magnetic field the population of this trap is present within $1 \mu\text{s}$ after the nitrogen laser pulse. This is shown in Fig. VII.5 A. This implies that under these conditions excitons with a lifetime of $< 1 \mu\text{s}$ populate this trap for 100%. An additional slow build-up component becomes apparent, when the field increases (Fig. VII.5B). Although observable in a field of 1 to 2 Tesla, the effect becomes maximal at ~ 12 Tesla. Then 20% of the population builds up via the slow rate process. At this temperature (1.5 K) the time constant for the slow build-up is 400 - 500 μs and equals the lifetime of the EM2 state in the magnetic field (The EM2 lifetime is longer in a magnetic field than in the absence of a magnetic field). When the crystal is rotated in the field an anisotropy in the intensity of the slow build-up component is observed. This effect proceeds parallel to the changes in the steady-state EM2 emission intensity, when the crystal is rotated.

These observations show that deeper traps obtain population not only from excitons but also from EM2 states, when enough EM2 population is available. This is the case in a magnetic field, where the EM2 population is strongly enhanced. The trapping route from EM2 could proceed either via first detrapping or directly via long range interactions.

Much more complicated are the results obtained for the temperature dependence of this effect (Fig. VII.6). In a high magnetic field the slow component of the EM4 build-up rate decreases in magnitude with increasing

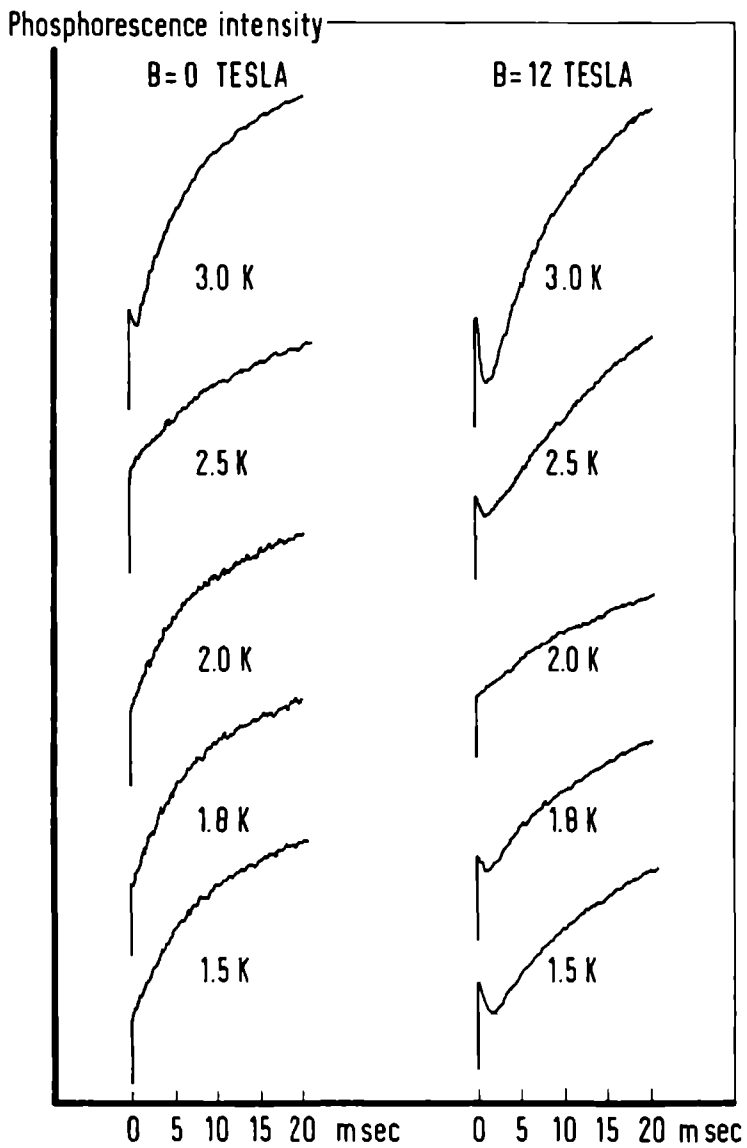


Fig. VII.6 *The temperature dependent time-resolved behaviour of the F_{M4} population after a λ_2 -laser pulse in zero-field (left part) and in high magnetic field (right part).*

temperature from 1.5 K until it has completely disappeared at 2.0 K. Increasing the temperature further makes the slow component to appear again, with a faster rate. This rate corresponds to the high temperature EM2 lifetime.

Since there is almost no temperature dependence of the zero field population build-up, the peculiar behaviour in a magnetic field most likely corresponds to properties of the EM2 state. A possible explanation may be found in the zero-field temperature dependent behaviour of the EM2 line position and line intensity. It was mentioned in Chapter IV, that the EM2 line position at 4.2 K was different from that at 1.2 K (20191.1 cm^{-1} and 20190.6 cm^{-1} , respectively). At 4.2 K the signal from the trap-like states is relatively weak and comparable to the intensity of the excitonic emission. Lowering the temperature until 2.0 K causes a decrease of the EM2-intensity. When the temperature is lowered further a huge increase of the EM2 emission intensity is observed and the low temperature line is found now at 20190.6 cm^{-1} .

In view of the temperature dependent time-resolved measurements described above, it is tempting to conclude, that it is probable that *two* different kinds of trap-like states are present close to the exciton band. One kind, found in the emission at 20190.6 cm^{-1} , is responsible for the slow component in the low temperature EM4 population build-up (1.2 K). A different kind, found in the emission at 20191.1 cm^{-1} , is responsible for the slow component found at 4.2 K. The curve presented in Fig. VII.6 for the behaviour at 2.0 K (no slow component present) then corresponds to the situation, where neither of the two kinds of trap-like states has enough population to influence the EM4 population build-up. No further evidence is available though, to confirm this qualitative explanation.

A time-resolved study of the EM3 population in large magnetic fields reveals similar effects as the study on the EM4 population. The results on EM3 are very irreproducible, though, and qualitatively vary considerably for different crystal specimens used. Therefore no further details on the study of the EM3 state will be presented.

VII.4 References

- [Sh71] M. Sharnoff, E.B. Iturbe, Phys. Rev. 27, 576 (1971).
- [Sw73] C.E. Swenberg, N.E. Geacintov, in "Organic Molecular Photophysics",
vol. 1, Wiley and Sons (1973).
- [Ve70] W.S. Veeman, J.H. v.d. Waals, Chem. Phys. Lett. 7, 65 (1970).
W.S. Veeman, J.H. v.d. Waals, Mol. Phys. 18, 63 (1970).
- [Wh71] J.D. Whiteman, Ph.D. Thesis, University of Pennsylvania (1971).

PHYSICAL AND CHEMICAL IMPURITIES IN DBN

VIII.1 Effects of different crystal growing techniques

The main effort of the previous chapters was concentrated on properties of Bridgman grown DBN-crystals. Phosphorescence emission spectra obtained from these crystals showed close resemblance with the spectra presented in the literature previously. At 4.2 K excitonic emission as well as emission from deep traps may be observed. We found, that at low temperatures (1.2 K) the pure excitonic emission ($\sim 20193 \text{ cm}^{-1}$) was extremely reduced in intensity in our crystals. Instead, strong emission was observed from trap-like states appearing very close to the exciton origin (20190.6 cm^{-1}). At this temperature the emission intensity of shallow traps with a trap depth in the order of $20 - 40 \text{ cm}^{-1}$ is very intense, whereas the emission from the deep traps has almost disappeared from the spectrum. Deep traps, apparent at 4.2 K, however, should act as even better traps at 1.2 K. Therefore it must be concluded that there are more shallow traps present than deep traps.

An interesting feature, which was not discussed in the previous chapters, is the fact that it is possible to *increase* the number of shallow traps by growing the crystals in narrower tubes. If the tube diameter becomes smaller than 6 mm shallow trap emission is observed even at 4.2 K. This fact suggests that the presence of shallow traps in DBN must be correlated with the physical perfection of the crystal rather than with the chemical purity. Since the Bridgman method for crystal preparation is fairly crude, we started to grow neat DBN crystals from solution and from the vapour.

Phosphorescence spectra of solution grown crystals (needles) are identical to those of melt-grown crystals, when the growing period is short (one day). At 1.2 K the spectra exhibit only shallow trap emission. No exciton emission can be detected between 4.2 K and 1.2 K. When the growing period is made longer (one week) shallow trap emission becomes weaker and two new traps are apparent at 20056.1 and 20006.1 cm^{-1} . Under extremely careful crystal growing conditions, where crystals were grown in

a period of several weeks by cooling down slowly a supersaturated solution, shallow trap emission can be removed completely from the spectrum. In the spectra from all solution grown crystals no exciton emission could be detected.

A much faster method to remove the shallow traps is the method of vapour growing. The spectra of crystals grown in three days show no trap emission for trap depths of 20 - 40 cm^{-1} . Only the two deep traps at 20056.1 and 20006.1 cm^{-1} are observed. Again no exciton emission could be detected. Increasing the vapour growth period to several weeks did not affect the emission spectra.

It is obvious that the physical perfection of the crystals has a large influence on the optical properties. However, the fact that also chemical impurities are present in Bridgman grown DBN crystals can be concluded from the observation that delayed fluorescence arises from an impurity molecule. In a substituted aromatic compound the most probable contaminations are expected to be isomers of the compound under study. For halogenated naphthalenes it is even known that isomerization of the pure compound can occur at higher temperatures (zone-melting!)[Lo30]. For this reason and also for the reason that we wanted to check if the model presented in this thesis would be applicable to other dibromonaphthalene systems, the isomers 1,5-dibromonaphthalene, and 1,8-dibromonaphthalene were synthesized [Wh51] .

VIII.2 The isomer 1,5-dibromonaphthalene

Crystals of 1,5-dibromonaphthalene are very disagreeable to handle. They have the shape of very thin films and crystallographic measurements appear to be difficult. The molecules are stacked in a similar fashion as in 1,4-DBN. Some important crystallographic data are summarized in Table VIII.1. Fig. VIII.1 shows the molecular packing in 1,5-DBN. The absorption of the first triplet state accidentally coincides with the $S_0 \rightarrow T_1$ absorption of the fully deuterated 1,4-DBN- d_6 analog and has an energy 65 cm^{-1} higher than the normal 1,4-DBN- h_6 isomer. The phosphorescence emission spectrum of a Bridgman grown crystal is displayed in Fig. VIII.2 and does not show excitonic emission. The vibrational pattern, that is observed in this phosphorescence emission spectrum, is also found

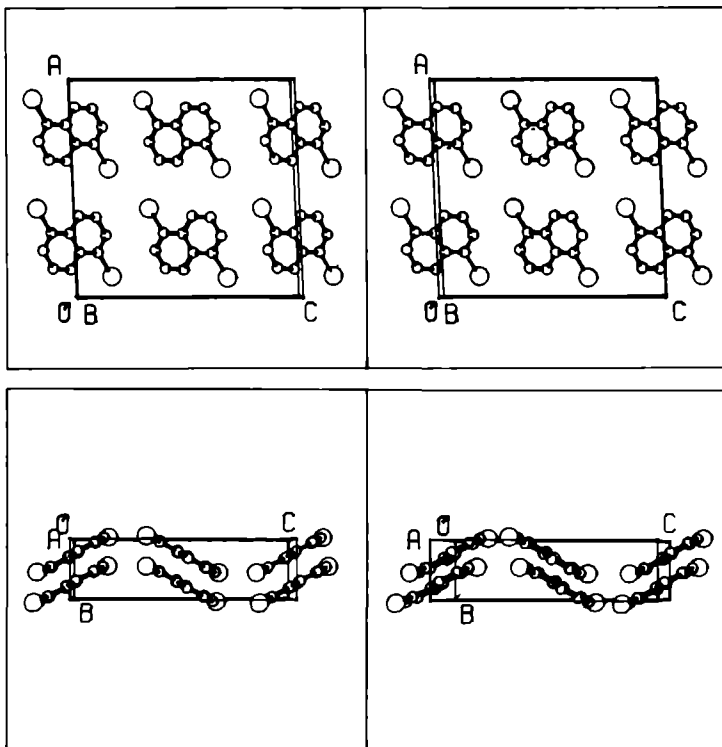


Fig. VIII.1 Stereoscopic views of the molecular packing in 1,5-dibromonaphthalene.

Table VIII.1 Crystal structure data of 1,5-DBN

Space group: C2/c
 Z: 4
 a(Å): 14.576
 b(Å): 4.049
 c(Å): 15.046
 β(°): 92.18

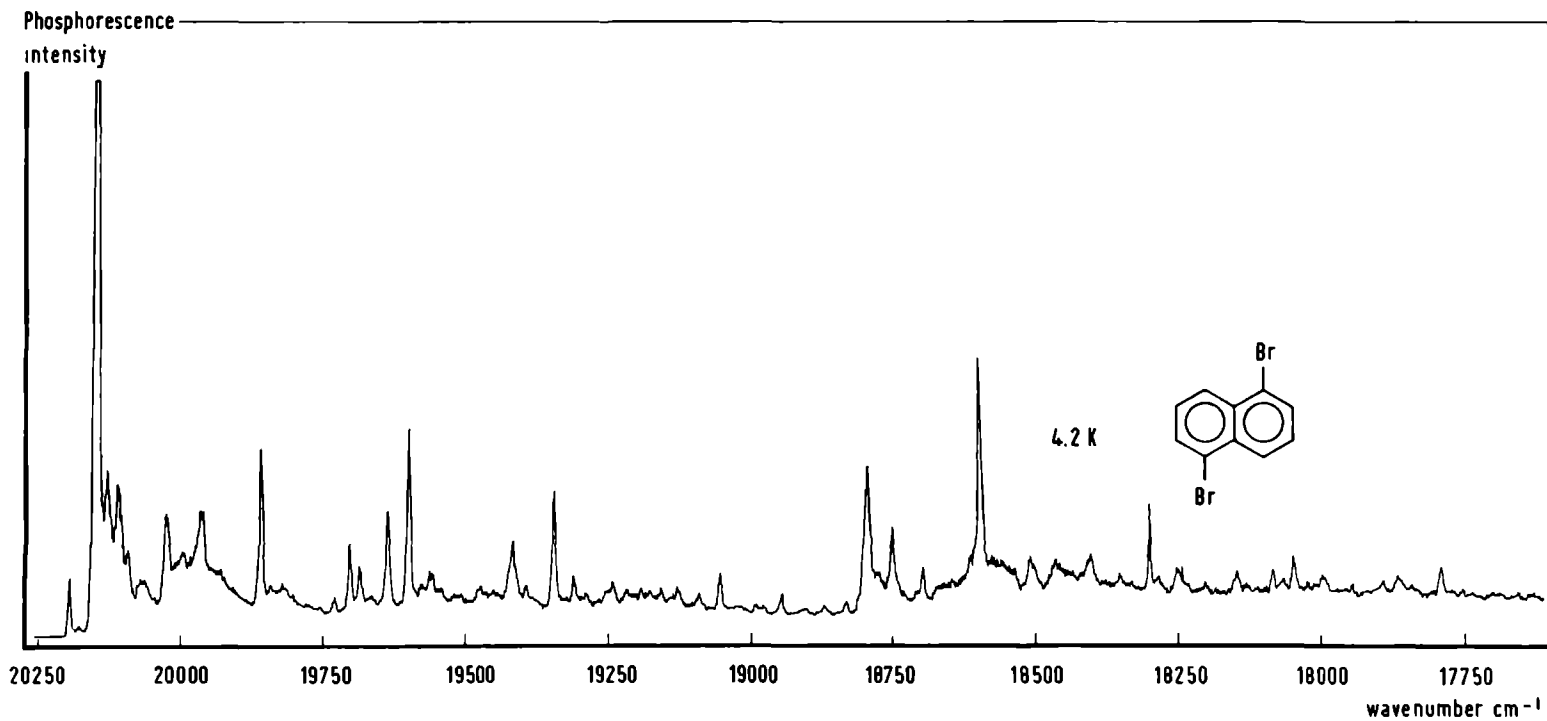


Fig. VIII.2 Phosphorescence emission spectrum of a Bridgman grown crystal of 1,5-DBN at 4.2 K.

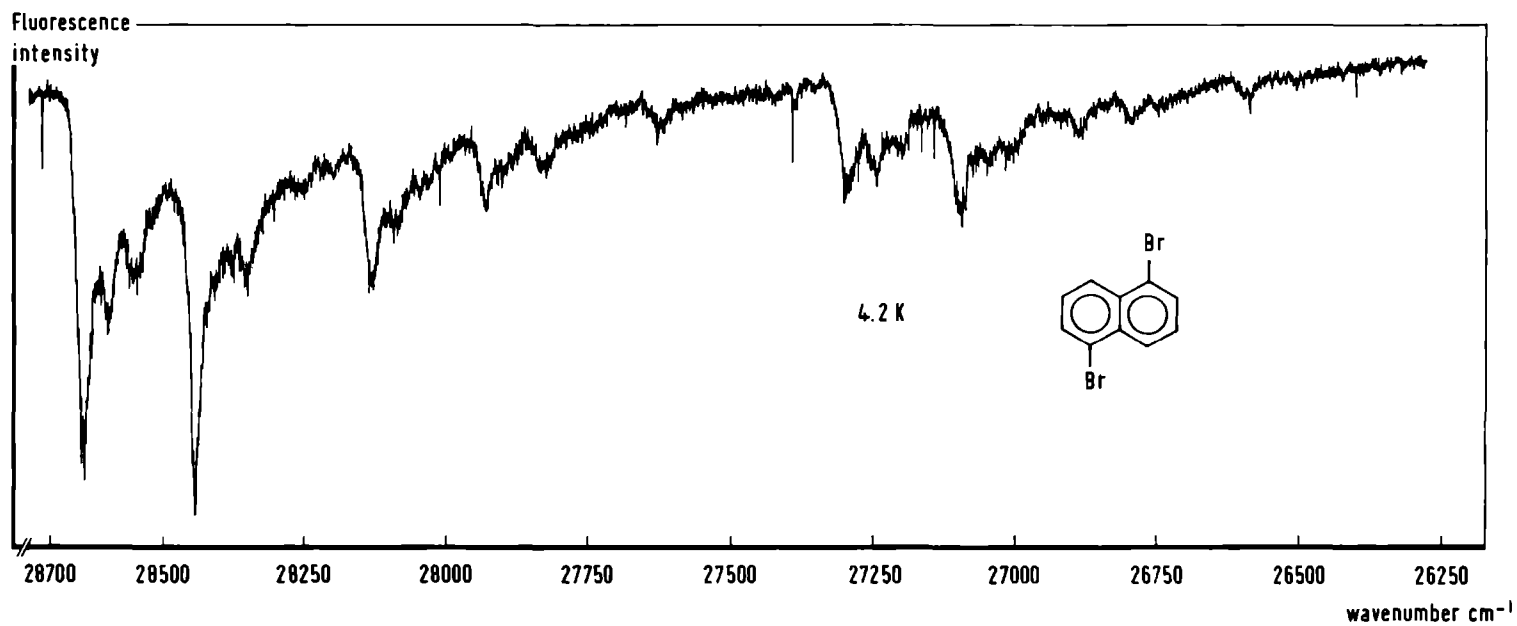


Fig. VIII.3 Fluorescence emission spectrum of a Bridgman grown crystal of 1,5-DBN at 4.2 K.

in the fluorescence emission spectrum (Fig. VIII.3), which indicates that both fluorescence and phosphorescence arise from 1,5-DBN molecules.

When we compare the fluorescence emission spectrum of Fig. VIII.3 with the spectrum found for the delayed fluorescence in 1,4-DBN (Fig. IV.7) we see that the spectra coincide almost exactly. Only the absolute energies are different due to the fact, that the two crystal lattices are different. This gives a strong indication, that the fluorescing species in 1,4-DBN is a 1,5-DBN molecule. To obtain additional proof for this hypothesis we isolated the second main component from the contaminated part at the bottom end of the zone-melting tube. Both ^1H - and ^{13}C -NMR spectra of this component were exactly identical with the NMR spectra of 1,5-DBN from independent synthesis. Therefore we conclude, that the zone-melting procedure does not remove all 1,5-DBN molecules from the 1,4-DBN system. The few remaining 1,5-molecules have a triplet state energy 65 cm^{-1} higher than 1,4-DBN. Consequently they can act as scattering barriers in the way described in previous chapters. EM2 trap states very close to the 1,4-DBN exciton origin were shown to be strongly involved in the triplet-triplet annihilation process. Since the phosphorescence emission from these states exhibits the typical 1,4-DBN vibrations we propose that EM2 states correspond to 1,4-DBN molecules, that have a slight misorientation due to the fact that they are in the neighbourhood of a chain disrupting 1,5-DBN molecule.

VIII.3 The isomer 1,8-dibromonaphthalene

Crystals of 1,8-DBN can be grown easily and are of good quality. The crystal structure has not yet been solved, but the probable space group and cell dimensions are listed in Table VIII.2. The $S_0 \rightarrow T_1$ absorption occurs at a much lower energy than in 1,4-DBN, namely at 19585.6 cm^{-1} . For this reason it is not very likely, that the 1,8-DBN isomer will act as a scattering barrier in the 1,4-system.

The $S_0 \rightarrow T_1$ absorption coincides within our experimental accuracy ($\sim 0.3\text{ cm}^{-1}$) with the highest energy line in the phosphorescence emission spectrum (Fig. VIII.4). This is an indication that this particular emission line may originate from excitonic emission. The lack of crystallographic data prohibits a prediction on the dimensionality of the exciton.

Table VIII.2 *Crystal structure data of 1,8-DBN*

Space group: $P2_1/c$

Z: 4

a(Å): 8.0496

b(Å): 10.8984

c(Å): 11.0827

$\beta(^{\circ})$: 107.834

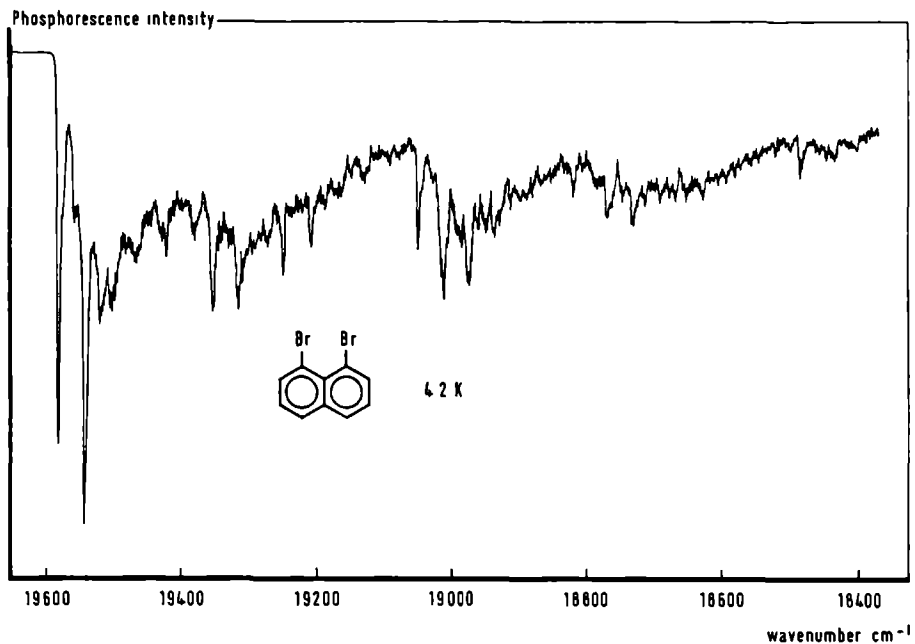


Fig. VIII.4 *Phosphorescence emission spectrum of a vapour grown crystal of 1,8-DBN at 4.2 K.*

The lifetime of the exciton phosphorescence varies for different crystals between 800 and 1000 μs . A trap at 19547 cm^{-1} builds up in $\sim 80\ \mu\text{s}$, showing again the presence of different excitons. In 1,8-DBN ODMR transitions can be detected between the exciton zero-field states, in contrast to 1,4-DBN. A strong transition is found at 3.8 GHz.

VIII.4 References

[Lo30] H. Lohfert, Ber. 63, 1939 (1930).

[Wh51] J.S. Whitehurst, J. Chem. Soc. 221 (1951).

SUMMARY

In the last decade linear triplet excitons have been investigated intensively. Until to date there is only a very limited number of well investigated systems, where the transfer topology is (quasi-) one-dimensional and 1,4-dibromonaphthalene (DBN) is one of them. The larger part of this thesis is dedicated to experiments on this particular compound.

Normally excitons are considered as collective excitations of the crystal as a whole and it is generally assumed, that to observe excitonic phosphorescence emission a crystal should be as perfect as possible. Of course this remains true in theory, but in practice the ideal perfect crystal is hard to obtain. Then, as shown in this thesis for DBN, the opposite of the above statement can be true: no exciton emission is observed in "perfect" crystals, grown from the vapour, whereas such emission is observed in less perfect crystals, grown from the melt.

In fact, it is described in this thesis that our DBN crystals, grown from the melt exhibit optical properties, which can be explained only by considering the crystal as a collection of 1-D-units ("cages"), strongly isolated from one another by high (triplet-) energy barriers. Optically accessible triplet excitons are found to exist simultaneously in different cages with different excitation frequencies and extremely different lifetimes.

When a trap is present in a cage, excitons generated within such cage will be very effectively trapped. Consequently, these excitons will have a very short lifetime. The probability of finding a trap in a cage will increase with increasing cagelength. This situation is most likely to be found in the more perfect vapour grown crystals where the 1-D-units may be rather large. Due to the very short exciton lifetime, no emission is observed from triplet excitons in these crystals.

For short chains the situation may occur that no traps are present. The lifetime of the exciton will become longer and emission may be observed when the lifetime is long enough. This situation is most likely to hold in melt-grown crystals. Ultimately, the lifetime of an exciton will be determined by the physical conditions describing a particular cage.

Many dynamical properties, different for the various different

excitons have been analyzed via measurements on phosphorescence emission, delayed fluorescence, and triplet absorption. A rather detailed picture of triplet exciton dynamics in DBN is obtained. This model may also be applicable to other systems.

Triplet-triplet annihilation is found to occur in melt-grown DBN crystals. At liquid helium temperatures it is found that delayed fluorescence occurs mainly from the interaction of one particular kind of excitons and a very particular trap (-like) state. In the phosphorescence emission spectrum the emission of this trap (-like) state is found very close to the emission of excitons. At very low temperatures ($T < 2$ K) we find a strong emission from this trap (-like) state and the emission may easily be confused with excitonic emission.

Delayed fluorescence, which is the final result of triplet-triplet annihilation is found to arise mainly from an impurity. This impurity acts as a very efficient trap for DBN singlet excitons, which are the primary result of the annihilation. We have been able to determine the exact nature of the impurity and it appears to be the 1,5-dibromonaphthalene isomer. This isomer has a much higher triplet energy than the 1,4-DBN system. Therefore it acts as a cage-terminator.

Triplet-triplet annihilative processes in DBN appear to be strongly affected by very high magnetic fields. These magnetic field effects have an influence not only on the delayed fluorescence but also on the phosphorescence emission. To describe these effects the theory of Merrifield, developed for low magnetic fields, is extended to very high magnetic fields.

In the last chapter of this thesis we present a new system for the study of triplet excitons in molecular crystals, 1,8-dibromonaphthalene. A large amount of excitonic emission is easily obtained and zero-field ODMR transitions are found for this emission.

SAMENVATTING

Gedurende de afgelopen tien jaar is er een intensieve studie gemaakt van lineaire triplet excitonen. Tot op heden is er slechts een zeer beperkt aantal goed onderzochte systemen waarin de transport topologie (quasi-) eendimensionaal is. Eén van die systemen is 1,4-dibroomnaftaleen (DBN). Het grootste gedeelte van dit proefschrift is gewijd aan experimenten met deze verbinding.

Normaal gesproken worden excitonen beschouwd als collectief aangeslagen toestanden van het kristal in zijn geheel en het wordt algemeen aangenomen dat een kristal zo perfect mogelijk moet zijn om fosforescentie emissie te kunnen detecteren van excitonen. In theorie blijft dit natuurlijk waar, maar in de praktijk is een echt ideaal perfect kristal moeilijk te verkrijgen. Zoals blijkt uit dit proefschrift, blijkt dan in DBN het tegengestelde het geval te zijn: geen exciton emissie wordt waargenomen in "perfecte" kristallen, gegroeid uit de damp, terwijl wel exciton emissie wordt waargenomen in minder perfecte kristallen, gegroeid uit de smelt.

In dit proefschrift wordt beschreven, dat de optische eigenschappen van DBN kristallen, die we uit de smelt gegroeid hebben, alleen verklaard kunnen worden door het kristal te beschouwen als een verzameling van eendimensionale stukjes ("kooien"). Deze kooien zijn sterk van elkaar geïsoleerd door barrières met een hoge (triplet) energie. Optisch toegankelijke triplet excitonen met verschillende excitatie energie en sterk verschillende levensduren blijken tegelijkertijd te kunnen bestaan in verschillende kooien. Wanneer een kooi een "trap" bevat, zullen de excitonen, die in deze kooi gegenereerd worden, heel effectief worden weggevangen (een "trap" is een energie-"val", waardoor de beweging van excitonen gestopt kan worden). Daarom zullen dit soort excitonen een zeer korte levensduur hebben. De kans om een trap in een kooi aan te treffen neemt toe met toenemende lengte van de kooi.

Een dergelijke situatie treft men waarschijnlijk aan in de bijna perfecte damp-gegroeide kristallen, waarin de eendimensionale kooien tamelijk lang kunnen zijn. Door de zeer korte levensduur van de excitonen kan men in deze kristallen geen exciton fosforescentie emissie waarnemen.

Voor kortere ketens is de kans groot dat géén trap aanwezig is. Zodoende wordt de levensduur van het exciton langer en als de levensduur lang

genoeg wordt kan men emissie waarnemen van deze excitonen. Waarschijnlijk treft men deze situatie aan in kristallen gegroeid uit de smelt. Uiteindelijk wordt de levensduur van een exciton dan bepaald door de fysische omstandigheden die een bepaalde kooi karakteriseren.

Veel dynamische eigenschappen, die verschillend zijn voor de diverse excitonen zijn geanalyseerd d.m.v. metingen aan de fosforescentie emissie, de vertraagde fluorescentie en de triplet absorptie. Een tamelijk gedetailleerd beeld van triplet exciton dynamica in DBN werd verkregen. Dit model is mogelijkwijze ook van toepassing op andere systemen.

Het optreden van triplet-triplet annihilatie is aangetoond in DBN kristallen, gegroeid uit de smelt. Het blijkt, dat vertraagde fluorescentie bij vloeibare helium temperaturen voornamelijk ontstaat door de botsing van één bepaald type excitonen met een zeer speciale trap(-achtige) toestand. In het fosforescentie emissie spectrum ligt de emissie van deze trap(-achtige) toestand vlak bij de emissie van excitonen. Bij temperaturen onder twee Kelvin vinden wij een sterke emissie van deze trap(-achtige) toestand en deze emissie kan dan gemakkelijk verward worden met exciton emissie.

De vertraagde fluorescentie, die het uiteindelijke resultaat is van triplet-triplet annihilatie blijkt voornamelijk te komen van een verontreiniging. Deze verontreiniging is een zeer efficiënte trap voor DBN singlet excitonen, die het primaire resultaat zijn van de annihilatie.

Wij hebben kunnen achterhalen om welke verontreiniging het hier gaat en het blijkt de isomeer 1,5-dibroomnaftaleen te zijn. Deze isomeer heeft een veel hogere triplet energie dan het 1,4-DBN systeem. Daarom functioneert hij als barrière tussen kooien.

De triplet-triplet annihilatie in DBN blijkt zeer sterk te worden beïnvloed door zeer hoge magneetvelden. Deze magneetvelden hebben niet alleen effect op de vertraagde fluorescentie maar ook op de fosforescentie emissie. Om deze effecten te kunnen beschrijven is de theorie van Merrifield, die is ontwikkeld voor lage magneetvelden, uitgebreid naar zeer hoge magneetvelden.

In het laatste hoofdstuk van dit proefschrift geven we een nieuw systeem aan voor de bestudering van triplet excitonen in moleculaire kristallen, 1,8-dibroomnaftaleen. Een grote hoeveelheid exciton emissie is makkelijk te verkrijgen en nulveld ODMR overgangen zijn gevonden voor deze emissie.

CURRICULUM VITAE

Jo Vankan, geboren 21 maart 1955 te Heerlen, behaalde zijn eindexamen gymnasium β (oude stijl) aan het St.-Bernardinuscollege te Heerlen in 1973. Aansluitend ging hij scheikunde studeren aan de Katholieke Universiteit te Nijmegen. Het kandidaatsexamen werd "met genoeg" afgelegd in juni 1976. In februari 1979 werd het doctoraalexamen cum laude afgelegd, met als hoofdvakken molecuulspectroscopie (Prof.dr. E. de Boer) en organische chemie (Prof.dr. B. Zwanenburg) en als caput het tentamen quantumchemie (Prof.dr.ir. A. van der Avoird). Tevens werd de eerstegraads lesbevoegdheid chemie behaald. Voor het onderzoek op de afdeling Molecuulspectroscopie werd in januari 1978 de Faculteitsprijs verkregen (NMR aan vaste stoffen).

Aansluitend aan het doctoraalexamen werd begonnen met het in dit proefschrift beschreven onderzoek en in dit verband trad hij in juli 1979 in dienst van ZWO/SON als wetenschappelijk medewerker. Het onderzoek stond onder de dagelijkse leiding van Dr.ir. W.S. Veeman.

Tijdens de studie- en promotieperiode assisteerde hij bij diverse practica (fysische chemie voor biologie studenten, fysische chemie voor chemie studenten en spectroscopische technieken) en verzorgde hij het werkcollege chemische binding.

STELLINGEN

I

Antisymmetrische exchange (AE) kan slechts voorkomen in systemen zonder inversiesymmetrie. Bencini et al. stellen voor de bijdrage van AE aan ESR spectra te bepalen uit het niet samenvallen van de \bar{g} en \bar{D} tensor assen van dimere systemen.

In dimere systemen, die de vereiste lage symmetrie hebben vallen de \bar{g} en \bar{D} tensor assen i.h.a. niet samen, waardoor het voorstel weinig zinvol is.

A. Bencini, D. Gatteschi, Mol. Phys. 47, 161 (1982).

II

De wijze, waarop Davey et al. α_{hkl} waarden gebruiken is niet juist, omdat de kritische α_{hkl}^R factoren niet berekend zijn.

R.J. Davey, J.W. Mullin, M.J.L. Whiting, J. Cryst. Growth 58, 304 (1982)

III

In tegenstelling tot wat Schlothauer en Alig verwachten, is het verband tussen het quotiënt van het piekoppervlak van twee methine koolstof resonanties in het ^{13}C -NMR spectrum en het vinylacetaat gehalte niet lineair maar parabolisch.

K. Schlothauer, I. Alig, Polym. Bull. 5, 299 (1981)

IV

De begrippen chiraliteit en optische activiteit worden in de literatuur op een verwarrende wijze naast elkaar gebruikt.

M.E. Jung, T.J. Shaw, J. Am. Chem. Soc. 102, 6304 (1980)

H. Hiemstra, H. Wijnberg, J. Am. Chem. Soc. 103, 417 (1981)

V

De bewering van Eaton en Eaton, dat exchange menging veroorzaakt van singlet en triplet $m_s = 0$ niveau en bovendien de andere triplet niveaus niet beïnvloedt, is onjuist.

S. Eaton, G. Eaton, J. Am. Chem. Soc. 104, 5002 (1982)

VI

Het opschrift "geldvervoer" op auto's, die geld transporteren is cognitief dissonant met de ervaring, dat geld normaliter met de grootste omzichtigheid behandeld wordt.

VII

Het feit, dat men tegenwoordig veelal de voorkeur geeft aan zogenaamde "authentieke" uitvoeringen van oude muziek boven zogenaamde "romantische" uitvoeringen daarvan, getuigt van het romantische karakter van onze tijd.

